

Syracuse University

**SURFACE**

---

Dissertations - ALL

SURFACE

---

May 2020

# Evaluating the Hydrologic and Thermal Performance of a Green Roof in Syracuse: Measurements and Modeling of a Full-Scale System

Yige Yang  
*Syracuse University*

Follow this and additional works at: <https://surface.syr.edu/etd>



Part of the [Engineering Commons](#)

---

## Recommended Citation

Yang, Yige, "Evaluating the Hydrologic and Thermal Performance of a Green Roof in Syracuse: Measurements and Modeling of a Full-Scale System" (2020). *Dissertations - ALL*. 1180.  
<https://surface.syr.edu/etd/1180>

This Dissertation is brought to you for free and open access by the SURFACE at SURFACE. It has been accepted for inclusion in Dissertations - ALL by an authorized administrator of SURFACE. For more information, please contact [surface@syr.edu](mailto:surface@syr.edu).

## ABSTRACT

Climate change and urbanization have increased the risk of flooding and combined sewer overflows as well as other stormwater related problems. Given the high costs of traditional infrastructure rehabilitation, green infrastructure, which mimics natural systems, has become a popular solution. Green roofs are one prominent example of green infrastructure. These are engineered vegetative systems positioned on the top of roof structures have been widely adopted around the world, owing to an abundance of roof area in urban neighborhoods. However, their hydrologic performance and thermal properties are unclear, due to a lack of qualitative and quantitative analyses on monitored full-scale green roofs. In particular, few studies have focused on factors that impact the hydrologic performance of green roofs, such as soil properties which change as the roof ages, and evapotranspiration (ET) which dries the soil and enables the green roof to store water from the next storm. Understanding water exchange on a green roof also requires investigation into the thermal properties of the system. To quantify thermal impacts, field measurements and a model that couples energy with soil moisture would be of value.

My study aims to fill these gaps by advancing understanding of green roof behavior, including the aging effect of soil media, ET, and heat transfer, and by developing methods to predict the hydrologic performance and related thermal properties of green roofs. In this research, rainfall, runoff, soil moisture content, and meteorological data have been measured in a green roof system at the Onondaga County Convention Center in Syracuse, NY (OnCenter) since 2015. This study included controlled laboratory experiments for soil characterization, monitoring the OnCenter green roof under a variety of weather conditions, and use of computer modeling to predict green roof performance.

In the first phase of the study, in which I investigated the effects of aging on green roof functions, virgin and 7-year-old growth media were characterized and the impact of the observed changes on hydrologic performance was assessed. Differences in structure (particle size distribution, porosity, organic content, density) and some hydrologic properties were observed. The aged growth medium experienced a shift to finer particles and smaller pores with a 60% increase in the organic content. An increase in water filled porosity indicated more water can be stored in aged growth medium than in the original medium. The observed aging effects on hydrologic performance were modelled using HYDRUS-1D. Five 24-hour design storms were applied to predict the retention and detention performance. A 4% improvement in retention performance was calculated for 7-year-old growth medium for significant storms over the original medium. Runoff was detected around an hour later in simulations in aged growth medium compared to original medium. Better retention and detention performance of the green roof was suggested from both monitored data and simulated data from HYDRUS-1D.

The second phase of the study focused on evapotranspiration (ET), a vital component of the water balance and also an important term in the soil surface energy balance of green roofs. Quantifying ET for green roofs helps quantify the thermal and hydrologic benefits of green roof systems, enabling informed design and installation decisions. In this work, a soil water balance method was applied to quantify ET using continuous field monitoring for the period May through November during 2015, 2016, and 2017. Results show daily ET ranged from 0 to 5.4 mm/day with an average of 0.76 mm/day. No clear seasonal variation of ET in the seven-month period was observed. The ET rate was significantly influenced by initial soil moisture content and solar radiation. The ET measurements were also compared to fourteen potential ET models

together with soil moisture extraction functions (SMEF), the Thornthwaite-Mather (T-M) equation, and antecedent precipitation index (API). The crop coefficient ( $K_c$ ) was obtained through backward least squares optimization. When soil moisture data are available, the Blaney-Criddle model and the Priestley-Taylor model together with SMEF and monthly  $K_c$  values are recommended for predicting ET for the northeastern U.S. due to their limited data input requirements. When soil moisture data are not available, the modified API model with monthly  $K_c$  is recommended.

In the third phase of the study, the focus shifted to energy storage and transfer. Green roofs have the potential to improve thermal performance of building systems through evapotranspiration, thermal mass, insulation and shading, thus decreasing the cooling energy consumption in summer. A combined energy and moisture model for the retrofit green roof at the OnCenter was developed in CHAMPS software with a hourly time step. Reasonable agreement was observed between the simulated output and monitored data. From the simulated data, the green roof demonstrated the ability to significantly reduce the temperature fluctuations of the roof membrane. In summer, the green roof moderated the heat flow through the roofing system and reduced the air conditioning cost. In winter, under the accumulation of snow, the protection provided by the growth medium was negligible compared with the protection provided by the snow. The temperature of the growth medium on the Convention Center remained slightly above freezing and was relatively steady when heavy snow coverage was present, even during extremely cold air temperatures. Heat flux is dominated by the temperature gradient between interior space and the snow layer.

Overall, this research provides valuable understanding on the hydrologic and thermal behavior of green roofs, especially extending knowledge of the effect of soil aging, quantification of the ET process, and prediction of energy flows. The methods and results in this study are valuable for informing future green roof design, planning, retrofit, maintenance, and policy decision making.

Evaluating the Hydrologic and Thermal Performance of a Green Roof in  
Syracuse: Measurements and Modeling of a Full-Scale System

by  
Yige Yang

B.S., Sun Yat-sen University, 2013  
M.S., Syracuse University, 2015

Dissertation

Submitted in partial fulfillment of the requirements for the degree of  
Doctor of Philosophy in Civil Engineering

Syracuse University  
May 2020

Copyright © Yige Yang May 2020

All Rights Reserved

## **ACKNOWLEDGMENTS**

During my PhD journey, I have faced many challenges. This dissertation would not have been completed without support and love of faculty members, family, and friends. I would especially thank my advisor, Professor Cliff Davidson. You gave me the freedom to choose the research topics, and mentored me throughout the entire research period. Especially, you have taught me to treat my work seriously and sincerely on another level. I would also like to thank all faculty and staff of the Department of Civil and Environmental Engineering for their help and support. For the guidance, comments, and suggestions on my thesis, I would like to thank my dissertation committee: Professor Charles Driscoll, Professor Jensen Zhang, Professor David Chandler, Professor Svetoslava Todorova. In addition, I would like to thank Professor Peng Gao for agreeing on serving as the oral exam chair on short notice. I would also like to thank the Onondaga County Department of Facilities Management for their assistance and permission to work at the Convention Center, especially Han Pham, Chris Denny, Charles Campbell, and Archie Wixson. The following students assisted with work on the green roof: Katie Duggan, Endla Feustel, William Guida, Mallory Squier, and Chris Weiman. The thesis was reviewed by Zach Monge, which is very much appreciated.

I want to also express my gratitude to the family and friends that I am extremely lucky to have. In particular, I would like to thank my parents, Jinsong Yang and Hong Wei, for always believing in me and having my back during difficult times. The annual family vacations are always relaxing and full of laughs. I would also like to thank: Mallory Squier for starting the green roof monitoring program and sharing experiences with me; Carli Flynn for encouraging

me like a big sister; Basak Keskin for all the fun activities after school; Tony Zheng, for being a close friend. I would also thank my boyfriend, William Shaw, for always being there for me. Finally, the dissertation would not be finished without the academic and financial support of the EMPOWER program and UREx Sustainability Research Network. I have not only gained technical knowledge, but also professional skills from these two programs.

# TABLE OF CONTENTS

LIST OF FIGURES .....	xiii
LIST OF TABLES .....	xv
<b>1. INTRODUCTION.....</b>	<b>1</b>
1.1 Dissertation Structure .....	3
1.2 Background .....	6
1.2.1 Green Roof Hydrology .....	6
1.2.1.1 Green Roof Hydrologic Benefits .....	6
1.2.1.2 Factors Affecting Green Roof Hydrology .....	7
Growth Medium.....	7
Plants and other Biota.....	8
Age of the Green Roof .....	9
Climate .....	10
Slope of the Roof .....	11
1.2.1.3 Prediction of Green Roof Performance .....	11
Hydrologic Modeling .....	12
Rain Simulator .....	15
1.2.1.4 Summary of Green Roof Hydrology .....	16
1.2.2 Evapotranspiration .....	17
1.2.2.1 ET Measurement Methods .....	17
1.2.2.2 ET Modeling .....	19
1.2.2.3 Summary of ET .....	20
1.2.3 Green Roofs Thermal Performance .....	20
1.2.3.1 Green Roofs Thermal Benefits .....	20
1.2.3.2 Factors affecting Green Roof Thermal Performance .....	22
Plants .....	22
Growth Medium .....	23
Snow .....	24
1.2.3.3 Green Roof Thermal Modeling .....	25
1.2.3.4 Summary of Green Roof Energy Performance .....	26

<b>2. GREEN ROOF AGING EFFECT ON PHYSICAL PROPERTIES AND HYDROLOGIC PERFORMANCE .....</b>	<b>27</b>
2.1 Introduction .....	27
2.2 Methods .....	28
2.2.1 Study Site and Monitoring System .....	28
2.2.2 Data Processing and Event Analysis .....	30
2.2.3 Extraction and Physical Tests of Growth Media .....	31
2.2.4 Hydrologic Analysis .....	32
2.2.5 Green Roof Hydrologic Modeling .....	34
2.3 Results and Discussion .....	35
2.3.1 Growth Medium Physical Properties .....	35
2.3.2 Green Roof Hydrologic Performance .....	39
2.3.2.1 Weather and Rainfall Profiles .....	39
2.3.2.2 Retention .....	40
2.3.2.3 Detention .....	43
2.3.3 Green Roof Hydrological Modeling .....	45
2.4 Conclusions .....	47
2.5 Practical Implications .....	49
<b>3. QUANTIFYING EVAPOTRANSPIRATION ON A GREEN ROOF: A COMPARISON OF SOIL WATER BALANCE METHOD WITH COMMONLY USED PREDICTIVE METHODS .....</b>	<b>50</b>
3.1 Introduction .....	50
3.2 Methods .....	52
3.2.1 Study Site and Instrumentations .....	52
3.2.2 ET Estimates .....	53
3.2.3 ET Measurement – Soil Water Balance Method .....	57
3.2.4 Energy Balance Model .....	58
3.2.5 Statistical Methods .....	59
3.3 Results and Discussion .....	60

3.3.1	Weather Condition and ET Measurement Results .....	60
3.3.2	Factors Affecting the ET Process .....	62
3.3.3	Daily ET Rates .....	64
3.3.4	ET Estimates from the Energy Balance Model .....	65
3.3.5	Actual ET (ETa) Estimates Comparison .....	66
3.3.6	Model Sensitivity and Improvement .....	70
3.4	Conclusion .....	73
<b>4.</b>	<b>EVALUATION OF THERMAL PERFORMANCE OF GREEN ROOFS VIA FIELD MEASUREMENTS AND HYGROTHERMAL SIMULATIONS.....</b>	<b>76</b>
4.1	Introduction .....	76
4.2	Methods .....	78
4.2.1	Experimental Campaign .....	78
4.2.2	Description of Green Roof Components .....	80
4.2.3	CHAMPS Simulation .....	81
4.3	Results and Discussion .....	83
4.3.1	Summer Thermal Performance .....	83
4.3.2	Winter Thermal Performance .....	84
4.3.3	Model Validation .....	86
4.3.4	Thermal Impacts of Green Roofs in Summer .....	87
4.3.5	Thermal Impacts of Green Roofs in Winter .....	90
4.3.6	Parametric Studies .....	92
4.4	Conclusion .....	93
<b>5.</b>	<b>CONCLUSIONS .....</b>	<b>96</b>
5.1	Key Findings .....	96
5.2	Proposed Areas of Future Work .....	100

<b>Appendices .....</b>	<b>102</b>
A: HYDRUS-1D Equations .....	102
B: HYDRUS-1D Design Storms .....	104
C: Daily Snowfall and Temperature data for Syracuse .....	105
D: Thermal Properties of the OnCenter Green Roof .....	106
E: The moisture mass balance and energy balance in CHAMPS .....	106
 <b>References.....</b>	 <b>108</b>
 <b>Vita.....</b>	 <b>131</b>

## LIST OF FIGURES

Figure 1.1. Structure of the dissertation. Main thesis topics are effect of green roof aging, prediction of evapotranspiration, and modeling of thermal performance. ....	5
Figure 2.1. Average monthly rainfall depth (rain only) and monthly snow depth recorded at the Syracuse Hancock Airport (1938 - 2018). Snow depth is typically divided by 10 to obtain meltwater depth.....	29
Figure 2.2. Positions of drain conduits, roof drains, and growth medium sample collection locations on the OnCenter green roof. ....	30
Figure 2.3. Samples collection illustration. ....	32
Figure 2.4. Particle size distributions for the virgin and aged growth medium. ....	37
Figure 2.5. Data for air-filled and water-filled porosity and for organic matter content in virgin (2011) and aged (2018) growth medium. ....	39
Figure 2.6. Monitored annual Rainfall and runoff data for 2015 – 2018. ....	40
Figure 2.7. Depth-frequency curves for 2015 and 2017 from the monitoring data. ....	42
Figure 2.8. Peak intensity-frequency curves for 2015 and 2017 from the monitoring data. ....	44
Figure 3.1. Monthly precipitation solar radiation, and ET from 5/1/2015 to 11/30/2017. ....	62
Figure 3.2. Variable importance in projection (VIP) plots for partial least squares analysis (PLS). The red line is the threshold value of 0.8 defining influential variables. ....	64
Figure 3.3. Daily precipitation and ET depth from 5/1/2015 to 11/30/2017. Tick marks on the x-axis indicate the first day of each month. ....	65
Figure 3.4. Energy Flux monthly average (mean daily value for each month). ....	66
Figure 3.5. Predicted ET from the five satisfactory models and the measured ET for the OnCenter green roof for the study period. Measurements and model results are shown as continuous lines, even though all measurements and calculations shown above are for days without rain. ....	70
Figure 3.6. Scatter plot of measured ET values and modeled ET using the original API model with a single $K_c$ , and using the modified API model with monthly $K_c$ values. ....	72
Figure 3.7. Monthly average measured ET results compared with three models: (1) the original API values ( $ET_a-API+K_c$ ), (2) an API model with fitted $\alpha$ , $K = 0.8$ , $n = 12$ , maximum API = 50, and one unified $K_c$ ( $ET_a$ -modified API+ $K_c$ ), and (3) an API model with modified $\alpha$ and monthly $K_c$ ( $ET_a$ -modified API+monthly $K_c$ ). ....	72

Figure 4.1. Photos of the OnCenter green roof during different seasons.....	79
Figure 4.3. Thermal conductivity for different water content measured in the lab. ....	80
Figure 4.4. Solar radiation and rainfall intensity during a typical summer week (Aug 1-7, 2017). .....	83
Figure 4.5. Temperature profile time series of the green roof during a typical summer week (Aug.1-7, 2017).....	84
Figure 4.6. Temperature profile time series of the green roof during a winter week in November (no snow). ....	85
Figure 4.7. Temperature profile time series of the green roof during a winter week in January (snow cover). ....	85
Figure 4.8. Comparison of simulated and measured temperatures of the growth medium on the green roof for the first week of August (a) and the first week of November (b).....	86
Figure 4.9. Comparison of the measured soil temperature of the green roof and simulated temperature of a traditional roof. The measured curve is identical to the curve in Figure 5.7 a. ...	88
Figure 4.10. Temperature fluctuations at the membrane of the simulated traditional roof and measured on the green roof in summer. ....	88
Figure 4.11. Comparison of heat flow through the insulation for the green roof and the traditional roof during a typical summer week (Aug 1-7, 2017).....	89
Figure 4.12. Temperature fluctuations at the membrane of the simulated traditional roof and measured on the green roof in winter.....	91
Figure 4.13. Temperature of the membrane for two conditions: simulated result with no snow cover and measurements with snow cover. ....	92
Figure 4.14. Comparison between measured and simulated (with and without water balance) soil temperature for the green roof. ....	92
Figure 4.15. Soil temperature on the green roof for different albedo values. ....	93
Figure B.1. Simulated hydrographs with rainfall (grey line), runoff for 2011 virgin soil (blue line), and runoff for 2018 aged soil (orange dot line). ....	<b>Error! Bookmark not defined.</b>
Figure C.1. Daily snowfall and daily minimum and maximum air temperature (1938-2016). .....	<b>Error! Bookmark not defined.</b>

## LIST OF TABLES

Table 1.1. Evapotranspiration measurement methods. ....	18
Table 2.1. Definition of the event rainfall and runoff characteristics used for analysis. ....	33
Table 2.2. Physical properties of the OnCenter growth medium.....	36
Table 2.3. Retention by season for the OnCenter green roof. ....	41
Table 2.4. Green roof average rainfall detention statistics.....	43
Table 2.5. Growth medium retention curve fitting statistics for 2011 and 2018 soil (RETC). ....	45
Table 2.6. Retention and detention performance for the virgin and aged growth media.....	46
Table 3.1. Previously reported ET measurement from green roofs. ....	51
Table 3.2. Potential ET estimate models.....	54
Table 3.3. Crop coefficient $K_c$ and statistical performance measures of the actual ET estimates. The simulations with satisfactory performance are shown in bold. Criteria for satisfactory performance are $RMSE < 0.5$ , $PBIAS < 12\%$ (positive or negative), $NSE > 0.6$ , $D > 0.85$ , and $R^2 > 0.6$ . ....	69
Table 3.4. Monthly crop coefficients ( $K_c$ ) derived from the observed and simulated data from the OnCenter green roof from five satisfactory ETa models for the three-year study period. ....	73
Table 3.5. Statistical performance of applying one single $K_c$ and also monthly $K_c$ values for the five satisfactory models.....	73
Table 4.1. Estimated summer energy demand and cost for 5600 m <sup>2</sup> green roof and traditional roof. ....	90
Table A.1. Average values of $\theta_s$ , $\theta_r$ , $\alpha$ , $n$ , Porosity and $K_s$ of the Carsel and Parrish (1988) calibration data set. ....	<b>Error! Bookmark not defined.</b>
Table D.1. Thermal properties of the Conventional Center green roof. ....	<b>Error! Bookmark not defined.</b>

# Chapter 1

---

## INTRODUCTION

Green roofs are not a recent development. The modern green roof industry began in the early 20<sup>th</sup> century, when German roofers employed vegetation on roofs to reduce solar radiation and protect roof structures. Active research on growth media, vegetation, roof construction, and design contributed to the development of the modern green roof and design guidelines (FLL, 1995). Green roofs typically consist of vegetation, engineered growth medium or other substrate, drainage layer, waterproof membrane, and the layers of material that make up the roof structure. Due to an abundance of roof area in urban neighborhoods and increasing environmental concerns, green roofs have become widely adopted around the world.

The adoption of green roofs is known to have numerous benefits. For example, green roofs can mitigate the urban heat island effect (Sharma et al., 2016; Theodoridou et al., 2017), reduce stormwater runoff (Mentens et al., 2006; Gregoire and Clausen, 2011), increase biodiversity (Metselaar, 2012), reduce air pollution (Bianchini and Hewage, 2012), improve building insulation (Li et al., 2017), and reduce noise (Besir and Cuce, 2018). However, research on hydrologic benefits has focused on understanding overall green roof volume retention and detention performance (Viola et al., 2017; Todorov et al., 2018). Fewer studies have focused on underlying factors that impact this performance, such as how properties of the growth medium change as the roof ages, and the role of evapotranspiration (ET) which controls soil moisture. Because of the importance of ET in hydrology, a better understanding of the effectiveness of models in simulating ET would be useful in their application of roof design and evaluation of performance. Furthermore, although research on heat flow through conventional roofs has been

explored in detail, only limited studies have considered thermal properties of green roofs (Squier and Davidson, 2016).

To predict green roof performance, models are available but the accuracy of input parameters is a major concern. Experimental characterizations of green roof growth media are especially needed.

Green roof hydrologic performance is a function of the effects of a range of interacting bio-physical processes. As green roof systems age, both the vegetation and the growth medium experience changes through a number of natural processes, such as root development, insect tunneling, soil consolidation, organic matter turnover, and media weathering. Those processes have potential to change the physical properties and green roof hydrologic performance over time. Currently there is limited understanding of the evolution of green roof systems and their hydrologic performance as systems age (De-Ville et al., 2017).

The installation of a green roof should enhance evapotranspiration (ET). Water fluxes from evaporation and plant transpiration have the potential to reduce building energy use and decrease stormwater runoff. ET during dry periods affects the soil moisture prior to a rainfall event (Berretta et al., 2014). The soil water retention capacity of a green roof is known to be highly sensitive to the initial moisture prior to a rainfall. In addition, ET contributes to latent heat losses and reducing the surface temperature (Gunkel and Lange, 2017). Studies of green roof evapotranspiration can improve understanding of the thermal and hydrologic benefits of these systems and enable informed design and implementation decisions. Furthermore, ET measurements or predictions are required for numerous green roof hydrologic and energy models (Schneider, 2011). The gap of investigation of ET performance on green roofs needs to be filled.

Thermal benefits of green roofs include energy savings for space heating and cooling, mitigating urban heat island effects, and protecting the base roof membranes from extreme temperature fluctuations. Several studies have analyzed the heat flow impact of green roofs in hot weather, but few studies have examined the thermal performance during cold conditions (Jaffal et al., 2012). It is economically beneficial to provide a reliable method to predict thermal performance of a green roof prior to installation. Models can estimate the impact of a green roof on heat flow, but the validation studies of those models lack long-term, accurate data (Zhang et al., 2017). Furthermore, a thermal model coupled with a soil moisture model is needed to understand and evaluate the influence of soil moisture on thermal conductivity.

The primary objective of this study is to advance our understanding of green roof behavior by reducing uncertainties in the prediction of its hydrologic and thermal performance. Through my research I aim to fill a gap in current research by exploring three aspects of green roof hydrology, namely the effect of aging of a green roof, prediction and estimation of evapotranspiration using measurements, and the development and application of a combined heat and moisture model. I used the following methods: direct field observations, controlled laboratory experiments, and computer modeling to predict green roof performance over a range of environmental conditions.

## **1.1 Dissertation structure**

The overarching question for this research is: **How can knowledge of the hydrology and thermal performance of green roofs be advanced through the combination of controlled laboratory experiments, simulation models, and continuous monitoring of a green roof?**

Studies that correspond to each chapter of this dissertation are conducted to answer this question. The structure of the dissertation is illustrated in Figure 1.1.

This thesis contains five chapters. In Chapter 1, I present a background, literature review, identification of current research gaps, and an outline of how the research fills these gaps. In Chapter 2, I describe two aspects of the effect of aging of the OnCenter green roof: changes in the physical characteristics and changes in hydrologic performance. In Chapter 3, I quantify ET behavior of the roof using the soil water balance method, and evaluate the effectiveness of various ET models. In Chapter 4, I evaluate the thermal performance of the OnCenter green roof in summer and winter, both with and without snowpack. Field observations were used to validate the proposed combined heat and moisture model. In Chapter 5, I summarize the main conclusions of the research and discuss potential avenues of future research.

The structure of this research is illustrated in Figure 1.1 including three phases.

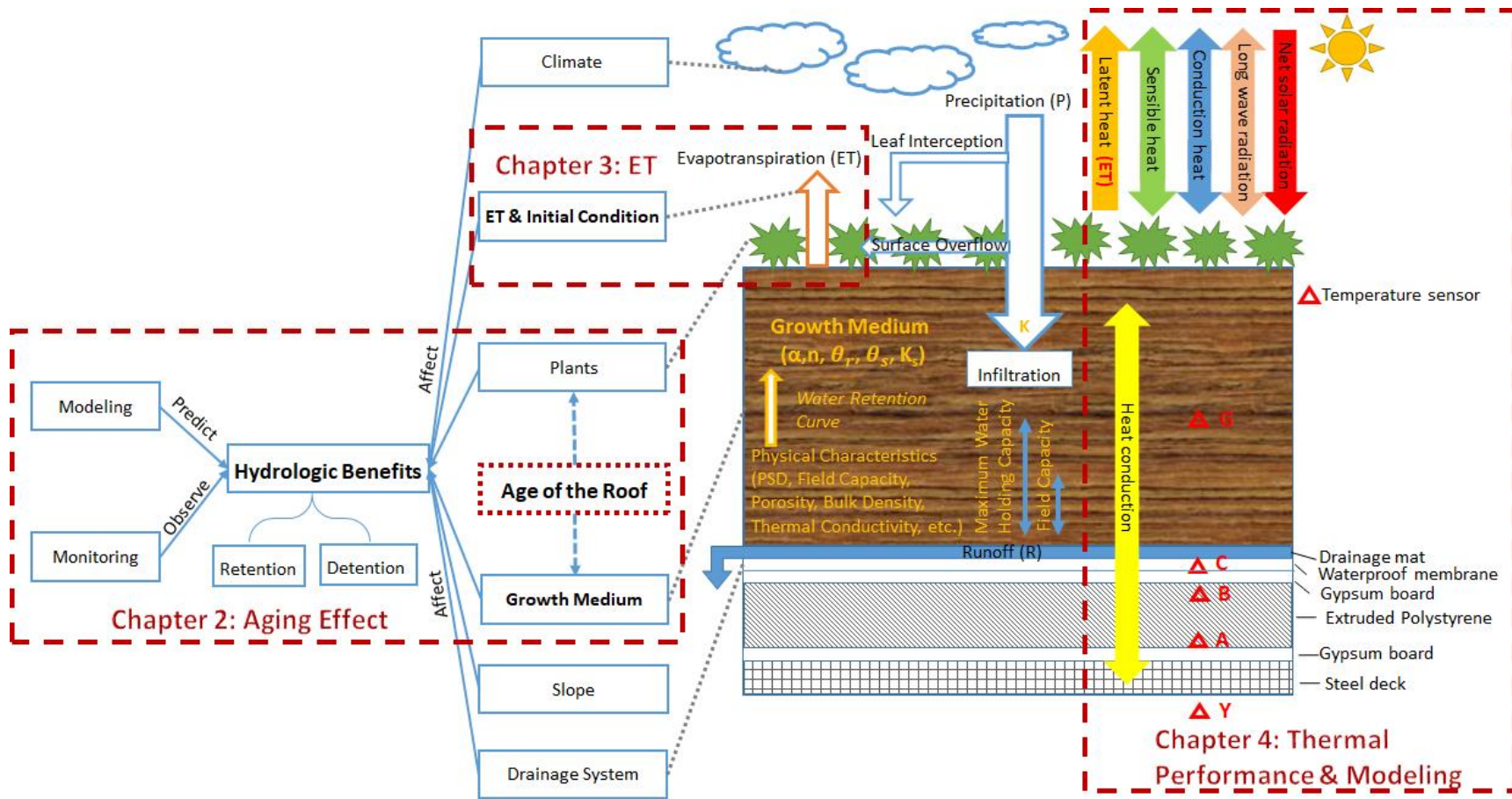


Figure 1.1. Structure of the dissertation. Main thesis topics are effect of green roof aging, prediction of evapotranspiration, and modeling of thermal performance.

## **1.2 Background**

### **1.2.1 Green Roof Hydrology**

#### **1.2.1.1 Green Roof Hydrologic Benefits**

In recent years, green roofs have become a notable method to mitigate combined sewer overflow (CSO) problems because they have the capacity to retain rainfall and detain and decrease runoff (De-Ville et al., 2017). At the onset of rainfall events, water begins to infiltrate into the growth medium. As the rain continues, flow through the growth medium is limited by its hydraulic conductivity, slope, evapotranspiration, and water on the surface of the green roof (She and Pang, 2010).

The potential infiltration rate is defined as a maximum infiltration rate, which depends on the soil moisture content (Getter et al., 2007). The potential infiltration rate decreases with an increase in soil moisture (Weil and Brady, 2017). When the rainfall intensity is smaller than the potential infiltration, rain can infiltrate through the growth medium. As the rainfall intensity increases, the infiltration rate will also increase but only up to the potential infiltration rate. Rainfall intensity greater than the potential infiltration rate will not increase the infiltration rate further.

In general, runoff occurs as the amount of water stored in the growth medium approaches field capacity. Some of the water within the media is taken up by the vegetation and transpired to the atmosphere, and some of the water simply evaporates from the soil. Both transpiration and evaporation are considered retained water lost from the system. In contrast to retention, some of the rainwater is detained temporarily in the growth medium, which reduces the peak runoff flow

rate and increases the lag time between peak rainfall and peak runoff (known as the “peak lag time”). Retention performance of extensive green roofs is well reported in the literature, where the volume retained varies from 27 to 81% (Mentens et al., 2006; Palla et al., 2018; Wong and Jim, 2014). Detention performance is much less documented (Marasco, 2014). Peak intensity reduction, peak lag time, and the lag time between onset of rainfall and onset of runoff (runoff lag time) are the most common measurements to represent detention. Stovin et al. (2012) reported that the peak runoff reduction ranges from 20-100%, with an average of about 59%.

### **1.2.1.2 Factors Affecting Green Roof Hydrology**

#### **Growth Medium**

The growth medium is generally lightweight and composed of highly porous engineered blends of organic matter to provide nutrients and inorganic material to provide structure (VanWoert et al., 2005). The selection of growth medium composition depends on local climate, maintenance level, required function, and intended vegetation (Vijayaraghavan and Raja, 2014). In general, depth, composition, and physical properties govern the water storage capacity. Two major types of green roofs are intensive roofs and extensive roofs. Extensive roofs generally have a thin layer of growth medium and require minimum maintenance. Intensive roofs have a relatively thick layer of growth medium, and often require irrigation and constant maintenance (Bianchini and Hewage, 2012). Many studies have shown that increased growth medium depth will improve the retention performance (Chow et al., 2018; Stovin et al., 2015). Mentens et al. (2006) reviewed 18 studies and demonstrated that there is a correlation between growth medium depth and retention volume. They showed that the average percent of retention was 75% for intensive green roofs, and 50% for extensive green roofs.

Green roof hydrologic performance depends on interacting physical properties such as particle size distribution, pore size distribution, porosity, organic content, and overall material texture (De-Ville et al., 2017). The particle size distribution is related to the pore size distribution which affects retention performance (McLaren and Cameron, 1996). Organic content typically has larger adhesion of water compared to inorganic. Thus, high organic content implies a larger maximum retention capacity. In contrast, detention performance is influenced by porosity, pore-scale permeability, and hydraulic conductivity (Coles and McDonnell, 2018). Based on a literature review, little attention has been given to quantifying the importance of these properties on detention (Johannessen et al., 2018).

### **Plants and other Biota**

Studies suggest that growth medium characteristics impact green roof retention capacity more than plant cover and type (VanWoert et al., 2005; Nagase and Dunnett, 2012). Nevertheless, plants and other biota play an important role in the stormwater retention capacity of green roofs. During precipitation, plants generally retain rain water through interception by leaves and water uptake by roots. Nagase and Dunnett (2012) investigated the influence of various plant species on the retention performance in green roof test beds in a greenhouse. They found grasses were the most effective for reducing runoff, followed by forbs, and sedum. They also found that plants with taller height, larger stem diameter, and larger root biomass retained more water. The authors reported poor performance of sedum, which they attributed to its smaller roots compared to forbs and grasses. Larger roots can fill large voids in the growth medium, thus increasing water holding capacity. However, plants with larger roots typically have poor drought tolerance (Lu et al., 2014). Sedums are considered succulents and are believed to be the more

suitable for extensive green roofs because of their drought tolerance, shallow soil adaptability, and low maintenance. Sedum stores water in its leaves during wet periods. During drought, sedums enable the crassulacean acid metabolism (CAM) pathway, meaning they open their stomata and absorb CO<sub>2</sub> at night, which coincides with minimal ET demands, while their stomata are closed during CO<sub>2</sub> assimilation to carbohydrates in the daytime (Nektarios et al., 2014).

Some of the hydrologic benefits of plants are also related to their ability to transpire.

Transpiration decreases the soil water uptake and can prevent wetting under small rainfall events, which help green roofs to extend their retention capacity. Berretta et al. (2014) set up three test beds with various plants and one test bed without vegetation, to investigate the temporal changes in soil moisture content during a dry period. They found that the presence of plants resulted in higher daily moisture loss after a few dry days. Ouldboukhitine et al. (2012) investigated ET water loss for grass, sedum, and bare growth medium and found that ET for grass was 60% higher than sedum, and almost 50% higher than bare growth medium. DeNardo et al. (2005) investigated three green roofs located in Pennsylvania and suggested that water loss rate would be around 3 mm/day for vegetated and 1.5 mm/day for bare growth medium.

### **Age of the Green Roof**

Both vegetation and growth medium are subject to natural processes which have the potential to change their characteristics over time. These changes may alter hydrologic performance.

Inconsistent trends were shown in previous studies that relate physical property changes to aging of green roofs. One study of a green roof in a Mediterranean climate reported that organic content and pore volumes had nearly doubled over five years (Getter et al., 2007). Emilsson and

Rolf (2004) reported that the organic content decreased over four months from 3% to 1% in one sample, and from 10% to 1.6% in a second sample. The authors assumed it may be because of different type of organic matter decay at different rate. Bouzouidja et al. (2018) found a decrease in organic content from 5% to 2% in four-year-old growth medium, possibly due to degradation of organic carbon and loss through drainage. However, the porosity and density of the medium remained constant. De-Ville et al. (2017) reported there was an unchanged density but a significant increase in the fraction of fine particles (< 2 mm) in the growth medium over a 5-year period. Porosity decreased and saturated hydraulic conductivity decreased from 0.0067 to 0.005 cm/s. A low saturated hydraulic conductivity was associated with an increase in detention. De-Ville et al. (2017) also examined physical properties using non-invasive X-ray microtomography (XMT) imaging. The effect of aging on hydrologic performance was evaluated using two models: a moisture-flux model for retention and an unsaturated-flow finite element model for detention. Small improvements in retention performance (< 5%) and detention performance (no statistically significant difference) due to increasing growth media age were observed in this study. The studies above applied different methods and are geographically distributed, which may account for the inconsistent results.

### **Climate**

Many studies show that rainfall characteristics, initial water content of the growth medium, solar radiation, and humidity can affect the hydrologic performance of a green roof (Palla et al., 2018; Sun et al., 2014; Nawaz et al., 2015). Nawaz et al. (2015) observed an inverse correlation between retention performance and both rainfall depth and storm duration. Stovin et al. (2012) analyzed a monitored green roof under climatic conditions of the United Kingdom and found

mean retention averaged 70% for all events but was only 43% for storms with a return period greater than one year. The roof retained 13.2 percent of stormwater for large events with a 16 year return period. Carpenter et al. (2016) reported an inverse relationship between the size of the storm and water retention of a green roof in Syracuse. This green roof could retain between 98% to 100% of the rainfall under low intensity rainfall events, while it only could retain 88% of the rainfall under high intensity rainfall events.

Green roof moisture retention capacity is highly sensitive to the antecedent conditions prior to a rainfall event. This is a function of antecedent dry weather period (ADWP) and weather conditions. Retention percentage increases as the ADWP increases (Stovin et al., 2015).

Higher temperatures and greater wind speeds increase ET and offer faster restoration of soil storage capacity following precipitation events. Generally, volume retention is higher in summer than in winter (Berndtsson et al., 2009; Mentens et al., 2006; Schwarz, 2015; Fassman-Beck et al., 2013). However, this pattern only occurs in regions which tend to have dry-warm summers and cold winters. Voyde et al. (2010) investigated a green roof in Auckland and did not observe significant seasonal variation in retention performance. This was due to small seasonal meteorological variations. Wong and Jim (2014) found that a seasonal effect on mean retention was not significant in Hong Kong, which has hot-wet summers.

### **Slope of the Roof**

Water retention of green roofs decreases as roof slope increases (Villarreal and Bengtsson, 2005; VanWoert et al., 2005). Getter et al. (2007) investigated runoff from 12 green roof platforms

with 4 slopes, 2%, 7%, 15%, and 25%. The retention was 86% for 2% slope and 76% for the 25% slope.

### **1.2.1.3 Prediction of Green Roof Performance**

Determining the limits of precipitation storage capacity and timing and volume of runoff is important to estimate green roof performance. In general, two methods are used to predict the performance of a green roof, namely computer models and laboratory experiments using a rain simulator.

### **Hydrologic Modeling**

Hydrologic modeling of green roofs have been done using (1) physically based models solving the equations for unsaturated and saturated flow; (2) analytical models that treated green roofs as storage reservoirs; and (3) water-balance models based on inputs and outputs. Further, various computational methods exist including the EPA “Storm Water Management Model” (SWMM) (Rossman, 2010), HYDRUS (Šimunek et al, 1994), and the Soil Water Atmosphere and Plant model (SWAP) (VanDam et al., 1990).

### ***SWMM***

SWMM is a widely used analytical model in the industry (Rossman, 2010). In SWMM 5.1 version, a green roof module is developed as part of Low Impact Development (LID) controls. SWMM is an efficient tool, however it does not simulate the detailed physical processes of LID controls (Li and Babcock, 2015; Burszta-Adamiak and Mrowiec, 2013). The inputs are precipitation data and estimates of retention capacity of the growth medium. Alfredo et al. (2010)

calibrated a SWMM model using two methods, namely Curve Number and Storage Node. In the Curve Number approach, each roof subcatchment was linked to an outlet node and the infiltration was computed. In the Storage Node approach, a storage node and two conduits were added between subcatchment and outlet. The authors found that the Curve Number approach underpredicted the volume and rate of discharge, possibly due the assumption that some infiltration would occur during the best-fit simulation run. The authors also suggested that caution needs to be paid when predicting green roof performance using SWMM, especially if validation is not conducted. Burszta-Adamiak and Mrowiec (2013) simulated the stormwater performance of a green roof using SWMM with the LID control module and found the simulation results had a weak fit compared to measured flowrates. Nash-Sutcliffe coefficient (Nash and Sutcliffe, 1970) was used to assess how well the runoff performance was predicted by the SWMM. With a value greater than 0.5, an acceptable model performance is indicated. Negative values of Nash-Sutcliffe coefficient for more than a half of the analyzed rainfall events were observed (Legates and McCabe Jr., 1999). Akdogan and Guven (2016) found the area of subcatchments, precipitation depth, and conduit depth are the most significant parameters in SWMM. To better simulate the infiltration process, She and Pang (2010) added the Green-Ampt infiltration module (Dussailant et al., 2003) to SWMM. By implementing the infiltration module, the simulation results agreed with measured data to within 11%.

### ***SWAP***

The Soil Water Atmosphere and Plant model (SWAP) is a physically based model developed to simulate flow and transport processes for a long term time series. It simulates the physical movement of water, air boundary conditions, and plant water uptake. This is a 1-dimensional

model for water in unsaturated conditions. It is based on the Darcy–Buckingham equation (VanDam et al., 1990). The model uses soil water retention curve and hydraulic conductivity as input parameters and suction per numerical layer, storage in the growth medium, ET and drainage as output parameters. Metselaar (2012) applied SWAP to determine the effects of growth media properties on water balance, and the influence of growth media properties on vegetation type. The results suggested that growth medium with a strong mineral component could be more sensitive to local conditions.

### ***HYDRUS***

HYDRUS (Šimunek et al, 1994) is the commercial graphical edition of the soil water movement of solutes (SWMS) model, a soil physics model for simulating water, heat, and solute movement in porous media of various dimensions and shapes. SWMS was developed by the Agricultural Research Service in FORTRAN code (Palla et al., 2009). HYDRUS is appropriate for green roofs because it can simulate the infiltration process and predict the variation in soil moisture. The model solves the Richards equation for saturated-unsaturated water flow in well-described porous media, e.g., various soil textures (USDA). The Van Genuchten –Mualem relationship (Van Genuchten, 1980) is applied with Richards equation by determining the unsaturated hydraulic conductivity in terms of soil hydrologic parameters. The model has a minimum temporal resolution of 1 second and flexibility in water flow boundary conditions, which make it suitable for a single facility system (Meng et al., 2014). Multiple studies have successfully simulated the hydrologic performance of green roofs using HYDRUS-1D/2D (Hilten et al., 2017; Ma et al., 2010; Hakimdavar et al., 2014; Palla and Gnecco, 2015). Palla et al. (2009) applied SWMS-2D to a green roof system at the University of Genoa, Italy. The model was calibrated

using eight rainfall events. After the calibration, the model was able to predict the retention and detention performance of the green roof with less than 15% error. The authors found that predicted water content closely matched the observed data at various depths along the vertical profile well. Hilten et al. (2008) simulated volume retention and peak flow of a green roof using HYDRUS-1D. The simulation results were validated by monitored data of the study site. For small events, HYDRUS accurately simulates runoff. For large events, the model tends to over-predict. However, additional large events at the study site are needed to verify the over-prediction.

### **Rain Simulator**

A rain simulator is a device used for study rainfall-runoff scenarios under controlled rainfall intensity. Rain simulators have been widely used in agriculture and environmental studies (Abudi et al., 2012). The advantage of a rainfall simulator is that rainfall can be controlled. The approach is especially applicable for research in arid areas where rainfall is not frequent and data collected under natural rainfall may take a very long period. In addition, the installation of monitoring systems on green roofs is not practical for most roof systems due to the high cost, necessary technical support, and maintenance. Samples of soil in the laboratory rather than *in situ* can be tested for physical properties and related directly to performance. In addition, rain simulators can be applied to test the performance of different growth medium compositions in order to evaluate alternatives for use in green roofs. Several disadvantages of simulator use must also be considered, including: (1) edge effects at the plot boundaries which occur due to the small plot size, (2) less variability in the drop size distribution compared to natural rainfall, (3)

difficulties of mimicking drain conditions, and (4) heavy logistic demands of replicate experiments, such as time, water, and labor (Bowyer-Bower and Burt, 1989).

Studies have applied rain simulators to test green roofs under varied precipitation conditions. Alfredo et al. (2010) simulated both low-intensity and short duration, high-intensity rainfall conditions successfully. They found the green roofs delayed, prolonged, and reduced the peak intensity to 22%-70% of that on a traditional roof surface. They also found that nearly all of the rainfall was discharged over a 24 h period immediately following the experiment.

#### **1.2.1.4 Summary of Green Roof Hydrology**

In general, hydrologic performance of green roofs (retention + detention) improves as rainfall depth, rainfall intensity, initial water content, and roof slope decrease. The effects of the growth medium on retention and detention are a function of its physical properties, such as organic content, particle sizes and pore sizes. The effects of plants on retention and detention vary due to species and root structure. Compared to the overall retention performance of green roofs, there is less understanding of how the age of a green roof affects hydrologic performance due to changes in growth medium characteristics over time. Among the multiple models that have been applied in green roof studies, SWMM is a fast assessment tool, while SWAP, SWMS, and HYDRUS simulate the physical processes of water flow through green roofs. A rain simulator can investigate soil response to various controlled rainfall intensity.

## **1.2.2 Evapotranspiration**

Evapotranspiration (ET) is the combination of evaporation and transpiration (Shuttleworth, 2008). Many factors affect ET, including: weather parameters such as solar radiation, air temperature, relative humidity, and wind speed; soil factors such as soil texture, structure, density, chemistry, and initial soil moisture; and plant factors such as plant type, root depth and foliar density, height, and stage of growth (Pickering et al., 1993). ET is an important process in the water balance in green roofs. ET is also an important term in the soil surface energy balance, due to the large latent heat of vaporization of water (Wadzuk et al., 2013).

### **1.2.2.1 ET Measurement Methods**

Direct and indirect methods have been applied to measure ET. The various methods of determining ET are summarized in Table 1.1. Direct methods use equipment to obtain gas measurements, either CO<sub>2</sub> or water vapor, from the vegetation surface. A common method is to use a chamber to isolate the gas sample. The benefit of the chamber method is that it measures the actual water flux from the transpiring vegetation rather than inferring it from climate parameters. The chamber method is widely used in the agriculture field and the history of applying chambers to evaluate ET can be traced back to the 1930s (Thomas and Hill, 1937). The open chamber method measures ET through the difference of vapor concentration between inlet and outlet points using a big hemispherical chamber (Long et al., 1996). The outlet gas is assumed to have the same water vapor concentration as in the system. This requires long-term measurement, and portability is a limiting factor (Centinari et al., 2009). For the closed chamber method, the objective is to place the chamber over the surface, lower the chamber, rapidly collect the data to determine the changes in water vapor concentration inside the chamber, and then

move the chamber to a new location to repeat the measurement. The assumption is that all sources and sinks of the measured water vapor are from within the system, so leaks need to be controlled by adding an airtight layer at the bottom edges. Clearly, the presence of the closed chamber will have some effects on the ET process, such as uptake or release of water from the chamber walls, reduction in total radiation, enhancement of the proportion of diffuse radiation, blocking of near-surface winds, and increasing air temperature (Reicosky and Peters, 1977; Davidson et al., 2002). But rapid measurements can minimize those effects with only minor impact on ET. Litvak et al. (2014) applied a small enclosed chamber to measure ET of irrigated turfgrass with and without a fan attached. They suggested calibration is important prior to field measurement, due to the relatively large calibration coefficient they found ( $k=4.26$ ).

Table 1.1. Evapotranspiration measurement methods.

			Brief Description	Assumption
Indirect methods	Water balance measurement	Lysimeter	Measure the change in the weight of a sample while measuring precipitation and drainage	Assume the sample is representative
		Soil water balance	Measure the change in the water content of a sample using a water content reflectometer while measuring precipitation and drainage	Assume the soil moisture sensors adequately determine a change in soil water
	Energy-based model	Bowen Ratio	Use the ratio of sensible heat to latent heat derived from the ratio between air temperature and humidity gradients	Assume the turbulent diffusion coefficient for sensible heat and latent heat are the same
		Eddy Correlation	Calculate ET from the correlation coefficient between fluctuations in vertical wind speed and fluctuations in relative humidity above the vegetation	Assume only turbulent transfer of water vapor at sample point
Direct Methods	Components of evaporation	Open chamber	Measure the difference of vapor concentration between inlet and outlet point	Assume the output air has the same water vapor concentration as air which has been fully mixed in the chamber
		Closed chamber	Measure the CO <sub>2</sub> or water vapor change in the chamber for a short time period	Assume all sources and sinks of the measured gases are from within the system

Indirect methods include the use of a water balance or surface energy balance. Those methods calculate ET based on the water flux and energy flux in the vegetation layer and growth medium surface. For the water balance method, ET is estimated from the measured difference between incoming and outgoing water fluxes. A method considered to be indirect involves the use of lysimeters, which are designed to provide continuous data in ET through weight change (Reicosky et al., 1983). However, installation of lysimeters in green roofs is usually impractical due to the high cost, labor, and time-intensive involvement. In addition, the lysimeter method cannot simulate the drainage system of the green roof, and typically the lysimeter retains more water than the unaffected growth medium (Schneider, 2011). The soil water balance has also been applied to full-scale green roofs to estimate ET. This method requires capturing continuous data on precipitation, runoff, and soil moisture change. Berretta et al. (2014) evaluated ET with the soil water balance method for three commercially-available growth media, Heather with Lavender Substrate (HLS), Sedum Carpet Substrate (SCS), and Lightweight Expanded Clay Aggregate (LECA) at the University of Sheffield. The mean values of ET for those three substrates were 0.76, 0.81, and 0.79 mm/day in March, and 1.83, 1.44, and 1.38 mm/day in May. Breña Naranjo et al. (2011) showed that the soil water balance method can provide a reasonable approximation of summer ET with appropriate computational time step. These results were validated by eddy covariance measurement.

#### **1.2.2.2 ET Modeling**

Equations and models have been developed to predict ET from available data, which is referred to as potential ET ( $ET_0$ ). Some studies suggested that the potential ET estimates could be applied to predict the actual ET from green roofs with a crop coefficient that depends on the type of

vegetation (Stovin et al., 2012). The crop coefficient ( $K_c$ ) is a function of the stomatal resistance, the ability of the roots to absorb water, and the leaf coverage and density (Allen et al., 1998). Various potential ET methods exist based on measured climate parameters, such as the Penman-Monteith method (Howell and Evett., 1965; Penman, 2008), the Blaney-Criddle equations (1959), Priestley-Taylor (1972), Turc (1961), Hargreaves (1975), and the Makkink (1957) method. Numerous studies have shown that the Penman-Monteith model is the most accurate method for a range of climatic conditions (Jensen et al., 1990; Chen et al., 2005; Berretta, et al., 2014). The American Society of Civil Engineers (ASCE) introduced a revised Penman-Monteith model to allow for calculation over shorter time steps (Stewart and Howell, 2003). The revised method is more accurate because it uses daily to sub-hourly time steps and vegetation-specific input parameters. It should be noted that the method requires several climatic inputs including solar radiation, air temperature, relative humidity, wind speed, soil heat flux, and actual vapor pressure. The ASCE Penman-Monteith method is widely regarded as the standard method for calculating ET. Schneider (2011) reported that ET calculated with the Penman-Monteith method has a 1.01% difference from lysimeter-measured ET on the Villanova green roof over eight-month study. The default method to estimate ET in SWMM and EnergyPlus (USDOE, 2004) models is the Penman-Monteith model.

Potential ET ( $ET_o$ ) estimated methods, which were developed for agriculture to study the irrigation strategies under certain assumptions. These methods are not always applicable to urban green infrastructure.  $ET_o$  is estimated using the assumptions of a well-watered monoculture crop with a uniform plant height in an idealized climate. However, green roofs are commonly not irrigated, so the assumption of well-watered vegetation is not always true. The difference

between the actual ET ( $ET_a$ ) and  $ET_o$  is a function of whether there is sufficient water in the soil. In non-water-limiting time periods,  $ET_a$  is equal to  $ET_o$  times a crop coefficient.  $ET_a$  decreases as soil water decreases. In water-limiting periods, four models were developed in the literature to estimate  $ET_a$  from  $ET_o$ : soil moisture extraction functions (SMEFs) (Stovin et al., 2013), antecedent precipitation index (API) (Priestley, 1972), advection-aridity (A-A) (Ali and Mawdsley, 1987), and Localized Hargreaves equation (L- Hargreaves) (Allen, 2012). The SMEFs model is based on actual soil moisture and field capacity. In the absence of soil moisture data, the API, A-A and L-Hargreaves models can use precipitation data to estimate  $ET_a$ .

### **1.2.2.3 Summary of ET**

Evapotranspiration is an important factor affecting both hydrologic and thermal performance of green roofs. However, the quantification of ET on green roofs has received limited attention. Because the ET process is difficult to measure directly, models have been developed. Potential ET models have been developed based on measured climate parameters. Various computational software, such as SWMM (USEPA, 2013) and EnergyPlus (USDOE, 2004), apply Penman-Monteith (Penman, 2008) to represent ET for green roofs. However, potential ET models neglect factors that affect the actual ET such as soil moisture availability of growth media. An ET model accounting for soil moisture is required for more accurate prediction of  $ET_a$ .

## **1.2.3 Green Roof Thermal Performance**

### **1.2.3.1 Green Roof Thermal Benefits**

Compared to traditional roofs, green roofs include three additional roof layers, namely vegetation, growth medium, and drainage layer. Thermal benefits of green roofs include saving

energy for space heating and cooling, and mitigating urban heat island effects by cooling the microclimate. Many studies explored the potential energy savings in buildings via green roofs both experimentally and numerically. According to those studies, the reductions of heat loss from the roofs are about 70-90% in summer, and 20-30% in winter (Besir and Cuce, 2018; Getter et al., 2011). However, Niachou et al. (2001) investigated a green roof in Athens and found the largest savings are for winter heating, rather than for summer cooling. This differed from the prevailing thinking that green roofs are predominately regarded as a cooling tool. Another benefit of a green roof is that it can block the solar radiation, thus protecting the base roof membranes from extreme temperature fluctuations. Liu and Baskaran (2003) observed the median daily temperature fluctuation was 6°C for an extensive green roof in Ottawa, Canada from November 2000 to September 2002, compared to 45°C for a traditional roof.

The role of green roofs in providing insulation for buildings has been well reported in the literature. However, green roofs are not always effective insulators. Zhao et al. (2014) suggested that standard commercial insulation diminished the differences in growth medium heat fluxes for different green roof assemblies. Thus, the influence of the growth medium and plants on a green roof energy balance is limited. In winter, a green roof can also shield the roof membrane from extreme cold and from sudden changes in ambient air temperatures.

### **1.2.3.2 Factors affecting Green Roof Thermal Performance**

#### **Plants**

Foliage absorbs a significant proportion of solar radiation through biological functions such as photosynthesis and transpiration. Their shading effects can provide a significant degree of local

sunlight reduction (Kumar and Kaushik, 2005). Foliage height, foliage density, and plant spectral reflectivity are three main factors affecting thermal performance. Foliage height is strongly related to the shading of the growth medium surface and to the transpiration levels. Greater foliage height contributes to increased cooling provided by a green roof (Theodosiou, 2003). Greater foliage height often results in greater shaded area, increasing heat flux through a green roof. In addition, greater foliage increases the aerodynamic displacement height and provides a weaker thermal connection between hot atmospheric air and the air contained within the foliage zone. Thus, not much cool air from the foliage is diffused into the atmosphere, keeping the foliage zone at a lower temperature. Foliage density also affects shading and transpiration from plants. A high foliage density of a green roof can reduce the cooling energy consumption during the summer due to the shading effect, although it can increase the heating consumption in winter by preventing some solar radiation from reaching surface of a green roof (Sailor, 2008). Zhao et al. (2014) compared thermal performance of seven plant species and found that plants with a lower reflectivity resulted in larger values of the net radiation absorbed by the roof. In the Chicago area, *S.tomentosum* is the preferred choice to minimize cooling load in summer.

### **Growth medium**

Several studies suggested that the depth of the growth medium and the water content in the growth medium have significant impacts on thermal performance. The influence of depth of growth medium on thermal performance is based on thermal inertia. A thicker growth medium exhibits a longer time lag and smaller variation of thermal flux. Permpituck and Namprakai (2012) compared the thermal insulation feature of two green roofs with growth medium depths of 10 and 20 cm to a bare roof. They found the heat transfer decreased by 59% and 96%,

respectively, compared to the bare roof. Similar results were obtained by other studies (Coma et al., 2017).

The thermal properties of the growth medium such as thermal conductivity and specific heat capacity can affect heat flow through a green roof. These thermal properties depend on soil composition, dry density, temperature, and water content. Barrio (1998) assessed the summer cooling potential of green roofs in Athens and found that as the density of the media decreased from 1500 to 1100 kg m<sup>-3</sup>, the thermal conductivity also decreased, thus the heat flux through the roof decreased. When a green roof growth medium is saturated, the thermal conductivity and specific heat capacity is higher compared to when it is dry. Niachou et al. (2001) found the change in water content of the growth medium between 30% and 60% alleviates heat storage by 24%. The growth medium with high water content can also enhance heat dissipation due to evapotranspiration in summer. Lazzarin et al. (2005) suggested that when the green roof was wet, not only the thermal gain was cancelled, but a slight outgoing flux was produced.

### **Snow**

Snowpack acts as an insulator, decreasing temperature fluctuations and increasing growth medium temperature. For extensive green roofs, shallow growth media can impair vegetation vigor in extremely cold regions. Alternatively, snow cover can increase plant survival due to warmer growth medium temperature. Snow cover can also reduce the frequency of freeze-thaw cycles, which is essential for the survival of overwintering plants (Boivin et al., 2001). Zhao et al. (2015) evaluated the snow effect on a green roof in Pennsylvania. Compared to a traditional roof, the green roof reduced the building energy consumption for heating by 23% without snow,

but only by 5% with a snow layer. They also found that the snow conductivity depends on the water content in the snow layer. Getter et al. (2011) investigated seasonal heat flux of an extensive green roof in the midwestern U.S. and found temperatures at the top of the insulation layer were more variable with no snow cover than days with snow for both green and traditional roofs.

### **1.2.3.3 Green Roof Thermal Modeling**

Thermal simulation modeling has often been applied to assess the potential thermal benefits of green roofs. Some studies have used numerical models such as DesignBuilder, VISUAL DOE PHPENICS, TRNSYS, and EnergyPlus for energy consumption simulations of green roofs (Ran and Tang, 2017; Zhang et al. 2017; Lazzarin et al. 2005; Foustalieraki et al., 2016). However, in most cases, validation was confined to a short-term period. Moreover, these simulations provide no information on the thermal function of the green roof under various climatic conditions. Model validated with extended long-term monitoring data is needed. In addition, many models are complex. Architects and developers need a user-friendly model to quantify the benefits of green roofs. Sailor (2008) developed a green roof energy balance model to be used with the EnergyPlus model. This model enables users to add a green roof as a retrofit layer on any existing roof. The model takes into account ET effects using the Penman-Monteith model by default. However, the Penman-Monteith model cannot represent actual ET under water limited conditions. The evaporative and conductive heat are a function of the water content in the growth medium. This limitation underscores the importance of considering the thermal capacity and latent heat fluxes associated with moisture transfer when modeling heat flow in green roofs (Feng et al., 2010).

#### **1.2.3.4 Summary of Green Roof energy performance**

Many studies showed that green roofs can reduce a building's surface cooling load in summer. However, few studies have explored a green roof heating load and the influence of snow dynamics on heat flux through the roof in winter. Various models have been developed to simulate heat flow through green roofs. However models need to be validated with long-term monitoring data and observations during summer and winter. Furthermore, it is important to consider the moisture transfer phenomenon in thermal modeling of green roofs, since soil moisture content is an important controller of ET and conductive heat fluxes.

## Chapter 2

---

### **EFFECT of GREEN ROOF AGING ON PHYSICAL PROPERTIES AND HYDROLOGIC PERFORMANCE**

#### **2.1 Introduction**

Growth of cities worldwide has increased the area of impervious land cover. This has reduced the rate at which rainwater can infiltrate the soil, sometimes leading to flooding. In communities with combined sewer systems, the capacity of the wastewater treatment plant can be exceeded during high flow events, and stormwater runoff and sanitary waste may be discharged to rivers, lakes, estuaries, and coastal waters with minimal or no treatment (Bricker et al., 2008). Rainfall events with intensity as low as 3 mm/hr can cause combined sewer overflows (CSOs) (Novotny, 2002).

Grey infrastructure solutions such as storage tanks and piping systems are designed to rapidly move stormwater away from urban neighborhoods. But cost and social issues of this approach to stormwater management may be problematic. Green infrastructure such as rain gardens, bioswales, street trees, and green roofs is becoming a popular alternative. These forms of stormwater control use less manufactured materials and energy, and they take advantage of ecosystem services to process rainwater by promoting infiltration and evapotranspiration.

Changes in hydrologic performance as a green roof ages remain largely unknown due to the scarcity of long-term monitoring records. Yet the physical properties of the growth medium will change due to root development, weathering of media, accumulation and turnover of soil organic

- A shorter version of this Chapter is being submitted to the *Journal of Sustainable Water in the Built Environment*.

matter, and consolidation. Previous studies that relate physical property changes to the aging of green roofs show inconsistent trends (Getter et al., 2007; Emilsson and Rolf, 2004; De-Ville et al., 2017). This study provides new information on the effects of aging on green roof hydrologic performance by investigating a full-scale extensive green roof installed in 2011. This study has the following objectives:

- 1: To characterize the physical properties of virgin and aged green roof growth medium via physical tests.
- 2: To evaluate retention and detention of precipitation inputs based on real-time monitoring data on a green roof over several years.
- 3: To assess the impact of physical changes in growth medium on hydrologic performance using observation data and appropriate modeling tools.

## **2.2 Methods**

### **2.2.1 Study Site and Monitoring System**

The green roof is located on the Onondaga County Nicholas Pirro Convention Center (OnCenter) in Syracuse, NY (43.044 N, 76.148 W). Syracuse is located at the northeast corner of the Finger Lakes region. The local weather features snowy winters (monthly average air temperature: -9°C to 2.4°C, monthly average snow depth: 591 mm) and humid summers (monthly average air temperature: 13°C to 28°C, monthly average precipitation depth: 75.2 mm), in part due to the lake effect from nearby Lake Ontario. Snow falls between November and March, while rain can occur any time of the year (Fig. 2.1) (NOAA, 2018).

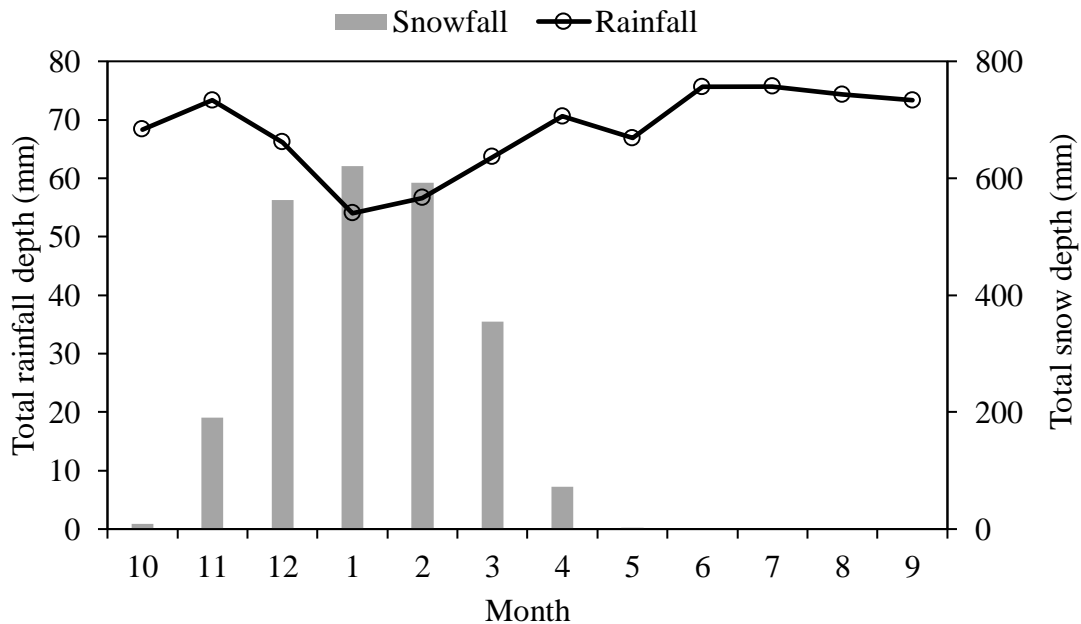


Figure 2.1. Average monthly rainfall depth (rain only) and monthly snow depth recorded at the Syracuse Hancock Airport (1938 - 2018). Snow depth is typically divided by 10 to obtain meltwater depth.

The OnCenter has an extensive green roof with an area of 5550 m<sup>2</sup>. The roof consists of the following layers, starting at the bottom: steel deck, gypsum board, extruded polystyrene insulation, gypsum board, waterproof membrane, drainage mat, and coarse growth medium (18% fines) layer of thickness 7.62 cm. Vegetation species include *Sedum album*, *Sedum sexangulare*, *Sedum rupestre*, *Sedum floriferum*, and *Phedimus taksimense*.

Thirteen roof drains are located on the east side of the roof and twelve on the west side (Fig. 2.2). The roof peak runs approximately north-south for the full length of the roof, midway between the east and west walls, and the roof has a 1% downward slope from the peak to both east and west drains. Triangular drain conduits 5.1 cm high positioned at the bottom of the growth medium convey stormwater from the middle of the roof to each roof drain.

The hydrologic monitoring system is equipped with CR1000 Dataloggers and AM 16/32B Multiplexers (Campbell Scientific). A weather station on the roof measures air temperature, relative humidity, windspeed, and wind direction. A tipping bucket (TE525, Campbell Scientific) measures rainfall. An electromagnetic flow meter (M2000, Badger Meter) indicates runoff from eight drains over the southeast area of the roof. All the sensors are scanned every minute and the data are averaged every five minutes.

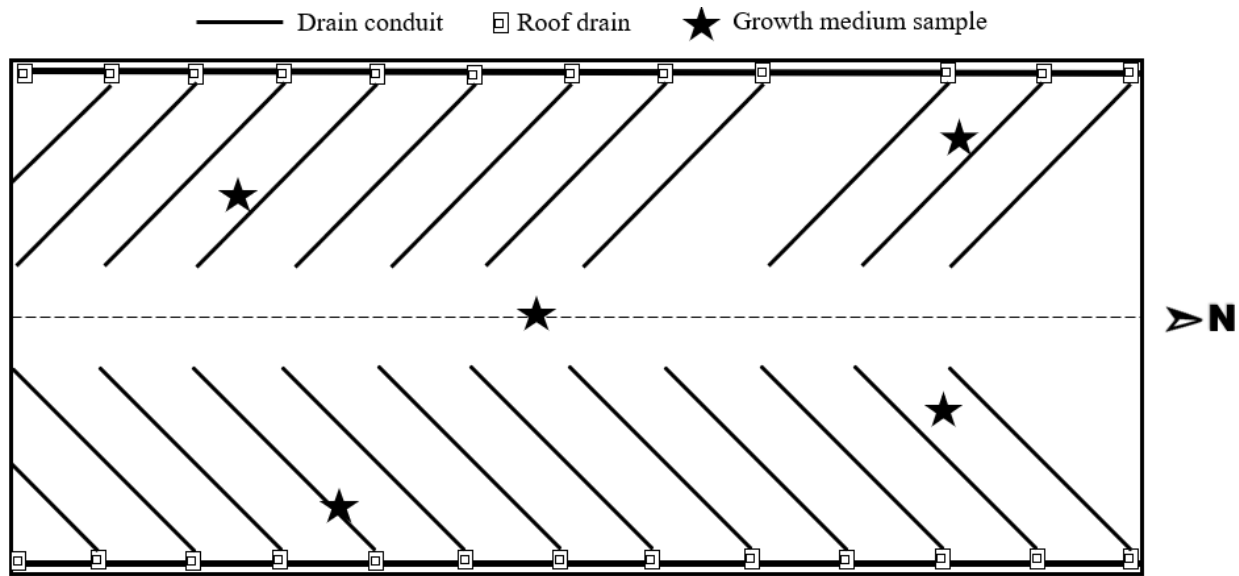


Figure 2.2. Positions of drain conduits, roof drains, and growth medium sample collection locations on the OnCenter green roof.

### 2.2.2 Data Processing and Event Analysis

The monitoring campaign reported here took place over three years (4/20/2015 – 6/30/2018). Data were downloaded using Loggernet software (Campbell Scientific). Statistical analysis has been performed in the open-source software R. The replicated measurements from the lab were applied to run the F-test to determine if the variances of the two populations were equal. A two-sample t-test assuming unequal variances (Welch’s t-test) has been applied to evaluate the

differences between physical properties in virgin and aged growth media. If p value is smaller than Alpha (0.05), the hypothesis of no significant difference in the means of each sample is rejected.

For hydrologic performance analysis, an event-by-event method was applied (Carson et al., 2013; Nawaz et al., 2015; Fioretti et al., 2010). Continuous data were separated into a series of rainfall events. Two event criteria were applied: a) each event was separated by a dry period of at least 6 hours, and b) runoff from a rainfall event must cease before the start of the next event. This approach ensures the values reported are directly comparable to other studies in the literature (e.g., Voyde et al., 2010; Fassman-Beck et al., 2013). After the application of these criteria, 387 events were identified over the three year study period. Then events were evaluated further based on two additional criteria. First, any event that included snow, either in the precipitation or previously accumulated on the roof, was excluded (58 events). Snow days were determined using snow depth measurements by NOAA at the Syracuse Hancock International (NOAA, 2018). Second, any events where total runoff exceeded total rainfall were excluded (31 events). Thus 298 events were analyzed in this study.

### **2.2.3 Extraction and Physical Tests of Growth Media**

Samples of growth medium were analyzed when the green roof was first constructed in 2011, and analyzed again in 2018 using identical test procedures (Penn State University, 2018). The 2018 samples were collected from widely spaced locations across the roof from the full depth of the growth medium and mixed to obtain a composite sample. The tested physical properties include particle size distribution, dry weight density, total porosity, air-filled porosity, hydraulic

conductivity, and organic matter. Two replicated samples for each physical property were tested at the Penn State agricultural lab. Methods used for testing followed the specifications of the FLL guideline for the planning, execution and upkeep of green roof sites (FLL, 2018).

To determine if characteristics of the growth medium would change with depth, samples were collected from five locations of the OnCenter green roof in 2016. At each location, three samples were collected vertically, at one inch intervals (Fig. 2.3). In the lab, a particle size distribution test was performed using the ASTM standard sieve analysis method for each sample with two replicates. All samples were oven dried at 105°C for 24 hours prior to sieving. Bulk density was determined from a sample of a known volume on a dry weight basis with two replicates. To test the organic content, samples were first oven dried under 105°C for 24 hours, and then combusted under 550°C for 2 hours.

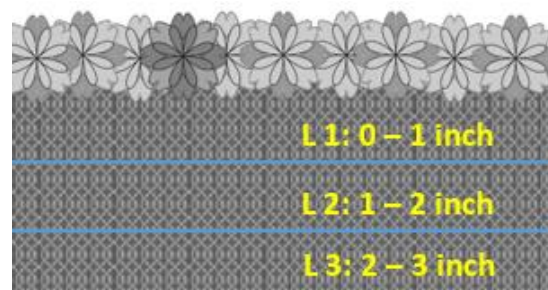


Figure 2.3. Samples collection illustration.

#### **2.2.4 Hydrologic Analysis**

To analyze green roof hydrologic performance, rainfall and runoff characteristics need to be determined by event. Definitions for each characteristic are listed in Table 2.1. For retention performance, retention % is the main parameter in the analysis. For detention performance, peak runoff intensity reduction, peak lag time, and the runoff lag time are three main parameters. The

peak rainfall intensity and peak runoff intensity are expressed in the units of  $\text{mm hr}^{-1}$ , based on 5-minute data collected in the monitoring campaign.

Depth-frequency and peak flow-frequency curves were applied to describe the OnCenter green roof response to storms in 2015 and 2017. The monitoring campaign started from April 2015, however, a few events in 2015 were missed. Most of events during December to March in Syracuse could not be analyzed due to snow. Runoff response is clearly a combination of multiple factors (Starry et al., 2016 ; Carson et al., 2017). Applying frequency analysis considers all factors including antecedent dry weather period (ADWP), meteorological conditions, plant conditions, and rainfall characteristics. Rainfall events were separated into four seasons based on Syracuse historical temperature, rainfall and snowfall records: Spring (March, April, May); Summer (June, July, August); Fall (September, October, November); Winter (December, January, February).

Table 2.1. Definition of the event rainfall and runoff characteristics used for analysis.

	Term	Unit	Description
Rainfall	Rainfall depth	mm	Total rainfall depth over full event
	Peak rainfall intensity	$\text{mm hr}^{-1}$	Highest 5-min rainfall rate over full event
	Rainfall duration	hr	Time between event start and end
	Average rainfall intensity	$\text{mm hr}^{-1}$	Rainfall depth / Rainfall duration
Runoff	Runoff depth	mm	Total runoff depth over full event
	Peak runoff intensity	$\text{mm hr}^{-1}$	Highest 5-min runoff rate over full event
	Runoff duration	hr	Time between runoff start and end
	Average runoff intensity	$\text{mm hr}^{-1}$	Runoff depth / Runoff duration
Retention	Retention	%	$(\text{Rainfall depth} - \text{Runoff depth}) / \text{Rainfall depth} \times 100$
	Peak intensity reduction	%	$(1 - (\text{Peak runoff intensity} / \text{Peak rainfall intensity})) \times 100$
Detention	Peak lag time	hr	Time between peak rainfall and peak runoff
	Runoff lag time	hr	Time between start of rainfall and start of runoff

### 2.2.5 Green Roof Hydrologic Modeling

Retention and detention performances within the virgin and aged growth media were modeled in HYDRUS-1D. Multiple studies have simulated the hydrologic performance of green roofs using HYDRUS-1D/2D successfully (Hilten et al., 2017; Ma et al., 2010; Hakimdavar et al., 2014; Palla and Gnecco, 2015). A description of HYDRUS-1D is given in the literature review (1.2.1.3) with relevant equations given in Appendix A.

The model requires four input parameters to describe the growth medium, namely residual water content ( $\theta_r$ ), saturated water content ( $\theta_s$ ), and independent parameters  $\alpha$  and  $n$ . Saxton and Rawls (2006) developed new soil water characteristic equations from the currently available USDA soil database using only the readily available variables of soil texture and organic content. A graphical computer program was developed to provide equation solutions (USDA, 2009). First, based on the tested soil texture and organic content of the virgin and aged growth media of the OnCenter green roof, two seven-point water retention curves were generated based on this USDA soil water characteristic graphical model. Second, those data points of the water retention curves were analyzed by RETC version 6.02 applying the Van Genuchten-Mualem function to obtain the model inputs (Van Genuchten et al., 1991). Details of the Van Genuchten-Mualem function are described in Appendix A.

The hydrologic performance was determined for five Soil Conservation Service 24-hour design storms, namely a typical small event (rainfall depth of 25.4 mm) and storms with return intervals of 2, 5, 50, and 100 years (SCS, 1992). Data from the New York Department of Environmental Conservation (NYDEC, 2010) for these return times for Syracuse show rainfall depths of 60.25,

88.1, 118.1, and 131.6 mm, respectively. Based on the SCS method, the Syracuse region belongs to a Type II distribution, which was used to obtain rainfall intensities at 0.1 hour intervals over a 24-hour period for each of the five rainfall depths. Initial water content prior to each storm was assumed to be 0.11, which was the average initial soil water moisture content prior to storm events in the study period.

## **2.3 Results and Discussion**

### **2.3.1 Growth Medium Physical Properties**

The physical properties for virgin and aged growth media are shown in Table 2.2. Bulk density and porosity showed significant changes ( $p < 0.05$ ). The organic matter content increased by 60%. There were also changes in the particle size distribution. The mass fraction of particles with diameter  $< 0.05$  mm increased by around 40%. Furthermore, the mass median diameter decreased from about 4 mm to 3 mm (Fig. 2.4). But the change in mass fraction of particles with diameter  $< 2$  mm was not small, as both 2011 and 2018 data showed values around 31%. The overall fraction of silt (0.002 mm to 0.05 mm) plus clay ( $< 0.002$  mm) increased relative to the fraction of sand ( $> 0.05$  mm) in the growth medium. Weathering and root growth are believed to be at least partly responsible for the decrease in particle sizes (De-Ville et al., 2015). The shift to smaller sizes suggests that these factors are probably more important than the loss of small particles transported by infiltrating rainwater (Schwager and Schaal, 2015), which would tend to increase the average particle size.

The OnCenter findings are somewhat consistent with one aging study reported by De-Ville et al. (2017). They found a large reduction in mass median diameter in growth medium particles over

a five-year period, from 2.53 mm to 0.42 mm. However, the OnCenter findings are contrary to one study reported by Bouzouidja et al. (2018). They reported that the fraction of particles with diameter < 2 mm in pozzolana-based growth medium decreased from 18.2% to 12.5% over four years. These inconsistencies among studies suggest a lack of understanding of variability in the effects of aging on different growth media.

Table 2.2. Physical properties of the OnCenter growth medium.

	*Bulk Density	*Porosity	Air-filled Porosity	Particle diameter <0.05mm	Soil moisture	Saturated Hydraulic Conductivity	Organic matter Content	Maximum water holding Capacity
Unit	(g/cm <sup>3</sup> )	(Vol %)	(Vol %)	(%)	(mass %)	(cm/s)	(%)	(Vol %)
2011	0.79	51.2	12.6	5.9	11.9	0.02	2.7	38.6
2018	0.89	55.1	9.3	8.4	16.1	0.02	4.3	45.9

\*An asterisk means the difference is statistically significant in the t-test. No replicates were tested for the organic matter content, and consequently statistical tests cannot be performed.

Bulk density is an indicator of soil compaction, and usually there is a negative correlation between bulk density and organic matter content. Organic matter acts as a filler to prevent the mineral portion of the soil from binding tightly and provides a matrix that can rebound when there is compression (DeVecchia et al., 2014). However, in this study, the bulk density increased with an increase of organic matter content. Weathering and degradation of organic matter in the roof growth substrate and gravitational transport of that material has filled larger pores in the roof substrate. This sedimentation process has thereby increased the bulk density of the roof substrate, especially near the roof surface. This process may also incorporate dust flux from the urban setting of the site and will likely continue to densify unless there is sufficient biotic turbidation or root decay to provide endogenous structure to the soil mat. The growth medium changed from a relatively homogeneous layer to a system where characteristics varied with depth with time. Data from a separate study conducted on the roof in 2016 showed that density averaged 0.83 g/cm<sup>3</sup> in the top third of the growth medium, 0.92 g/cm<sup>3</sup> in the middle

third, and 0.99 g/cm<sup>3</sup> in the bottom third. Although based on only one set of samples from three locations on roof, the results suggest that the density has changed as the roof ages. Furthermore, tests of the organic content of the three layers showed that the surface layer had almost twice as much organic matter compared to the middle and bottom layers (top: 9.9%, middle: 4.5%, bottom: 4.3%). Organic matter has a charged surface that attracts water, and under this condition, water adheres to the particle surface, which would increase the water holding capacity of the top layer. Hudson (1994) demonstrated that soils high in organic content had significantly greater water holding capacity than soils of similar texture that contained less organic matter. For example, a silt loam soil with 4% organic matter held more than twice the water of a silt loam containing 1% organic matter. The increase in organic content in Table 2.2 is thus consistent with the increase in maximum water holding capacity. The increase in organic content is also consistent with the shift to smaller particle sizes, as organic matter is associated with fine particles (Yio et al., 2013).

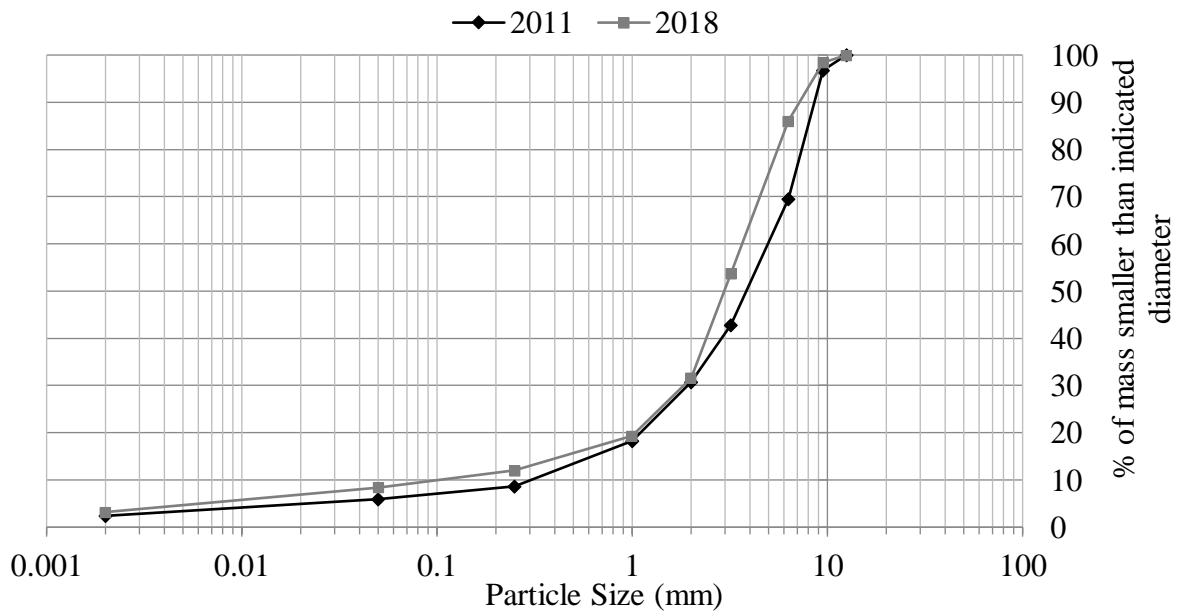


Figure 2.4. Particle size distributions for the virgin and aged growth medium.

A significant increase in porosity was observed from 2011 to 2018 ( $p < 0.05$ ). Root growth can reduce pore volumes due to local compression and pore filling (Dexter, 1987), thereby reducing hydraulic conductivity. On the other hand the decay of dead roots results in channels which may increase pore volume and create flow paths, increasing hydraulic conductivity (Schwen et al., 2011). Air-filled porosity indicates the volume percentage of macropores (pore diameter  $> 50 \mu\text{m}$ ). Moisture can only be held against gravity inside micropores or water-filled pores.

Micropores control water movement and retention in soils and determine the amount of water stored in the soil for plant use (Arshad et al., 1996). Although porosity overall increased, air-filled porosity showed a decline, indicating an increase in water-filled porosity (Fig. 2.5). Thus, more water can be stored in the growth medium, which indicates a greater maximum water holding capacity and better retention performance. The observed 7% increase in maximum water holding capacity in Table 2.2 is consistent with this understanding, and with other published results (Getter et al., 2007; De-Ville et al., 2017).

The saturated hydraulic conductivity ( $K_{\text{sat}}$ ) did not change between 2011 and 2018. The value of 0.02 cm/s for  $K_{\text{sat}}$  satisfies the German FLL standard (FLL, 2008). According to this widely accepted German standard, the minimum  $K_{\text{sat}}$  for extensive green roofs is 0.001 cm/s. We anticipated a decrease in  $K_{\text{sat}}$ , given the increase in water-filled porosity for the aged growth medium. The lack of change in  $K_{\text{sat}}$  is not surprising as other factors could govern hydraulic conductivity, including cracks, root holes, worm holes, and stability of soil crumbs (Kirkham, 2004).

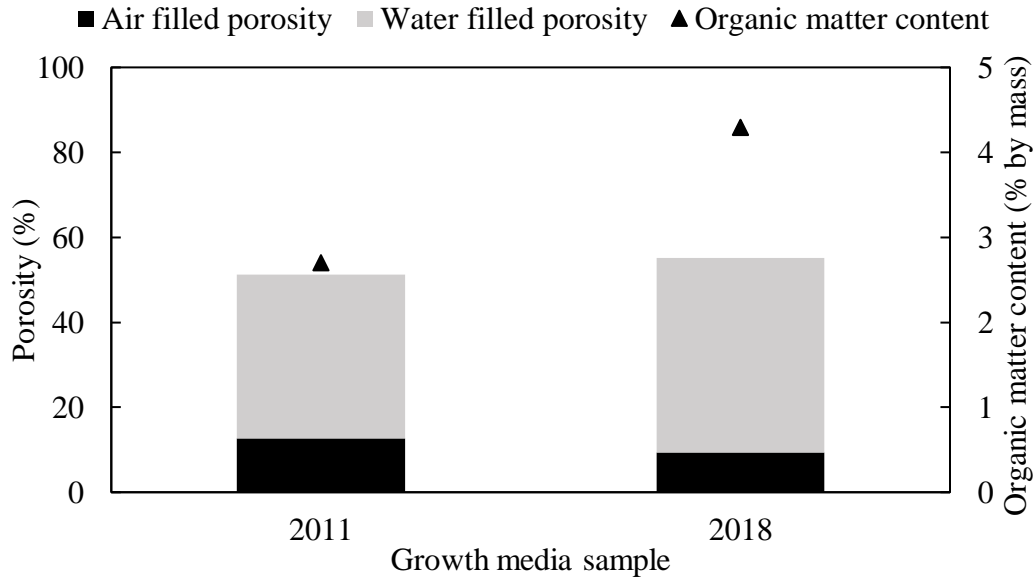


Figure 2.5. Data for air-filled and water-filled porosity and for organic matter content in virgin (2011) and aged (2018) growth medium.

## 2.3.2 Green Roof Hydrologic Performance

### 2.3.2.1 Weather and Rainfall Profiles

The yearly total rainfall and runoff collected at the OnCenter for the monitoring period (April 2015 – July 2018) is shown in Figure 2.6. Years 2015 and 2017 shared a similar rainfall pattern with an annual rainfall at the OnCenter of about 780 mm. The year 2016 was relatively dry, with around 400 mm rainfall depth. Data were not available for the full year in 2018. Overall, data from 2015 and 2017 were selected to assess the aging effect on the green roof hydrologic performance due to data comparability and availability.

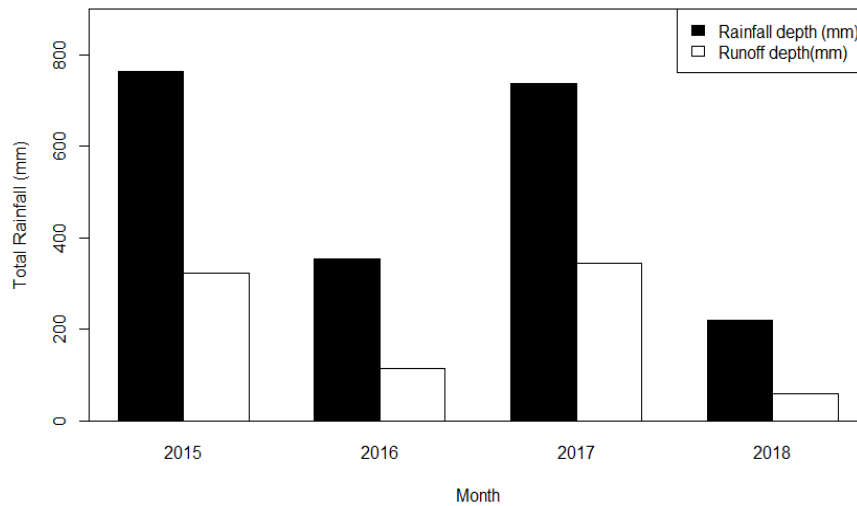


Figure 2.6. Monitored annual Rainfall and runoff data for 2015 – 2018.

### 2.3.2.2 Retention

The 298 rain events in this study had a total rainfall depth of 1844 mm. These events ranged from brief showers (event 66, rainfall depth: 0.3 mm, duration: 0.4 hr) to lengthy, intense storms (event 280, rainfall depth: 90.5 mm, duration: 70 hr). A total of 198 events had 100% retention. Based on the roof area of 5550 m<sup>2</sup>, the green roof retained 6400 m<sup>3</sup> water over roughly 26 months of rainfall for the three-year monitoring period, excluding times of snow. The fraction of retention was computed as the difference between total rainfall and total runoff divided by total rainfall, which was 62% over the monitored period. Retention for individual storms ranged from 14% to 100%. These values aligned with retention values in other studies with similar growth medium depth. Liu and Minor (2005) reported a 57% retention for a green roof with 100 mm depth growth medium in Toronto. Carson et al. (2013) reported the mean retention for three green roofs in New York City as 36%, 47%, and 61%. These sites are in the same climatic zone as Syracuse. The 96.8% retention for the green roof on the Center of Excellence in

Environmental and Energy Systems in Syracuse (Carpenter et al., 2016; Todorov et al., 2018), may be due to the specially designed large storage volume available below the growth medium.

Retention by season for 2015 and 2017 is shown in Table 2.3. The climatic patterns varied among seasons and years. Syracuse experienced greater precipitation during summer and winter in 2015 than in 2017, by a factor of two in summer and a factor of five in winter. In summer, a high retention is expected due to the high rates of evapotranspiration, not considering other factors. This was the case in 2017, but not in 2015. It appeared the higher total rainfall and larger number of events might have contributed to the poor retention in summer 2015. Retention values in spring and fall 2015 were higher than those in 2017 despite a similar number of events, rainfall depth and mean duration. This pattern suggested that the retention response could depend on many factors not accounted for in this table, such as the timing of rain events, evapotranspiration rates, rain intensity, and cloud cover.

Table 2.3. Retention by season for the OnCenter green roof.

	2015				2017			
	# of events	Rainfall depth (mm)	Duration (hr)	Retention %	# of events	Rainfall depth (mm)	Duration (hr)	Retention %
Spring	13	124	11.5	70.7	14	113	10.2	39.9
Summer	37	307	6.7	60.9	29	151	5.5	89.4
Fall	34	222	7.2	57.1	36	292	10.5	43.7
Winter	7	53.3	13	56.9	7	10.5	2.7	99.2
Total	91	707	8.4	60.3	86	566	8.1	56.2

The depth frequency curves for rainfall and runoff in 2015 and 2017 are shown in Fig. 2.7. The curves for rainfall showed very similar patterns for the two years up to 20 mm, yet the curves for runoff suggested that the probability of exceeding a given runoff value was greater in 2015 than in 2017, meaning more retention capacity in 2017 than 2015. For example, the exceedance

probability of 2 mm runoff depth was around 25% in 2015, while it was 17% in 2017. It was observed for small (0-2 mm), medium (2-10 mm), and large events (10-20 mm) that the aged green roof had a smaller exceedance probability, except in extreme events. In extreme events, where rainfall depth was larger than 20 mm, there was no clear pattern. Overall, the aged green roof provided better retention performance. Although many factors can affect retention performance, the similarity in depth frequency curves for rainfall for 2015 and 2017 suggested that the changes in physical properties of the growth medium shown in Table 2.2 might have provided improved retention performance as the growth medium continued to age between 2015 and 2017.

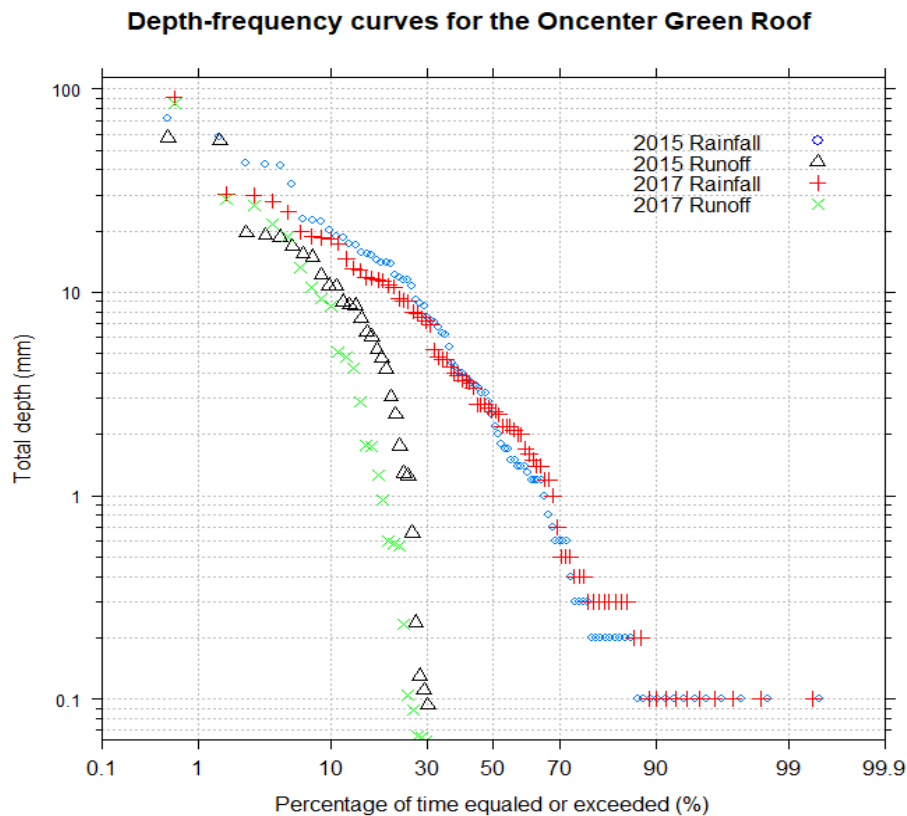


Figure 2.7. Depth-frequency curves for 2015 and 2017 from the monitoring data.

### 2.3.2.3 Detention

A well-designed green roof can reduce the peak intensity and delay the occurrence of runoff. Peak lag time (hr), runoff lag time (hr) and peak intensity reduction (%) are the three parameters used for the assessment of detention performance in this study. No runoff occurred in 198 out of 298 events in the monitoring period. In the events with runoff, the runoff was initiated around 3.6 hours (SD = 4.0 hours) after the beginning of rainfall for the study period of three years. Similarly, the peak in runoff occurred roughly three hours after the peak in rainfall. The maximum peak rain intensity was 90 mm/hr (event 179, 9/18/2016), and the maximum peak runoff intensity was 39 mm/hr (event 30, 6/30/2015), both 5-minute averages. The reduction in peak intensity for individual events ranged from 23% to 99%, with a mean value of 79%. Marasco (2014) assessed the detention performance of four green roofs in New York City, and reported the 5-minute mean peak reduction values were between 81% and 85%. But the runoff lag time ranged from 0.75 to 2 hours over these green roofs, which was shorter than the OnCenter green roof (3.6 hours on average). The roof configuration (e.g. size, slope, plants, non-vegetated areas, flow paths) influences the lag time, which may differ between the roofs in NYC and OnCenter (Marasco, 2014). The comparison of detention parameters in 2015 and 2017 are shown in Table 2.4. The year 2017 had a shorter peak lag time but a higher peak intensity reduction. The runoff lag time was about the same in both years.

Table 2.4. Green roof average rainfall detention statistics.

	2015		2017	
	Mean	Standard Deviation	Mean	Standard Deviation
# storm event	91	/	86	/
# with runoff	32	/	30	/
Peak lag time (hr)	3.2	5.5	1.4	4.3
Runoff lag time (hr)	3.4	3.1	3.5	4.4
Peak intensity reduction (%)	70.9	17.9	81.1	23.5

To compare the detention performance, peak flow frequency curves were developed for 2015 and 2017 (Fig. 2.8). Peak rainfall intensity for these years shared a similar pattern up to 40 mm/hr. For a given storm event, there was around 8% probability that the peak rainfall intensity exceeds 40 mm/hr in both 2015 and 2017. However, runoff peak intensity in 2017 was more likely to be smaller than in 2015. For example, for a given storm event, the exceedance probability of 3 mm/hr was 11% for 2017, and 20% for 2015. Overall, the aged green roof provided greater peak intensity reduction.

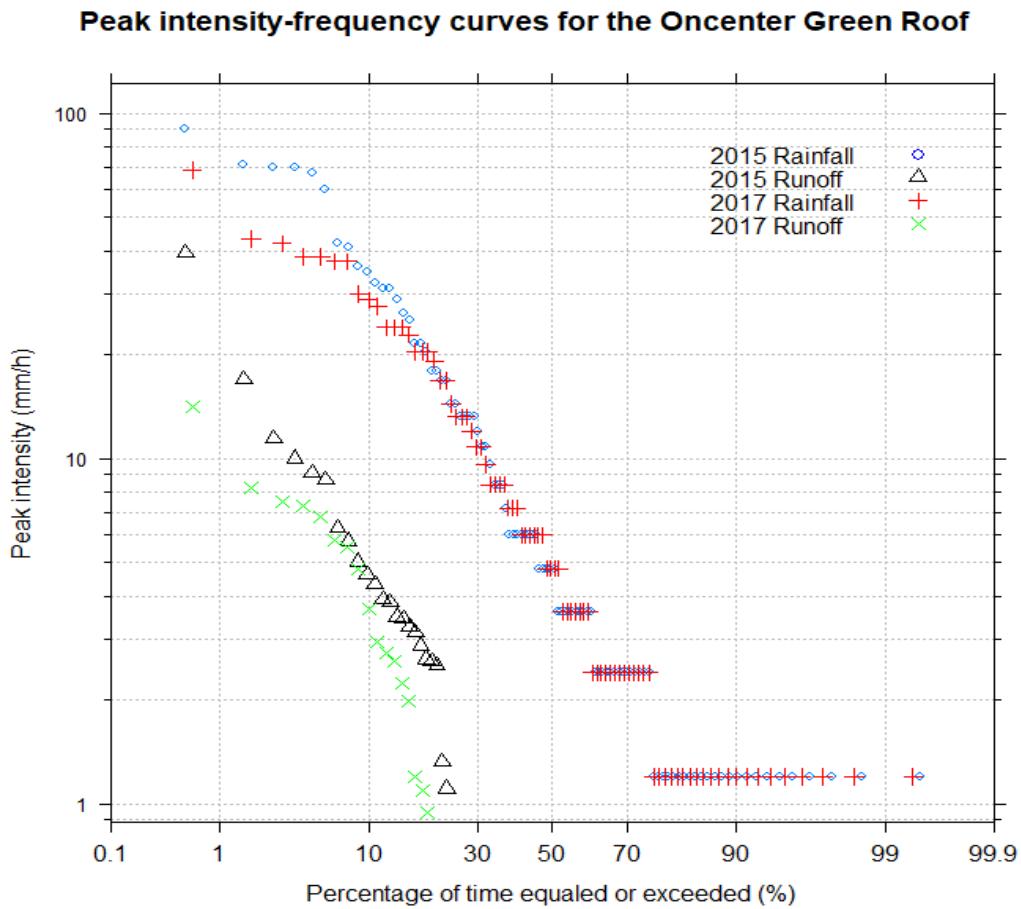


Figure 2.8. Peak intensity-frequency curves for 2015 and 2017 from the monitoring data.

### 2.3.3 Green Roof Hydrological modeling

The estimated residual water content ( $\theta_r$ ), saturated water content ( $\theta_s$ ), scaling parameter ( $\alpha$ ) and shape parameter ( $n$ ) are shown in Table 2.5. Those four parameters of the growth medium serve as the inputs for HYDRUS-1D simulation. The independent parameters  $\alpha$  and  $n$  obtained for the growth medium of the OnCenter green roof are in line with those found in other green roof studies. Palla et al. (2009) considered the growth medium of a green roof in Genoa, Italy as sandy loam ( $\alpha = 0.075 \text{ cm}^{-1}$ ,  $n = 1.89$ ) for a SWMS-2D simulation and validated this model using monitored data. Hilten et al. (2017) estimated the growth medium of a green roof in Georgia as sand ( $\alpha = 0.145 \text{ cm}^{-1}$ ,  $n = 2.68$ ) for HYDRUS-1D simulation. Metselaar (2012) applied ( $\alpha = 0.0103\text{-}0.0596 \text{ cm}^{-1}$ ,  $n = 1.320\text{-}2.167$ ) from the literature for the growth medium of a green roof in Netherlands for SWAP simulation. Li and Babcock (2015) measured the water retention curves for five growth media cores and found the values ( $\alpha = 0.25\text{-}0.47 \text{ cm}^{-1}$ ,  $n = 1.66\text{-}2.44$ ). In all those studies, Parameters  $\alpha$  and  $n$  were calibrated through monitored data.

Table 2.5. Growth medium retention curve fitting statistics for 2011 and 2018 soil (RETC).

	Variable	Value	S.E.Coeff	T-Value	Lower	Upper
2011	ThetaR	0.0324	0.0161	2.01	-0.0188	0.0836
	ThetaS	0.455	0.0017	268	0.45	0.460
	$\alpha$	0.0647	0.0614	1.05	-0.131	0.260
	$n$	1.26	0.0661	19	1.05	1.469
2018	ThetaR	0.01	0.0103	0.98	-0.023	0.043
	ThetaS	0.49	0.0006	864	0.49	0.494
	$\alpha$	0.064	0.016	3.92	0.012	0.115
	$n$	1.185	0.016	75.3	1.14	1.24

The maximum water holding capacity increased from 38.6% in 2011 to 45.9% in 2018 (Table 2.2). In the simulated rainfall-runoff results, an improvement in retention performance was

observed (Table 2.6). The retention performance in 2018 improved compared to 2011 from 25% to 3% for the design storms with an average of 8%.

Table 2.6. Retention and detention performance for the virgin and aged growth media.

	Year	Rainfall depth (mm)	Runoff depth (mm)	Retention (%)	Runoff lag time (hour)	Peak lag time (hour)	Peak reduction (%)
Small event	2011	25.4	12.4	51.3	12.5	1.1	92.5
	2018	25.4	5.9	76.8	13.8	3.5	97.6
2 year	2011	60.5	47.1	22.2	11.8	0	24.6
	2018	60.5	42.4	29.9	11.9	0.1	27.0
10 year	2011	88.1	74.6	15.4	10.5	0.0	5.5
	2018	88.1	69.7	20.9	11.5	0.0	3.1
50 year	2011	118.1	104.5	11.5	9.0	0.0	3.3
	2018	118.1	99.8	15.5	10.4	0.0	1.6
100 year	2011	131.6	117.5	10.7	6.3	0.0	2.7
	2018	131.6	113.3	13.9	9.9	0.0	1.2

Hydrographs of five design storms are shown in Appendix B. The difference in detention performance was small compared to retention performance between the two modeled years. An hour runoff lag time was observed in most design storms. However, for the 100-year storm, runoff in the virgin growth medium started 6.3 hours after the start of rainfall, which is a short time relative to the start of runoff in the aged growth medium, which occurred 9.9 hours after the start of rainfall. The relatively short time to onset runoff in the virgin growth medium may be due to the combination of high air-filled porosity in the growth medium and the action of an intense storm. High intensity storms can stimulate saturated flow conditions to occur near the surface, inducing gravitational fluxes. When gravity dominates, water can flow out of the growth medium through macropores (Weil and Brady, 2017). The relative high fraction of macropores in the virgin growth medium can result in a small runoff lag time. For peak lag time, peak runoff occurred immediately after peak rainfall for both virgin and aged growth media. The aged

growth medium exhibited a greater peak intensity reduction in small events. However, for events larger than the 10-year design storm, the aged growth medium exhibited a smaller peak intensity reduction. This is possibly because under the extreme peak rain intensity, aged growth medium with a smaller fraction of macropores, where water can flow through, exhibited a higher peak runoff intensity (Poë, 2016).

## **2.4 Conclusions**

In this study, the aging of growth medium of a 0.56 ha green roof was examined, using both measurements and computer modeling, to assess changes in hydrologic performance. Over seven years, the particle size distribution showed a decrease in the particle mass median diameter from 4  $\mu\text{m}$  to 3  $\mu\text{m}$ , as well as shifts in the overall distribution toward smaller particles. These changes are attributed to root growth and weathering. In addition, the organic content of the growth medium increased from 2.7% to 4.3%, consistent with the reduction in particle size. The aged growth medium showed an increase in water-filled pores smaller than 50  $\mu\text{m}$  (micropores) and an increase in the maximum water holding capacity from 38.6% to 45.9%. The hydraulic conductivity remained constant for both virgin and aged growth medium.

The changes in the growth medium are consistent with the hydrologic data, comparing 2015 and 2017. Meteorological data were somewhat similar in 2015 and 2017, permitting comparisons of overall rainfall and runoff quantities and also peak intensities of rainfall and runoff. Depth frequency curves of total rainfall showed that the curves for 2015 and 2017 were very similar, with little difference in the exceedance probability associated with any given rainfall depth except for extreme events. However, the exceedance probability of runoff depth was greater in

2015 than in 2017 for most runoff depths except extreme events. For example, the exceedance probability of 2 mm runoff depth was 25% in 2015, but only 17% in 2017.

The curves for exceedance probability of peak rainfall intensity for 2015 and 2017 were also similar except for extreme events. Yet the curves for peak runoff intensity showed probabilities of exceedance for most values that were greater in 2015 than in 2017 demonstrating that the growth medium was more effective in storing water in 2017 than two years earlier.

Simulations with HYDRUS-1D showed an average of 8% increase in retention for the five design storms. The simulated detention performance also showed improvement with age, longer runoff lag time and an identical peak lag time from the aged growth medium for large rainfall events. For an extreme event with 100-year return period, the virgin growth medium onsets runoff three hours before the aged growth medium. The peak intensity reduction of the aged growth medium is smaller than that of the virgin growth medium for large events (return period >10 years).

While physical property differences are observed between the virgin and aged growth medium, it is assumed that those differences are due to aging. However, growth medium heterogeneity may have contributed to the differences between the virgin and older samples. In addition, shipment of growth medium samples to the testing lab may have disturbed the physical characteristics.

## **2.5 Practical Implications**

Few studies have focused on aging effects of green roofs. Previous studies use various methods for testing the physical properties of growth media such as XMT and physically-derived tests. Different standards and methods are applied to measure porosity, hydraulic conductivity and other properties. In this study, improvement in the hydrologic performance was predicted over a 7-year period. However, the improvement is small when compared to weather and seasonal patterns. Standard methods should be established for investigating aging effects on green roofs.

## Chapter 3

---

### QUANTIFYING EVAPOTRANSPIRATION ON A GREEN ROOF: A COMPARISON OF SOIL WATER BALANCE METHOD WITH COMMONLY USED PREDICTIVE METHODS

#### 3.1 Introduction

Green roofs have become popular in recent years because they can mitigate several problems associated with urbanization. Research on hydrologic benefits has focused on green roof volume retention performance and to a lesser extent volume detention performance (Viola et al., 2017). However, only limited studies have considered green roof evapotranspiration (ET) performance and soil moisture storage behavior between storm events.

ET quantifies the loss of water to the atmosphere through the combined processes of evaporation (from soil and plant surfaces) and transpiration (from plant tissues) (Shuttleworth, 2008).

A summary of green roof ET studies is shown in Table 3.1. Several methods have been used to estimate ET, for example, the soil water balance, the lysimeter method, the energy balance, and chamber studies. Each of these methods has specific advantages and disadvantages; in this paper, the soil water balance and the energy balance methods were used.

Table 3.1. Previously reported ET measurement from green roofs.

Author	Location	Setup type	Study period	Growth medium depth (cm)	Irrigated	Measurement method	ET (mm day <sup>-1</sup> )
Berretta et al. (2014)	Sheffield, UK	Full-scale	4/2010 - 9/2013	8	No	Soil water balance method	HLS: 1.83 (warmer period), 0.76 (cooler period)
							SCS: 1.44 (warmer period), 0.81 (cooler period)
							LECA: 1.39 (warmer period), 0.79 (cooler period)
Stefferdud (2016)	Trondheim, Norway	Full-scale	8/2015-4/2016	5	No	Soil water balance method	0.6 (spring), 1 (summer)
DiGiovanni et al. (2013)	Bronx, NY, USA	Test-box	6/2009-6/2010	10	No	Weighing lysimeter	1.92 (annual average)
Sherrard and Jacobs (2011)	Durham, NH, USA	Test-box	8/2009-11/30/2009	10	No	Weighing lysimeter	1.24 (Aug), 0.91 (Sep), 0.75 (Oct), 0.52 (Nov)
Feng et al. (2018)	Salt Lake City, UT, USA	Test-box	Calendar year 2014	30.5-45.7	Yes	Weighing lysimeter	Annual average: 2.01 (non-vegetated), 2.52 (sedum), 2.69 (grass covered)
Berghage et al. (2007)	University Park, PA, USA	Greenhouse	2000-2003	10	Yes	Weighing lysimeter	1.9 (2 days after saturation), 0.4 (10 days after saturation)
Wadzuk et al. (2013)	Phila, PA, USA	Test-box	April-November of 2009 and 2010	10	No	Weighing lysimeter	2.9 (annual average)
Poë et al. (2015)	Sheffield, UK	Lab setup	4/7/2011-8/25/2011	8	No	Weighing lysimeter	0.6-1 (spring), 0.7-1.25 (summer)
Voyde et al. (2010)	Auckland, New Zealand	Greenhouse	4/28-5/26; 6/17-7/25 (2008)	7	Yes	Weighing lysimeter	1.9-2.2 (unstressed water condition); 0.2-2.1 (stressed water condition)
Cirkel et al. (2018)	Amsterdam, Netherlands	Test-box	4/2017 – 8/2017	4	Yes	Weighing lysimeter	3 (summer), 4 (spring)
Marasco et al. (2014)	W118, Manhattan, NY, USA	Full-scale	7/2009-12/2009	3.2	No	Dynamic chamber	4.8 (7/2009); 0.24 (12/2009)
	USPS, Manhattan, NY, USA	Full-scale	4/2012-10/2013	10			4.9 (7/2012) 0.72 (12/2012)
Coutts et al. (2013)	Melbourne, Australia	Test-box	10/2011-2/2012	1.5	Yes	Closed-chamber	0.7-7.8 (four clear sunny days)
Lazzarin et al. (2005)	Vicenza, Italy	Full-scale	Summer of 2002 and 2003; winter of 2004	20	No	computed as a residual term in the energy balance	0.69-6.9 with an average value of 1.6

\*HLS is Heather with Lavender Substrate; SCS is Sedum Carpet Substrate; LECA is Lightweight Expanded Clay Aggregate.

The overall goal of this study is to quantify the ET performance of a large extensive green roof over two-year period. There are four specific objectives: (1) to quantify ET on the 0.56 ha Onondaga County Convention Center (“OnCenter”) green roof in Syracuse, NY using the soil water balance method; (2) to evaluate the dominant factors that affect ET behaviors in water-limited and non-water limited time periods; (3) to use estimates of ET from the soil water balance method to assess the utility of several models for estimating ET on the OnCenter green roof; and (4) to modify existing models to arrive at a set of models that can be used when only limited input data are available to estimate ET on other green roofs in this region. The study results are expected to improve our understanding of ET behaviors and improve ET modeling for green roofs in Northeastern US and elsewhere.

## **3.2 Methods**

### **3.2.1 Study Site and Instrumentations**

This study extends work on the thermal properties of the OnCenter green roof (Squier and Davidson, 2016) to consider water storage and ET. The experimental period is 05/01/2015 to 12/31/2017 excluding times of snow and covers a range of weather and seasonal variation. Soil moisture sensors (CS616 Water Content Reflectometers, Campbell Scientific) were installed at four locations in the growth medium at roughly the midpoint of the depth. An LI200X pyranometer (Campbell Scientific) with silicon photovoltaic detector was deployed to provide global solar radiation measurements. Temperature sensors (Model 109 Temperature Probe, Campbell Scientific) were installed in different roof layers from the growth medium down to the steel deck to provide profiles at five locations (Squier and Davidson, 2016; Yang and Davidson, 2018). Ambient temperature and relative humidity were recorded using a Vaisala

Temperature/RH probe (HMP155A, Campbell Scientific). An RM Young model 03-102 cup anemometer/wind vane assembly was applied to measure wind speed and wind direction. The overall thermal conductivity was measured using a Decagon KD2 Pro Thermal Properties Analyzer.

### **3.2.2 ET Estimates**

It is important to define two terms before discussing the ET measurement methods, namely the “actual ET” or  $ET_a$ , and the “potential ET” or  $ET_o$ . Actual ET is defined as the measured amount of water that leaves a surface due to climatological demand and soil water availability, and is a combination of surface, subsurface, plant, and meteorological conditions (Wadzuk et al., 2013).

Potential ET is defined as the ET from actively growing short green vegetation, completely shading the ground and with sufficient water (Witmer and Brownson, 2011). The concept of potential ET was developed to estimate ET from agricultural crops; when there is sufficient water in the soil,  $ET_a$  can be estimated as  $ET_o$  multiplied by a crop coefficient  $K_c$ .  $K_c$  is a function of the stomatal resistance, the ability of the roots to absorb water, and the leaf coverage and density (Allen et al., 1998). The Penman-Monteith method is widely regarded as the standard method for calculating  $ET_o$  (Jensen et al., 1990; Penman, 2008). The American Society of Civil Engineers (ASCE) has introduced a revised Penman-Monteith model to calculate ET for short time periods. This revision adds the aerodynamic resistance and surface resistance factors (Stewart and Howell, 2003). But the method requires numerous meteorological measurements including solar radiation, air temperature, relative humidity, wind speed, soil heat flux, and water vapor pressure in hourly or daily time steps. Those data are not always available. As a result,

various simplified models that require less weather parameter input have been developed, such as the following methods: Blaney-Criddle (1959), Priestley-Taylor (1972), Turc (1961), Hargreaves (1975), and Makkink (1957). Gao et al. (2017) reported that the Turc method was the best of several models in a cold humid climate, while the Hargreaves equation performed best under a semi-arid condition. The various methods of determining potential ET are summarized in Table 3.2.

Table 3.2. Potential ET estimate models.

Category	Name	Equation	Eq.
<b>Penman</b>	ASCE standardized Penman-Monteith model (1998)	$ET_o = \frac{0.408\Delta(R_n - G) + \gamma \left( \frac{C_n}{T_{mean} + 273} \right) u_2 (e_s - e_a)}{\Delta + \gamma(1 + C_d u_2)}$ $C_n = 900 \text{ } ^\circ\text{C mm s}^3 \text{ Mg}^{-1} \text{ d}^{-1}; C_d = 0.34 \text{ s m}^{-1}$ for reference crop with height of 0.12 m, a fixed surface resistance of 70 s m <sup>-1</sup> , and an albedo of 0.23	3.1
	Schendel (1967)	$ET_o = 16 \frac{T_{mean}}{RH}$	3.2
<b>Simplified combined method</b>	Turc (1961)	$ET_o = a \frac{T_{mean}}{T_{mean} + 15} (R_s + b) \text{ (RH} \geq 50\%)$ $ET_o = \left( 1 + \frac{50 - RH}{70} \right) a \frac{T_{mean}}{T_{mean} + 15} (R_s + b) \text{ (RH} \leq 50\%)$ $a = 0.31 \text{ (m}^2\text{MJ}^{-1} \text{ mm}^{-1}), b = 2.094 \text{ (MJ m}^{-2}\text{day}^{-1})$	3.3
	Valiantzas (2013)	$ET_o = 0.00668 R_a \left( (T_{mean} + 9.5)(T_{max} - T_{min}) \right)^{0.5} - 0.06$ $* \left( (T_{max} - T_{min}) - 0.024 \right)$ $* (T_{mean} + 20) * \frac{1 - RH}{100}$ $- 0.00455 * R_a * (T_{max} - T_{dew})^{0.5}$ $+ 0.0984 * (T_{mean} + 17) * (1.03 + 0.00055 * (T_{max} - T_{min})^2 - RH/100)$ <p>The dew temperature (<math>T_{dew}</math>) was estimated by Allen et al. (1998)</p>	3.4
		$T_{dew} = \frac{116.91 + 237.3 \ln(e_a)}{16.78 - \ln(e_a)}$	3.5

Table 3.2 (continued)

Category	Name	Equation	Eq.
<b>Temperature-based method</b>	Blaney-Criddle (1959)	$ET_o = p(0.46T_{mean} + 8)$ $p = \text{fraction of daylight hours}$	3.6
	Original Hargreaves (1975)	$ET_o = 0.0135 \times 0.408R_a \times (T_{mean} + 17.8)$	3.7
	Hargreaves and Samani (1985)	$ET_o = 0.0135 \times KR_s \times 0.408R_a$ $\times (T_{mean} + 17.8)$ $\times (T_{max} - T_{min})^{0.5}$ $KR_s = 0.17 \text{ for Salt Lake City}$	3.8
<b>Radiation-based model</b>	Priestley-Taylor (1972)	$ET_o = 1.26 * \frac{\Delta}{\Delta + \gamma} \frac{R_n - G}{\lambda}$	3.9
	Makkink (1957)	$ET_o = 0.61 * \frac{\Delta}{\Delta + \gamma} \frac{R_s}{\lambda} - 0.12$	3.10
	Makkink (1967) modified Hansen (1984)	$ET_o = 0.7 * \frac{\Delta}{\Delta + \gamma} \frac{R_s}{\lambda}$	3.11
<b>Mass-transfer-based model</b>	Dalton (1802)	$ET_o = (0.3648 + 0.07223u_2)(e_s - e_a)$	3.12
	Trabert (1896)	$ET_o = 3.075\sqrt{u_2}(e_s - e_a)$	3.13
	Mahringer (1970)	$ET_o = 0.15072\sqrt{3.6u_2}(e_s - e_a)$	3.14

Note:  $ET_o$  is potential evapotranspiration ( $\text{mm d}^{-1}$ );  $\Delta$  is the slope of the saturation water vapor pressure–temperature curve ( $\text{kPa } ^\circ\text{C}^{-1}$ );  $R_n$  is the calculated net radiation ( $\text{MJ m}^{-2} \text{d}^{-1}$ );  $G$  is the soil heat flux density at the soil surface ( $\text{MJ m}^{-2} \text{d}^{-1}$ );  $\gamma$  is the psychrometric constant with a value of  $0.06642 \text{ kPa } ^\circ\text{C}^{-1}$  for the elevation of Syracuse (Allen et al., 1998);  $T_{mean}$  is the mean daily air temperature at 1.5 to 2.5 m height ( $^\circ\text{C}$ );  $u_2$  is the mean daily wind speed at 2 m height ( $\text{m s}^{-1}$ );  $e_s$  is the mean saturation water vapor pressure (kPa);  $e_a$  is the actual water vapor pressure (kPa); and RH is relative humidity in %.  $R_a$  is extraterrestrial radiation ( $\text{MJ m}^{-2} \text{d}^{-1}$ ).  $R_s$  is the solar radiation ( $\text{MJ m}^{-2} \text{d}^{-1}$ );  $\lambda$  is the latent heat of vaporization in  $\text{MJ kg}^{-1}$  ( $\lambda = 2.45$  at a temperature of  $20^\circ\text{C}$ ). The constant 0.408 in Eq. 3.1, 3.7, and 3.8 has units of  $\text{kg MJ}^{-1}$  and is the inverse of latent heat of vaporization. The temperatures denoted by  $T_{mean}$ ,  $T_{min}$ ,  $T_{max}$ , and  $T_{dew}$  are in degrees Celsius. All variables necessary for computing the potential ET are determined by direct measurements and computation according to the ASCE-specified daily Penman-Monteith methodology (Allen et al., 1998).

Under water-limiting conditions, in addition to the crop coefficient,  $ET_a$  must be corrected for soil water content:

$$ET_a = Kc \times \text{Soil moisture function} \times ET_o \quad \text{Eq.3.15}$$

Several models estimate water availability in the soil, for example, soil moisture extraction functions (SMEFs) (Stovin et al., 2013), Thornthwaite-Mather Equation (T-M) (Steenhuis and Van Der Molen, 1986), and antecedent precipitation index (API) (Priestley, 1972). The SMEFs and T-M model incorporate data on soil moisture (Eq.3.16-Eq.3.17). The crop coefficient ( $Kc$ ) is back-calculated given the computed  $ET_o$  and the measured  $ET_a$  by using the method of least squares. This coefficient accounts for the specificity of green roof sedum plants.

$$ET_{a-SMEF} = Kc \times \frac{\theta_t}{\theta_{fc}} \times ET_o \quad \text{Eq.3.16}$$

$$ET_{a-TM} = Kc \times \frac{\theta_t - \theta_{wp}}{\theta_{fc} - \theta_{wp}} \times ET_o \quad \text{Eq.3.17}$$

where  $\theta_t$  is the actual soil moisture,  $\theta_{fc}$  is the field capacity,  $\theta_{wp}$  is the wilting point of the growth medium.

In the absence of soil moisture data, the API model can use precipitation data (Eq.3.18-Eq.3.21). The API model is a modification of the Priestley-Taylor equation. This model predicts  $ET_a$  incorporating a function of precipitation over the previous 28 days to account for variations in soil water content (Ali and Mawdsley, 1987).

$$ET_{a-API} = 0.35\alpha \times \left( \frac{\Delta}{\Delta + \gamma} (Rn - G) \right) \times Kc \quad \text{Eq.3.18}$$

$$\alpha = 0.123(API) - 0.0029(API)^2 - 0.0000056(API)^3, \text{ for } API \leq 20 \quad \text{Eq.3.19}$$

$$\alpha = 1.26, \text{ for } API > 20 \quad \text{Eq.3.20}$$

$$API(d) = P_{(d-1)} + KP_{(d-2)} + K^2P_{(d-3)} + \dots + K^{27}P_{(d-28)} = \sum_{t=1}^{28} K^{(t-1)}P_{(d-t)} \quad \text{Eq.3.21}$$

where API(d) is the API value corresponding to day d, and  $P_{(d-t)}$  is the precipitation depth in mm for the day that is t days prior to d. API ( $\text{mm d}^{-1}$ ) is defined with K set to 0.9 for all values of t from 1 day to 28 days before present (Kohler and Linsley, 1951).

### 3.2.3 ET Measurement - Soil Water Balance Method

The ASCE Hydrology handbook describes the general soil water balance as follows:

$$\Delta\theta * z = P - R - ET_a - DP + GW \quad \text{Eq.3.22}$$

where  $\Delta\theta$  is the change of soil moisture content ( $\text{m}^3 \text{ water} / \text{m}^3 \text{ soil plus water}$ ), z is the depth of soil, P is precipitation, R is runoff,  $ET_a$  is the actual evapotranspiration, DP is deep percolation losses, and GW is the movement of ground water into the soil. Each variable on the right side of Equation 3.22 has the unit of mm.

Using this method, ET can be evaluated through daily change in soil moisture. For a green roof, DP and GW are 0. Eq.3.22 is applied on days when  $P=0$  and  $R=0$ . The water balance equation can be simplified to Eq.3.23 below. The change in soil moisture content is quantified for each day ( $\theta_0 - \theta_{23}$ ), where  $\theta_0$  is the hourly average value (12:00 AM-1:00 AM) at midnight beginning the day and  $\theta_{23}$  is the hourly average value (11:00 PM to 12:00 AM) at the end of the day. The daily actual ET is calculated by:

$$ET_a = -(\theta_{23} - \theta_0) * z \quad \text{Eq.3.23}$$

If a rainfall event is longer than one day, calculated  $ET_a$  can be negative due to the detention performance of the green roof, hence  $ET_a$  was set to zero on such days.

### 3.2.4 Energy Balance Method

ET, as the latent heat flux, can be calculated from the energy equation (Eq. 3.24)

$$Q_{latent} = R_{sw} + R_{lw} - Q_{sensible} - Q_{conduction} \quad \text{Eq.3.24}$$

where all terms have units of  $\text{W m}^{-2}$ ,  $R_{sw}$  is net shortwave radiation,  $R_{lw}$  is net longwave radiation,  $Q_{sensible}$  is sensible heat flux between the atmosphere and the soil surface on the roof, and  $Q_{conduction}$  is conductive heat flux between the soil surface on the roof and the interior of the building. Sensible heat flux can be calculated from Eq.3.25-3.26.  $Q_{conduction}$  can be determined from the difference in temperature between the roof  $T_{roof}$  and ceiling  $T_{ceiling}$  (Gaffin et al., 2010) (Eq. 3.27).  $T_{roof}$  refers to the temperature of the growth medium.

$$Q_{sensible} = 6.6 u_2^{0.8} (T_{roof} - T_{air}) \quad \text{when } u_2 > 1.75 \text{ m/s} \quad \text{Eq.3.25}$$

$$Q_{sensible} = 10.3 (T_{roof} - T_{air}) \quad \text{when } u_2 \leq 1.75 \text{ m/s} \quad \text{Eq.3.26}$$

$$Q_{conduction} = \kappa (T_{roof} - T_{ceiling}) \quad \text{Eq.3.27}$$

where  $u_2$  is the wind speed at 2 m above the roof (m/s) and  $\kappa$  is the thermal conductivity of the overall roof with a value of  $0.36 \text{ W m}^{-1}\text{K}^{-1}$ .  $T_{roof}$ ,  $T_{air}$ , and  $T_{ceiling}$  have been measured directly using the Campbell temperature probes described earlier. Since total radiation data are not available, the method of Allen et al., (1998) was used to estimate  $R_{lw}$ .

After  $Q_{latent}$  is determined, the ET value can be calculated from Eq.3.28 (Henderson-Sellers, 1984):

$$ET_a = \frac{Q_{latent}}{\lambda} = \frac{Q_{latent}}{1918.46 \left( \frac{T_{air}}{T_{air} - 33.91\text{K}} \right)^2} \quad \text{Eq.3.28}$$

where  $\lambda$  is the latent heat of vaporization ( $\text{kJ kg}^{-1}$ ),  $T_{air}$  is in degrees Kelvin.

### 3.2.5 Statistical methods

All the statistical analyses were conducted in the open-end software “R”. Partial least squares (PLS) analysis was applied to determine the influence of chosen environmental variables on the ET rates on a daily basis. This method is appropriate when the factors are many and collinear. The variable importance in projection (VIP) scores of each variable were used to present the influence of each variable in the PLS model. The method gives a measurable value to select the independent variable that contributes most to the dependent variable’s variance (Y. Feng et al., 2018). In general, variables with  $VIP < 0.8$  are less influential, while variables with  $VIP > 1$  are highly influential.

Correlation-based measures are inappropriate due to the effects of extreme values. Instead, the index of agreement (D), Nash-Sutcliffe efficiency (NSE), percent bias (PBIAS), and root mean square error (RMSE) are applied to evaluate the performance of simplified reference evapotranspiration models (Legates and McCabe Jr, 1999). R-squared is still presented as a common indicator of model performance. The modified index of agreement is a standardized measure of the degree of model prediction error and varies between 0 and 1 (Willmott, 1981). NSE indicates how well the plot of observed versus modelled data fits the 1:1 line. PBIAS measures the tendency of the modeled values to be larger or smaller than the observed values, and the optimal value is 0. RMSE gives the standard deviation of the model prediction error. Criteria for satisfactory performance are  $RMSE < 0.5$ ,  $PBIAS < 12\%$  (positive or negative),  $NSE > 0.6$ ,  $D > 0.85$ , and  $R^2 > 0.6$ .  $O_i$  is the ET observed by the soil water balance method,  $C_i$  is the  $ET_a$  calculated by ET estimates,  $n$  is the number of calculated values, and  $\bar{O}$  is average measured ET. In addition, the pair-wise comparisons are made using linear regression.

$$D = 1.0 - \left[ \frac{\sum_{i=1}^n (C_i - O_i)^2}{\sum_{i=1}^n (|C_i - \bar{O}| + |O_i - \bar{O}|)^2} \right] \quad \text{Eq.3.29}$$

$$NSE = 1.0 - \frac{\sum_{i=1}^n (C_i - O_i)^2}{\sum_{i=1}^n (O_i - \bar{O})^2} \quad \text{Eq.3.30}$$

$$PBIAS = \frac{100 \sum_{i=1}^n (C_i - O_i)}{\sum_{i=1}^n O_i} \quad \text{Eq.3.31}$$

$$RMSE = \sqrt{n^{-1} \sum_{i=1}^n (C_i - O_i)^2} \quad \text{Eq.3.32}$$

### 3.3 Results and Discussion

#### 3.3.1 Weather Condition and ET Measurement Results

Meteorological conditions in the study years of 2015, 2016, and 2017 varied greatly as shown in Fig. 3.1. The total precipitation depth in these three years were 640 mm, 400 mm, and 703 mm, respectively. The average monthly relative humidity ranged from 57% to 75% and roughly followed the change of the precipitation. No clear pattern of monthly windspeed was observed during the study period. An annual minimum in windspeed was seen in September.

The daily ET rates ranged from 0 to 5.4 mm with a mean value of 0.76 mm. The average daily ET rates in 2015, 2016, and 2017 were 0.7 mm (SD = 0.7 mm), 0.6 mm (SD = 0.7 mm), and 1.0 mm (SD = 1.0 mm), respectively. The measured values are within the range of ET reported from green roofs in the literature (Table 3.2). Both Berretta et al. (2014) and Stefferud (2016) applied the soil water balance method to measure ET and reported daily ET rates of 1.39 mm (LECA) and 1 mm for a warm period, respectively, and 0.79 mm (LECA) and 0.6 mm for a cool period, respectively. The results for HLC and SCS are similar to those for LECA (Berretta et al., 2014). The ET rates reported here tend to be smaller than those in studies with irrigation that use a lysimeter. For example, Wadzuk et al. (2013) reported an annual average daily rate of 2.9 mm in Philadelphia. They explained the high ET rates by the lack of a drain under the lysimeter.

Variations of ET rates among studies can be explained by the differences in climate, roof configuration (soil moisture capacity, plant coverage, etc.), irrigation practices, and measurement methods.

Higher ET rates are expected in summer because of larger storm events, warmer temperature, and higher solar radiation. For example, Digiovanni et al. (2013) and Marasco et al. (2014) reported higher ET rates in summer than in winter in New York City. Jim and Tsang (2011) found the transpiration rate on sunny days in Hong Kong were highest in autumn and lowest spring. The high values in autumn were explained by the end of the monsoon with warm, dry weather and sufficient photosynthetically active radiation. In contrast, the ET rates in Syracuse were highly variable from month to month and year to year, without a consistent seasonal trend. This is mainly due to the variability in timing, intensity, and total amount of rain occurring during the 3-year study period. Furthermore, the study in Syracuse is confined to months of the year with rain only; months with any snowfall are excluded.

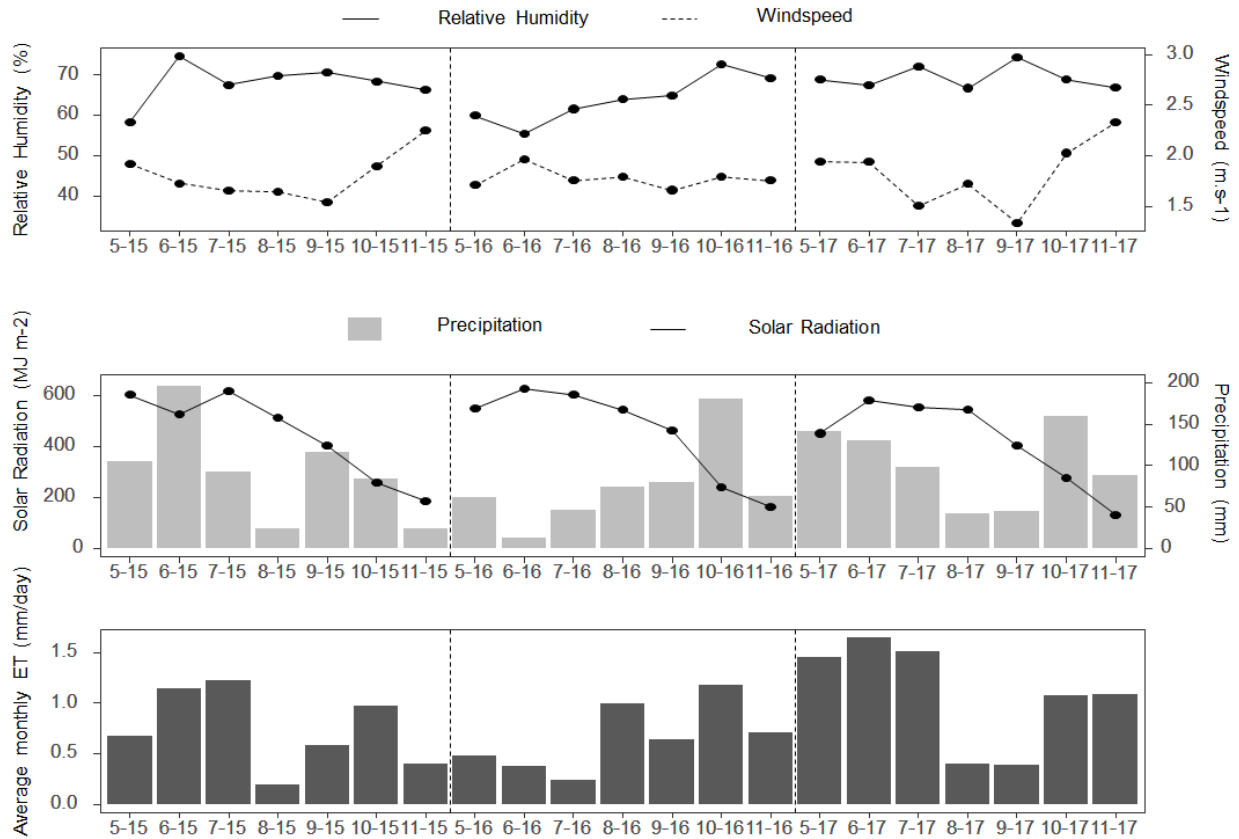


Figure 3.1. Monthly precipitation solar radiation, and ET from 5/1/2015 to 11/30/2017.

### 3.3.2 Factors Affecting the ET Process

Three variables were believed to have an important influence on the ET process according to the PLS analysis (Fig. 3.2). For the three-year study period, the VIP scores for initial soil moisture content, solar radiation, and maximum relative humidity were 4.9, 2.0, and 1.5, respectively; no other variables were above the threshold value of 0.8. Multiple regression analysis shows the initial soil moisture content explains 55% of the variability in ET consistent with the PLS analysis. Because soil moisture is so important, water-limiting and non-water-limiting periods were separated by the threshold of initial soil moisture exceeding the field capacity (0.14 for the OnCenter green roof growth medium), as was proposed by Crago and Brutsaert (1992). During a large rain event, water saturates the soil, and then the water will drain until the moisture content

decreases to the field capacity. When the water content is above the field capacity, there is no stress for plants to take water. For these conditions, the five factors that influence ET, in order of importance, were minimum, mean, and maximum air temperature, solar radiation, and water vapor deficit. For the water-limiting period, the five factors in order of importance were solar radiation, water vapor deficit, minimum and mean relative humidity, and minimum air temperature.

The initial soil moisture content was determined to be the most important factor controlling ET, followed by the solar radiation. When water content was above the field capacity, air temperature became the most influential variable. This selective importance of air temperature comes from the fact the higher air temperature leads to an increase in stomatal conductance and increases evaporation (Urban et al., 2017). When water content is below the field capacity, solar radiation controls ET, as higher energy was needed to break the bonds that act to retain water in the soil (Stovin et al., 2015). Water vapor deficit and minimum relative humidity were important in dry conditions; such conditions could promote enhanced ET from the plant leaf surface or soil into the air by diffusion and convection. These observations are in line with Lazzarin et al. (2005) who suggested that evapotranspiration was driven entirely by the water vapor deficit in the air in winter. Wind speed did not play a major role in augmenting ET rates in either water-limiting or non-water-limiting scenarios, which is consistent with the observation of Jim and Tsang (2011).

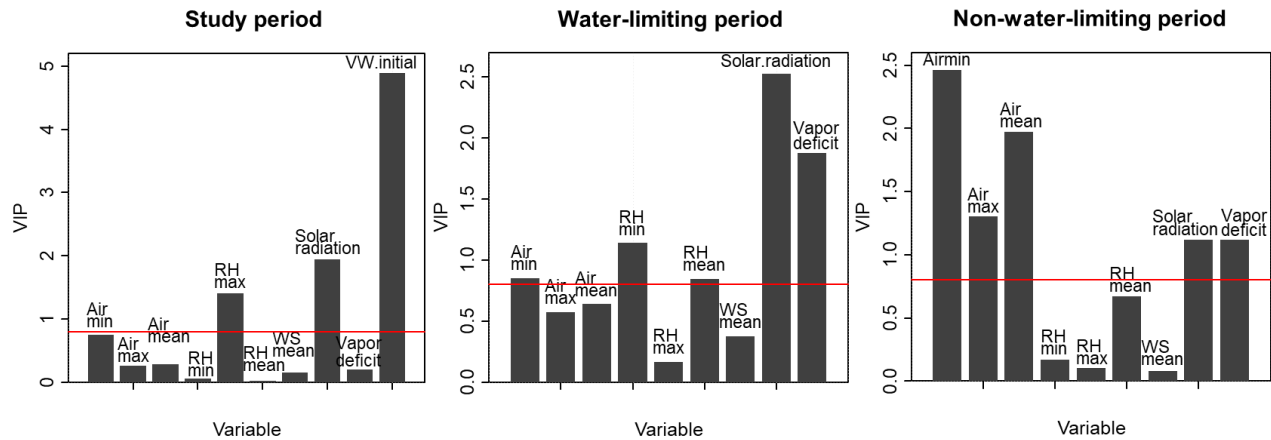


Figure 3.2. Variable importance in projection (VIP) plots for partial least squares analysis (PLS). The red line is the threshold value of 0.8 defining influential variables.

### 3.3.3 Daily ET Rates

Given that the amount of water in the soil governs the ET process, the ET rates immediately after a storm event should be high and then gradually decrease. This decline can be explained by a combination of short-rooted vegetation as well as highly porous growth medium which enables rapid drainage. The change in daily ET rates after storm events during the study period compared with the rainfall hydrograph are shown in Figure 3.3. The data show consistent behavior with an almost linear downward trend of ET observed after many events. In general, the ET rate is the highest one day after the event and continuously decreases from that value. For example, ET on 7/2/2017 was 5.4 mm/day when the initial soil moisture was 0.21. The next day, the ET rate decreased to 2.6 mm/day while the initial soil moisture decreased to 0.14. This pattern suggests that ET is an effective soil storage recovery mechanism after a rain event. In addition, the relationship between the change of ET and soil moisture availability indicates that it is necessary to include soil moisture terms when modeling ET.

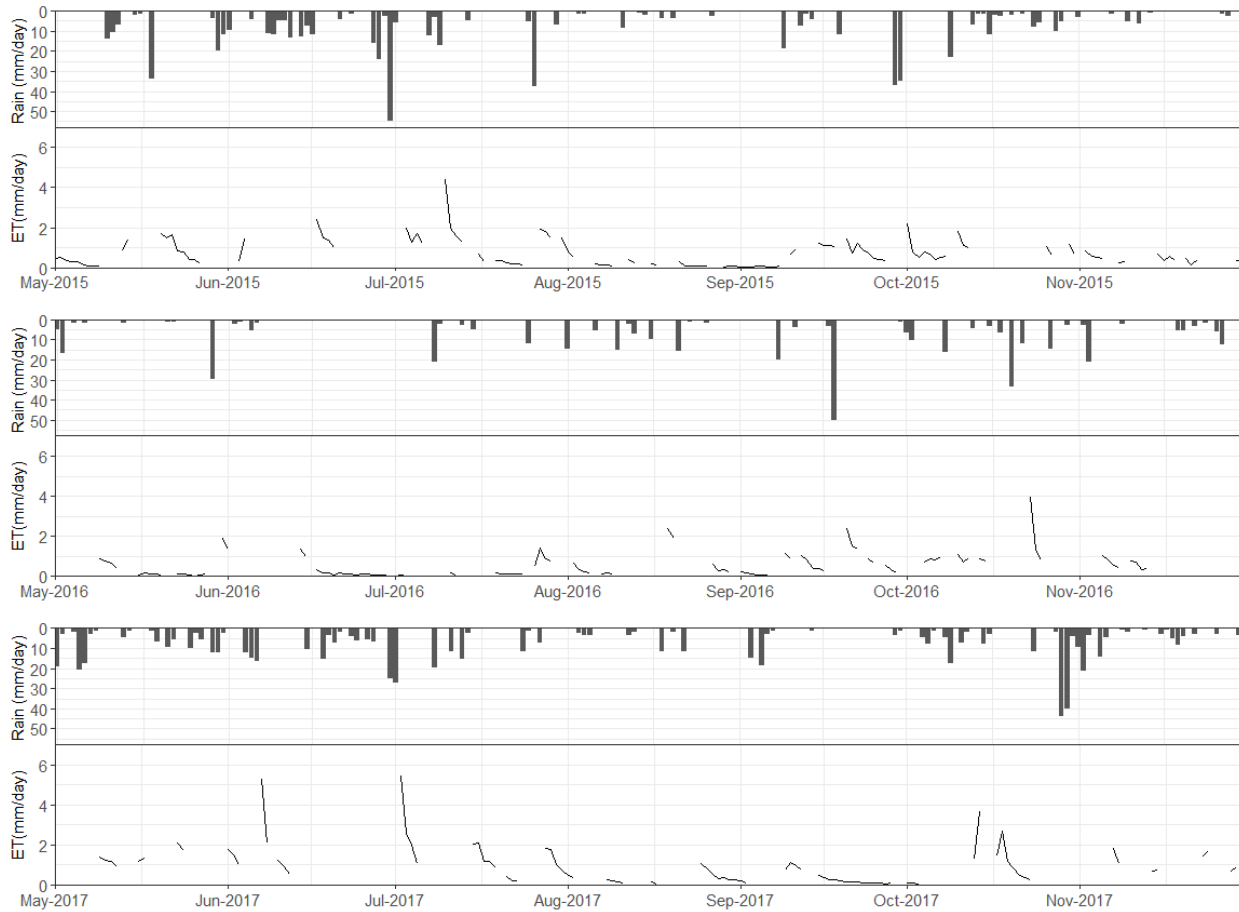


Figure 3.3. Daily precipitation and ET depth from 5/1/2015 to 11/30/2017. Tick marks on the x-axis indicate the first day of each month.

### 3.3.4 ET Estimates from the Energy Balance Model

Monthly average heat flux was calculated, including upward latent heat flux, downward net radiation, upward conductive heat, and upward sensible heat. Note that heat flux is defined as positive in the downward direction (Figure 3.4). Conductive heat flux was generally minimal, becoming negative in October and November, when the roof temperature was lower than the ceiling temperature. Net radiation peaked in June and July with a monthly average of  $140 \text{ W m}^{-2}$ . Sensible heat peaked in May and followed a downward trend in the subsequent months. Negative sensible heat flux was observed in October and November when the roof temperature was higher than the air temperature. Average latent heat followed a similar decreasing trend after a peak in

May. The similar temporal pattern of sensible heat flux and latent heat flux confirms that applying Bowen's Ratio ( $\beta=Q_{\text{sensible}}/Q_{\text{latent}}$ ) is sufficient for predicting latent heat from sensible heat on a green roof (Heusinger and Weber, 2017). For the warm months (May, June, July, and August), the average  $\beta$  was 0.2 in 2015 and 2017. For late June and early July 2016, when a drought occurred, the average  $\beta$  increased to 0.3. The calculated coefficient satisfies the expectation that green roofs ideally should have  $\beta$  similar to rural sites ( $\beta < 1$ ) in order to reduce urban warming. Martens et al. (2008) suggested  $\beta$  should be between 0.12 and 0.35 in models for non-irrigated extensive green roofs. The calculated values of  $\beta$  here are consistent with their suggestion. The energy balance model does not consider advection, water limitation, and increased surface resistance during drought.

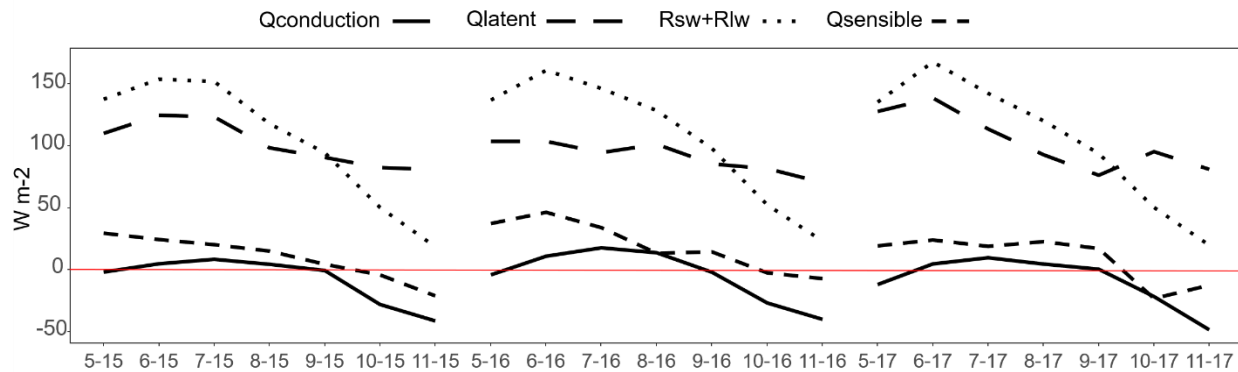


Figure 3.4. Energy Flux monthly average (mean daily value for each month).

### 3.3.5 Actual ET (ET<sub>a</sub>) Estimates Comparison

Simulated results from fourteen potential ET estimation methods have been tested against the measured ET<sub>a</sub> rates using the soil water balance method on the OnCenter green roof. Most methods overestimated the ET for the green roof as expected, since they did not account for water availability. To address water stress conditions, the SMEF, Thornthwaite-Mather, and API methods were applied. In the final step, a system-specific crop coefficient (K<sub>c</sub>) was developed

for each potential ET method using a least-squares linear regression of daily measured ET results.

The  $ET_a$  model performance statistics are summarized in Table 3.3. The table presents values of the five statistical performance criteria for each model, with those values satisfying the criteria shown in bold. Overall, applying SMEF produced better  $ET_a$  simulations compared to the Thornthwaite-Mather equation. This may be because the T-M method is highly sensitive to the input parameter of the wilting point, which is difficult to measure accurately (DiGiovanni et al., 2013). Feng et al. (2018) compared the simulated  $ET_a$  to lysimeter measured data and found that the T-M model had the lowest  $R^2$ . So no further analysis of the T-M model is presented. The API model significantly underestimated  $ET_a$  values.

By applying SMEF and Kc, five satisfactory potential ET models were the energy balance, the ASCE Penman-Monteith, the Blaney-Criddle, the Priestley-Taylor, and the 1957 Makkink model (Fig. 3.5). The results of the 1967 Makkink model were very similar to the 1957 model and thus were not shown. All five models showed results in rough agreement with the measured ET rates. However, none of the models successfully predicted ET rates greater than 4 mm/day.

The energy balance model achieved the best fit among the five satisfactory models. Using the energy balance model requires onsite monitored data including net radiation, sensible heat flux between the atmosphere and the soil surface on the roof, and conductive heat flux between the soil surface on the roof and the interior of the building. Those data are not commonly available for green roofs.

The performances of the other four models were all similar. The Blaney-Criddle model is a temperature-based potential ET method, which only requires monthly mean temperature and daily percentage of annual daytime hours. The Priestley-Taylor and the 1957 Makkink are radiation-based models, and they require inputs such as net solar radiation, heat flux density at the soil surface, and the slope of the saturation water vapor pressure-temperature curve. With less inputs and a less tedious computational process, the Blaney-Criddle, Priestley-Taylor, and 1957 Makkink models may be applied to replace the ASCE Penman-Monteith model for estimating the ET of green roofs. This finding is consistent with Marasco et al. (2015), who used Hargreaves, Priestley-Taylor, Penman, and ASCE Penman-Monteith models to simulate  $ET_a$  for two green roofs in NYC. Their results showed the Priestley-Taylor equation had the best agreement with dynamic chamber ET measurements. Based on input data availability and the results in Table 3.3, it is proposed that the best approaches to estimate  $ET_a$  for the OnCenter green roof are the Blaney-Criddle and Priestley-Taylor models coupled with SMEF. Crop coefficients  $K_c$  determined for the two models were 0.47 and 0.54 for the non-irrigated OnCenter green roof, respectively.

The sedum  $K_c$  found by this study is consistent with the values determined by other studies. A value of 0.64 was reported for a green roof test bed with Sedum Carpet Substrate (SCS) in Sheffield, UK using data from the soil water balance method (Berretta, et al., 2014). Under the same conditions,  $K_c$  for Lightweight Expanded Clay Aggregate with sedum was 1.36. A value of 0.53 was given for the sedum canopy in New Hampshire using data from a weighing lysimeter (Sherrard and Jacobs, 2011). The crop coefficient was around 0.5 for a well-watered condition and 0.3 for a stressed-water condition in Vicenza, Italy using the energy balance method

(Lazzarin et al., 2005). The crop coefficient was 0.59 for sedum on an irrigated green roof in Salt Lake City, an arid area (Feng et al., 2018). A range of Kc values of 0.98 to 1.04 was determined for the Priestley-Taylor and ASCE Penman-Monteith models for two green roofs in New York using data from a dynamic chamber (Marasco et al., 2014). A range of 1.0-1.7 for sedums was obtained from a green roof in Philadelphia using a lysimeter (Wadzuk et al., 2013).

Table 3.3. Crop coefficient Kc and statistical performance measures of the actual ET estimates. The simulations with satisfactory performance are shown in bold. Criteria for satisfactory performance are RMSE<0.5, PBIAS<12% (positive or negative), NSE>0.6, D>0.85, and R<sup>2</sup>>0.6.

		Kc	RMSE	PBIAS %	NSE	D	R <sup>2</sup>
SMEF	ASCE. PM	0.45	<b>0.46</b>	<b>9.8</b>	<b>0.66</b>	<b>0.88</b>	<b>0.69</b>
	Adjusted Hargreaves Samani	0.58	0.55	<b>2.1</b>	0.53	0.82	0.53
	Hargreaves and Samani	0.63	0.72	<b>5.5</b>	0.6	0.85	<b>0.61</b>
	Schendel	0.65	0.77	-23.2	0.07	0.59	0.18
	Mahringer	4.25	0.53	6.6	0.54	0.81	0.55
	Blaney-Criddle	0.47	<b>0.47</b>	<b>11.8</b>	<b>0.66</b>	<b>0.87</b>	<b>0.7</b>
	Priestley-Taylor	0.54	<b>0.46</b>	<b>1.2</b>	<b>0.64</b>	<b>0.88</b>	<b>0.64</b>
	Turc	0.82	0.55	<b>0.3</b>	0.52	0.82	0.52
	1957 makkink	0.64	<b>0.48</b>	<b>4.9</b>	<b>0.64</b>	<b>0.87</b>	<b>0.65</b>
	1967 makkink	0.54	<b>0.47</b>	<b>6.3</b>	<b>0.65</b>	<b>0.88</b>	<b>0.66</b>
	Valiantzas	0.50	0.49	<b>8.9</b>	<b>0.63</b>	<b>0.86</b>	<b>0.65</b>
	Energy balance	0.38	<b>0.43</b>	<b>6.3</b>	<b>0.71</b>	<b>0.9</b>	<b>0.71</b>
	Dalton	32.90	0.6	<b>-1.3</b>	0.44	0.77	0.44
	Trabert	0.39	0.53	6.6	0.54	0.81	0.55
T-M	ASCE.PM	0.40	0.6	<b>-9.7</b>	0.43	0.77	0.44
	Adjusted Hargreaves Samani	0.47	0.67	-23.7	0.31	0.7	0.36
	Hargreaves and Samani	0.53	0.63	-17.6	0.38	0.74	0.4
	Schendel	0.35	0.87	-60.8	-0.19	0.49	0.14
	Mahringer	3.70	0.65	-14.6	0.35	0.71	0.37
	Blaney-Criddle	0.44	0.6	<b>-2.9</b>	0.45	0.78	0.45
	Priestley-Taylor	0.42	0.65	-27.5	0.34	0.74	0.41
	Turc	0.64	0.68	-26.9	0.29	0.7	0.35
	1957 Makkink	0.53	0.62	-19.1	0.39	0.75	0.42
	1967 Makkink	0.45	0.62	-16.5	0.41	0.76	0.43
	Valiantzas	0.44	0.61	-10	0.41	0.75	0.42
	Energy Balance	0.60	0.88	57.4	-0.21	0.75	0.45
	Dalton	25.14	0.71	-30.4	0.22	0.64	0.3
	Trabert	0.34	0.65	-14.6	0.35	0.71	0.37
API	API	0.22	0.83	-42.7	-0.08	0.41	0.09

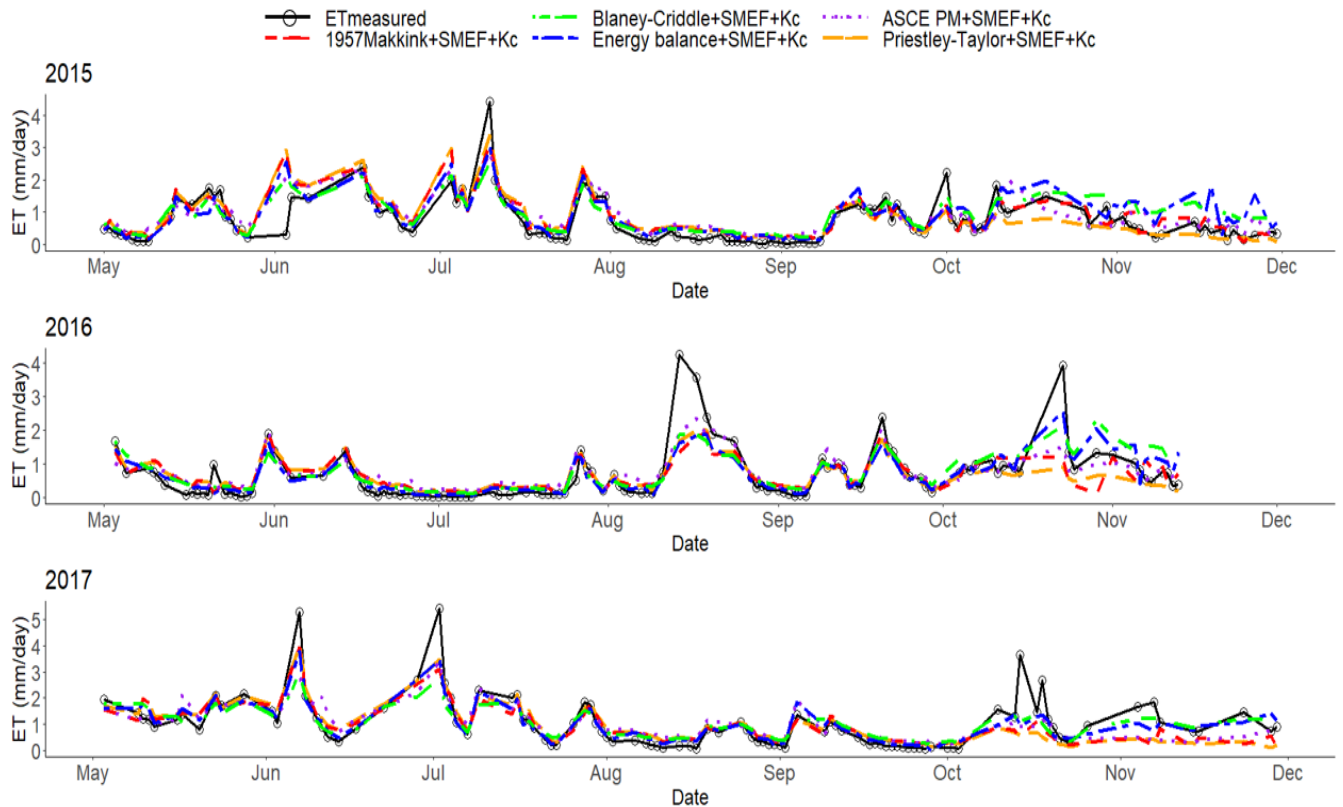


Figure 3.5. Predicted ET from the five satisfactory models and the measured ET for the OnCenter green roof for the study period. Measurements and model results are shown as continuous lines, even though all measurements and calculations shown above are for days without rain.

### 3.3.6 Model Sensitivity and Improvement

The API model underestimated ET rates significantly with poor statistics (%PIAS: 42.7, NSE:0.08,  $R^2$ :0.09). This can be explained, as the original API model was developed and tested with barley and turf in the United Kingdom (Mawdsley and Ali, 1985), where climate conditions, plant species, and growth medium characteristics are much different than for the OnCenter green roof. Even in the original paper, the author found the  $\alpha$  distribution of the turf differed from that of barley. To enable the  $ET_a$  model to better serve green roofs in northeastern U.S., the API model was revised.

The variables in the API formula and  $\alpha$  function (Eq. 3.26-3.28) have been analyzed to improve the model performance. The variables include the following: (1) the coefficient, K (0.8-0.95); (2) antecedent precipitation (4-32 days); (3) the maximum API for  $\alpha$  calculation (10-60); and (4) the maximum  $\alpha$  value. The coefficient  $\alpha$  was determined by a new cubic regression of  $ET_a/ET_o$  and the API index was determined with various K and antecedent precipitation values. The best API model was achieved with K = 0.8, antecedent precipitation days n =12, and maximum API = 50 mm (Eq. 3.33-3.35). In the last step, a crop coefficient was fitted by least squares optimization.

$$API(d) = \sum_{t=1}^{12} 0.8^{(t-1)} P_{(d-t)} \quad \text{Eq.3.33}$$

$$\alpha = 0.1143(API) - 0.0052(API)^2 - 0.00008(API)^3, \text{ for } API \leq 50 \quad \text{Eq.3.34}$$

$$\alpha = 2.51, \text{ for } API > 50 \quad \text{Eq.3.35}$$

The modified API model has a better model performance ( $R^2=0.42$ ), compared to the original API ( $R^2=0.09$ ) (Fig. 3.6). The average monthly measured ET and the original and modified API modeled ET rates are shown in Figure 3.7. The modified API model fitted the measured ET rates from May to September, but it underestimated ET in October and November. To address this problem, monthly crop coefficients were developed using the least squares optimization instead of one single coefficient for the entire year. The modified API model with monthly Kc yielded better estimates of the observations. The crop coefficients for October and November were almost doubled values compared to the other months. This pattern is consistent with the observation that the Priestley-Taylor method yielded relatively small potential ET values for October and November compared with the other potential ET models. The results also show the API model is sensitive to the K and n selection in the API formula, the maximum API value in the  $\alpha$  function, and the monthly crop coefficient.

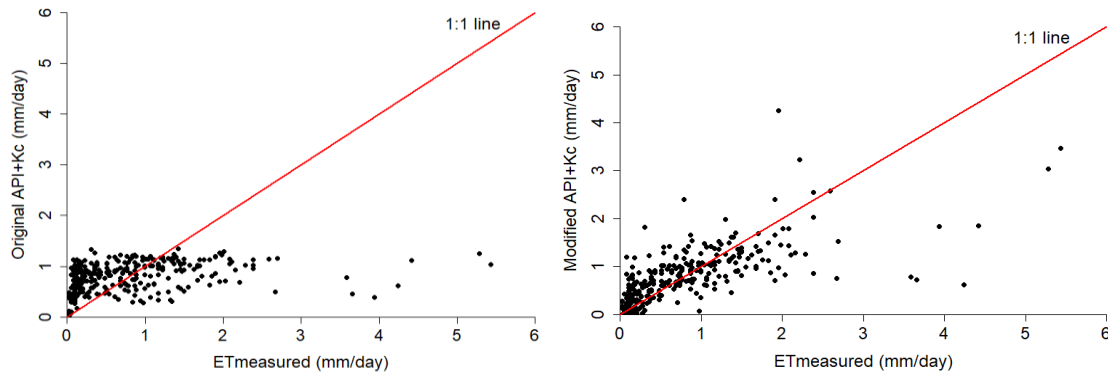


Figure 3.6. Scatter plot of measured ET values and modeled ET using the original API model with a single Kc, and using the modified API model with monthly Kc values.

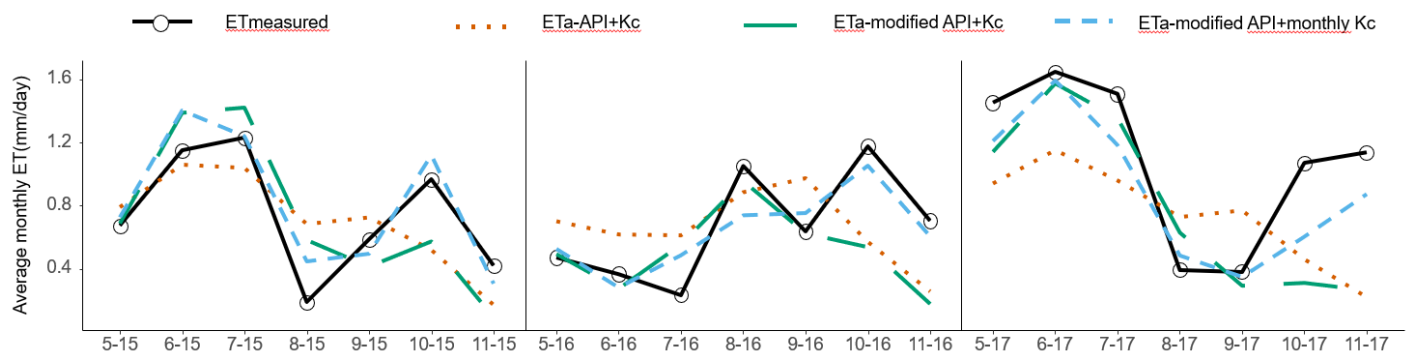


Figure 3.7. Monthly average measured ET results compared with three models: (1) the original API values ( $ET_a\text{-API+Kc}$ ), (2) an API model with fitted  $\alpha$ ,  $K = 0.8$ ,  $n = 12$ , maximum API = 50, and one unified Kc ( $ET_a\text{-modified API+Kc}$ ), and (3) an API model with modified  $\alpha$  and monthly Kc ( $ET_a\text{-modified API+monthly Kc}$ ).

The simplified potential ET models were sensitive to the resolution of the crop coefficient, while the ASCE Penman-Monteith was not. One single crop coefficient has been applied to the  $ET_a$  estimate methods in the previous section. To test the sensitivity of Kc, monthly Kc values have been developed for the five satisfactory models (Table 3.4). The crop coefficients were consistent through the year with a slightly smaller value in November in those five models except the Blaney-Criddle and Priestley-Taylor. For the Priestley-Taylor model, Kc values were larger in October and November than in the other months. For the Blaney-Criddle model, the Kc value was smaller in November. By applying monthly Kc, the statistics of the simplified models

improved somewhat, for example,  $R^2$  of Priestley-Taylor increased from 0.64 to 0.75, and  $R^2$  of Blaney-Criddle changed from 0.7 to 0.76. The detailed results of model performance metrics are shown in Table 3.5. The ASCE Penman-Monteith, a physically-based model, was not sensitive to the adjustments of crop coefficients.

Table 3.4. Monthly crop coefficients (Kc) derived from the observed and simulated data from the OnCenter green roof from five satisfactory ETa models for the three-year study period.

	Crop Coefficient (Kc)				
	ASCE PM	Blaney-Criddle	Priestley-Taylor	1957 Makkink	Energy balance ET
May	0.43	0.46	0.48	0.58	0.38
June	0.40	0.50	0.46	0.56	0.38
July	0.46	0.58	0.54	0.68	0.43
August	0.45	0.57	0.60	0.74	0.50
September	0.41	0.43	0.55	0.60	0.37
October	0.57	0.45	0.97	0.82	0.39
November	0.39	0.28	1.17	0.58	0.22

Table 3.5. Statistical performance of applying one single Kc and also monthly Kc values for the five satisfactory models.

	Single "all data" Kc					Monthly Kc					
	RMSE	PBIAS %	NSE	d	$R^2$	RMSE	PBIAS %	NSE	d	$R^2$	
ASCE PM	0.46	9.8	0.66	0.88	0.69	ASCE PM	0.45	9.6	0.68	0.88	0.71
Blaney-Criddle	0.47	11.8	0.66	0.87	0.7	Blaney-Criddle	0.42	11.4	0.72	0.9	0.76
Priestley-Taylor	0.48	1.2	0.64	0.88	0.64	Priestley-Taylor	0.42	9.9	0.72	0.9	0.75
1957 Makkink	0.48	4.9	0.64	0.87	0.65	1957 Makkink	0.46	6.1	0.66	0.88	0.67
Energy balance	0.43	6.3	0.71	0.9	0.71	Energy balance	0.39	6.3	0.76	0.92	0.77

### 3.4 Conclusion

This study aims to quantify ET performance and assess the ET<sub>a</sub> models for a green roof in the northeastern United States from the months of May to November of the year. The daily ET rates applying the soil water balance method ranged from 0 to 5.4 mm with a mean value of 0.76 mm in the study period. The weather patterns in years 2015, 2016, and 2017 varied greatly. In the summer of 2016, a drought stressed the plants on the green roof, in contrast to adequate rain in 2015 and 2017. The average daily ET rates were 0.7 mm (SD = 0.7 mm) in 2015, 0.6 mm (SD =

0.7 mm) in 2016, and 1.0 mm (SD = 1.0 mm) in 2017. Seasonal variations in ET were not observed in this study, because data were confined to the warmer months. Poë et al. (2015) suggested that the influence of season upon ET rates was apparent when soil moisture was abundant. Through the partial least squares analysis, the initial daily soil moisture content was discovered to be the most important factor influencing ET, and the next most important factor was solar radiation, as both govern the energy and water availability. Windspeed did not play a major role in the process. In daily ET observation, ET rates were high after storm events and then decreased, along with a simultaneous decrease in soil moisture availability. The change in ET related to the available soil moisture availability indicates the importance of including soil moisture content in the modeling procedure.

Fourteen potential ET models that are widely used for agricultural crops were applied to account for the influence of climate on ET. Almost all potential ET estimates were higher than the measured ET rates. The SMEF, T-M, and API models have been employed to account for soil moisture availability in the dry periods between storms. Only the SMEF method was able to yield satisfactory  $ET_a$  results. A system-specific crop coefficient has been introduced to account for vegetation type, climate pattern, and soil properties. The crop coefficients for the OnCenter green roof ranged from 0.38 to 0.64, which is consistent with previous green roof studies. In the future, a model of crop coefficients that relates to sedum productivity and weather condition is needed to improve model accuracy. In summary, when soil moisture data are available, the Blaney-Criddle ( $R^2=0.76$ ,  $NSE=0.72$ ) and the Priestley-Taylor ( $R^2=0.76$ ,  $NSE=0.72$ ) models together with SMEF and monthly  $K_c$  values are recommended for predicting ET as they provide satisfactory results even with limited data input requirements. When soil moisture data are not

available, the modified API model coupled with the Priestley-Taylor model, and monthly crop coefficients is recommended.

## Chapter 4

---

### EVALUATION OF THERMAL PERFORMANCE OF GREEN ROOFS VIA FIELD MEASUREMENTS AND HYGROTHERMAL SIMULATIONS

#### 4.1 Introduction

Buildings use a substantial fraction of the primary energy consumption in most countries (Mentens et al., 2006). Adding green roofs to the building envelope has become a popular strategy to mitigate the urban heat island effect, reduce energy consumption, and improve aesthetic appeal for buildings. Green roofs normally consist of multiple layers, for example, vegetation, growth medium, drainage, waterproof membrane, structural, and insulating layers of the roof. Regional climate influences the type of green roof design. While green roofs have been implemented in cities for years, the interest in installing green roofs in both retrofit and new construction is still increasing.

There are many thermal benefits associated with the adoption of green roofs. First, both plants and growth medium have a thermal insulation feature. A study demonstrated that only 13% solar radiation reaching the green roof was conducted through the roof and ceiling into the building interior beneath, while 27% was reflected, and 60% was absorbed by soil and plants (Eumorfopoulou and Aravantinos, 1998). Second, green roofs add thermal mass to help stabilize temperature through the roofing system, especially for the membrane. Temperature fluctuations can create thermal stresses on the membrane, affecting long-term performance and durability (Teemusk and Mander, 2010). Third, green roofs can mitigate heat flow through evapotranspiration (ET). A study reported that 58% of the heat from a green roof in China lost by ET in summer (Feng et al., 2010). Thus green roofs can stabilize the surface temperature, which

- Part of this Chapter is published in the *International building physics conference* (2018), “Simulating the thermal performance of the green roof based on CHAMPS model”.
- Part of this Chapter is being submitted to *Energy and Buildings*.

consequently reduce temperature fluctuations in the roofing system, and reduce the heating and cooling energy load of buildings. These benefits have been demonstrated through many field studies (Tabares-Velasco et al., 2012; Lazzarin et al., 2005; Ayata et al., 2011; Fioretti et al., 2010).

To assess the thermal impact of green roofs on building performance under various climate conditions, a combined heat and moisture transfer model can be used. It is noted that models in the literature are mostly limited to heat transfer (Djedjig et al., 2012). Sailor (2008) generated a green roof energy balance model, “Ecoroof”, within the U.S. Department of Energy building simulation program, EnergyPlus. Wong et al. (2003) applied the DOE-2 simulation program to compare the thermal performance of various plants on green roofs. However, the model was not validated with experimental results. To demonstrate the importance of including moisture in thermal modeling, Ouldboukhitine et al. (2012) developed a thermodynamic model for green roof temperature, finding that the average modeling error decreased from 2.9°C to 0.8°C when a water balance was included. A few mathematical models have been developed for green roofs; however, they are not user-friendly (Djedjig et al., 2012). To address this concern, a new modeling platform is presented to simulate the green roof performance in this study, the combined heat, air, moisture and pollutant simulation of building envelope systems (CHAMPS-BES) model. This model accounts for radiative, conductive, and convective heat transfer, evapotranspiration, and moisture effects. CHAMPS offers a user-friendly interface enabling users to add green roof layers to any building construction.

In this study, the thermal performance of a large extensive green roof was simulated using CHAMPS in both warm and cold periods. After the experimental validation, the model was applied to illustrate the thermal benefits of adding a green roof as a retrofit to a traditional roof. Next, the impact of a thick layer of snowpack on the green roof was analyzed. Further, the importance of including water balance terms and the albedo effect in model simulation was discussed. The results show that CHAMPS can be used by engineers and planners to assess the benefits of a green roof through consideration of thermal mass, passive cooling, membrane protection, and energy savings, especially for a retrofit decision to an existing building.

## **4.2 Methods**

### **4.2.1 Experimental Campaign**

The green roof is located on the Onondaga County Convention Center (OnCenter) in Syracuse, NY. The facility receives on average 104 cm of precipitation and 264 cm of snow (26.4 cm of snow meltwater) per year (NOAA, 2018). Snow falls mainly between the months of November and March. January is the coldest month with the largest amount of snowfall of 24 mm/day (Appendix C).

The OnCenter green roof with an area of 5600 m<sup>2</sup> was retrofitted in 2011. The building is surrounded by a few tall buildings, mainly to the North, and as a result, there is no shading from other buildings to the green roof surface during the day (Fig. 4.1). The green roof consists of the following material layers from top to bottom: (1) a growth medium and vegetation layer, (2) a drainage mat, (3) a waterproof membrane, (4) a gypsum board, (5) an extruded polystyrene insulation layer, (6) a second gypsum board, and (7) a steel deck (Fig. 4.2). The insulation layer

and layers below are original to the building. The main thermal properties of the layers of the green roof are described in Appendix D.

An experimental campaign to characterize the function of the green roof commenced in 2015. The thermal monitoring system of the green roof is equipped with CR1000 Dataloggers and AM 16/32B Multiplexers (Campbell Scientific). Temperature sensors have been installed between several of the roof layers to provide vertical temperature profiles (Fig. 4.2). Soil moisture sensors were positioned in the middle of the growth medium. Interior temperatures are controlled by HVAC system. Temperature sensor (Y) was mounted on the ceiling of the exhibit hall beneath the roof to measure the indoor temperature. A weather station was installed on the roof to record solar radiation, relative humidity, ambient temperature, rainfall, windspeed, and wind direction. The measured data have been collected every minute and the average reported every hour. The thermal analysis of the green roof was conducted from November 2017 to September 2018. Snow depth was measured once on 1/9/2018 along several east-west transects (Yang and Davidson, 2018).



Figure 4.1. Photos of the OnCenter green roof during different seasons.

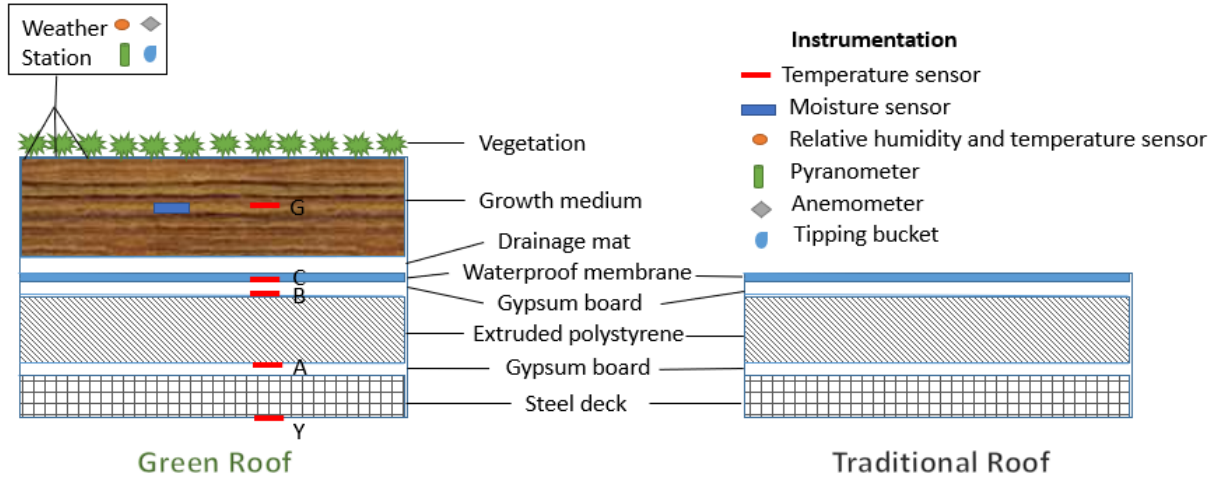


Figure 4.2. Roof layers and instrumentation locations on the OnCenter green roof. The traditional roof was simulated by removing the drainage mat, growth medium, and vegetation layers.

#### 4.2.2 Description of Green Roof Components

The rate of heat transfer and water vapor transfer on green roofs depends on both meteorological data and physical properties of the roof layers. The growth medium is coarse engineered mineral with an average bulk density of  $790 \text{ kg/m}^3$ . Laboratory results showed a 55% pore composition and a saturated hydraulic conductivity of  $0.002 \text{ m/s}$ . The effective saturation moisture content is  $0.234 \text{ m}^3/\text{m}^3$ . Thermal properties of the growth medium were measured using the Decagon KD2 Pro with an accuracy of  $\pm 10\%$  (Decagon, 2006). The thermal conductivity of soil from the OnCenter green roof increased from  $0.2$  to  $1 \text{ W/m K}$  as water content increased from  $1\%$  to  $40\%$  (Fig. 4.3).

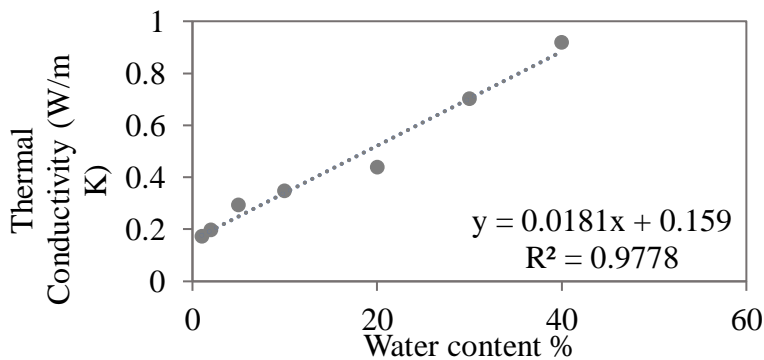


Figure 4.3. Thermal conductivity for different water content measured in the lab.

### 4.2.3 CHAMPS Simulation

The CHAMPS model simulates the combined heat and moisture transfer processes between the atmosphere and roof layers. The model has been built upon Delphin 5, and has a user-friendly interface. The moisture mass balance and energy balance are written as Eq. E.1-E.9 in Appendix E. The main inputs to the CHAMPS model include the following five groups: materials (thermal and moisture transport and storage properties of each layer), meteorological conditions (e.g., solar radiation, air temperature, windspeed, relative humidity, and rainfall), boundary conditions (e.g., heat conduction, vapor diffusion, shortwave radiation, longwave radiation, and rainfall), initial conditions (temperature, relative humidity, and soil moisture content), and field conditions (water/energy sources).

In this study, a green roof model was first developed in CHAMPS and validated by the monitored data from the OnCenter green roof during both warm periods (8/1/2017-8/7/2017) and cold periods (11/1/2017-11/7/2017). For the winter simulation, only the energy balance was applied due to the low impact of the roof water balance. For the summer simulation, both energy balance and water balance were applied. The albedo was assumed constant and did not change with soil moisture content during the simulation. A challenge in modeling the green roof is to account for the effect of evapotranspiration and water transport process in the plant layer. In the present study, we used a negative source account for such an effect. Since evapotranspiration has a substantial impact on the heat and water transfer processes on a green roof, hourly ET values were added as negative water sources in the model. ET was calculated using a soil moisture extraction function (SMEF) model (Eq. 4.1) (Zhao et al., 2013). The SMEF model describes ET as a function of the ASCE Penman-Monteith ET equation (Allen et al., 1998) multiplied by the

ratio of moisture content ( $\theta$ ) to the field capacity ( $\theta_{fc}$ ), and the crop coefficient ( $K_c = 0.45$ ). The crop coefficient value was obtained from the study of ET models suitability in Chapter 3 (Table 3.3).

$$ET = ET_{ASCE\ Penman-Monteith} \times \frac{\theta}{\theta_{fc}} \times K_c \quad (\text{Eq. 4.1})$$

A traditional roof model was developed by eliminating the growth medium and drainage layers from the green roof model in CHAMPS. An albedo of 0.2 was applied for the traditional model (Sharma et al., 2016). The output of the traditional roof is compared with experimental data from the green roof to determine the thermal benefits of the green roof. Analysis of variance (ANOVA) was applied to evaluate the differences between thermal performance of the traditional roof and the green roof, as well as green roof temperature with and without snowpack. In addition, simulations were conducted to understand the sensitivity of parameters on the energy modeling of the green roof, including water balance and albedo.

In general, two cases were performed based on the objectives of this study.

- To determine the impact of the green roof in warm and cold periods, CHAMPS was applied for the case of the OnCenter traditional roof before the green roof retrofit. The output of CHAMPS was compared with the experimental data from the green roof.
- To determine the impact of a snowpack on the green roof, CHAMPS was applied for the green roof without snow. The output of CHAMPS was compared with experimental data from the green roof with a thick layer of snowpack.

## 4.3 Results and Discussion

### 4.3.1 Summer Thermal Performance

During the week of used to simulate summer thermal characteristics of the green roof (August 1-8, 2017), the peak solar radiation ranged from 487 to 860  $\text{W m}^{-2}$  (Fig. 4.4). Moreover, a series of rainfall events occurred on August 4, 5, and 6. The temperature profile time series within the roofing system for this week is shown in Fig. 4.5. Diurnal temperature cycles were observed in layers above the insulation (B, C, G). However, temperatures below the insulation (A, Y) stayed relatively constant around  $22^{\circ}\text{C}$ , which indicates that the insulation layer contributes nearly all of the thermal resistance of the roof. During high solar radiation periods in summer (8/1-8/3), peak temperatures in daytime and minimum temperatures at night in layers B, C, and G were all higher than the air temperature. When solar radiation was low, temperatures in those three layers were closer to the air temperature. Solar radiation significantly impacts the temperature of the roof's upper layers.

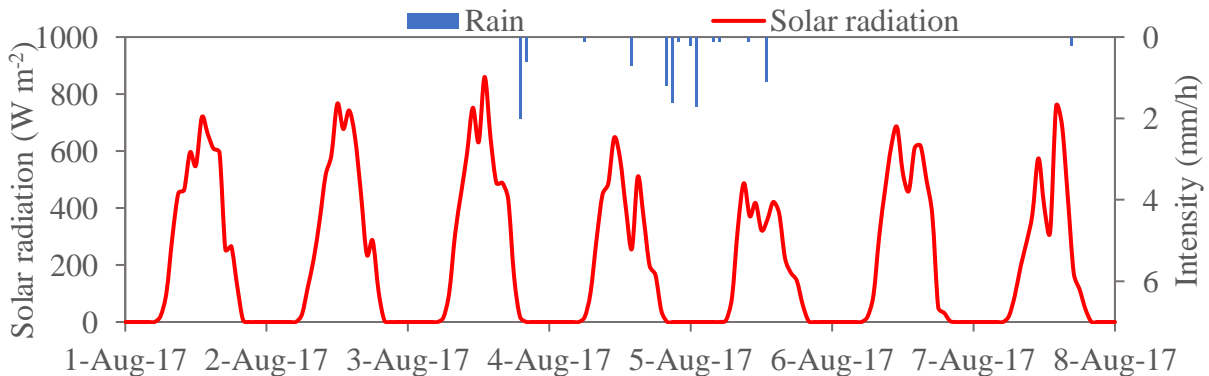


Figure 4.4. Solar radiation and rainfall intensity during a typical summer week (Aug 1-7, 2017).

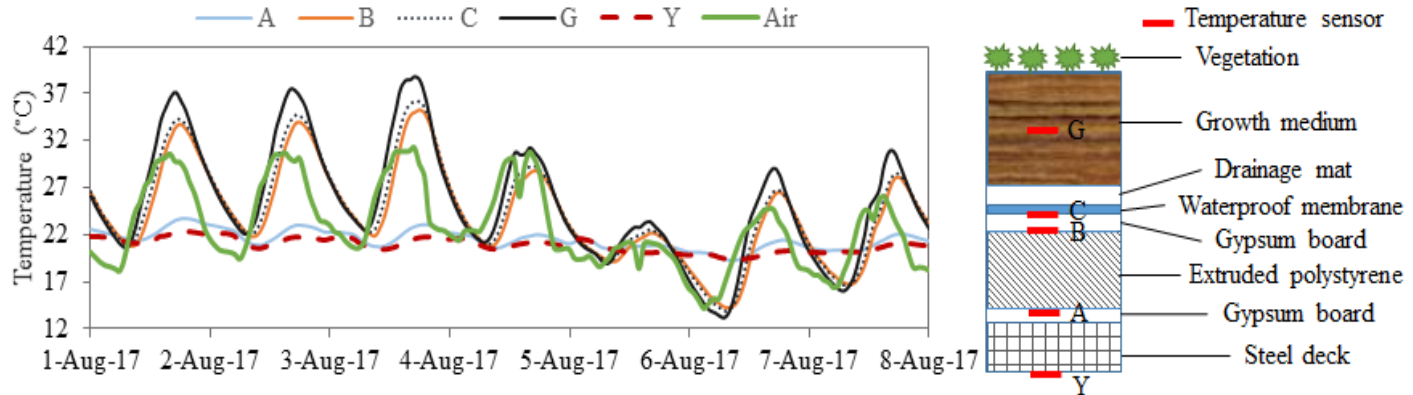


Figure 4.5. Temperature profile time series of the green roof during a typical summer week (Aug.1-7, 2017).

During and after a rainfall event, the growth medium increases in saturation. A greater moisture content not only increases the thermal conductivity, it also increases ET which increases the rate of transfer of the thermal energy in the growth medium to latent heat, and thus decreases the temperature of growth medium (Chapter 3). The lower temperature of the upper roof from 8/5-8/6 was the result of lower air temperature and lower solar radiation and ET following the rain on 8/5. This is consistent with the finding of Feng et al. (2010) that when the soil is wet, solar radiation accounts for 99% of total heat gain and ET accounts for 58% of total heat loss. The low temperature of the upper roof from 8/5-8/6 was possibly caused by a combination of lower solar radiation and higher ET rates following the rain on 8/5.

### 4.3.2 Winter Thermal Performance

The temperature profile time series for a typical week without snow in November (Nov. 1-8) was similar to the summer performance (Fig. 4.6). The temperatures of layers above the extruded polystyrene insulation (B, C, and G) followed the diurnal pattern of ambient air but with slightly smaller diurnal variation than the temperature of ambient air. An average of two hours delay in

peak temperature was observed based on the temperature in the growth medium (G) compared to the ambient temperature. In contrast, the temperature profile time series for a typical week with a thick snowpack in January (Jan. 1-8) did not show high variability in the temperature of the growth medium (G, Fig. 4.7). The temperature of the growth medium remained around 0°C even when the ambient air temperature was occasionally -20°C. The impact of snow accumulation was substantial on thermal profile of the roof. Similar findings were reported by Getter et al (2011) and Squier and Davidson (2016).

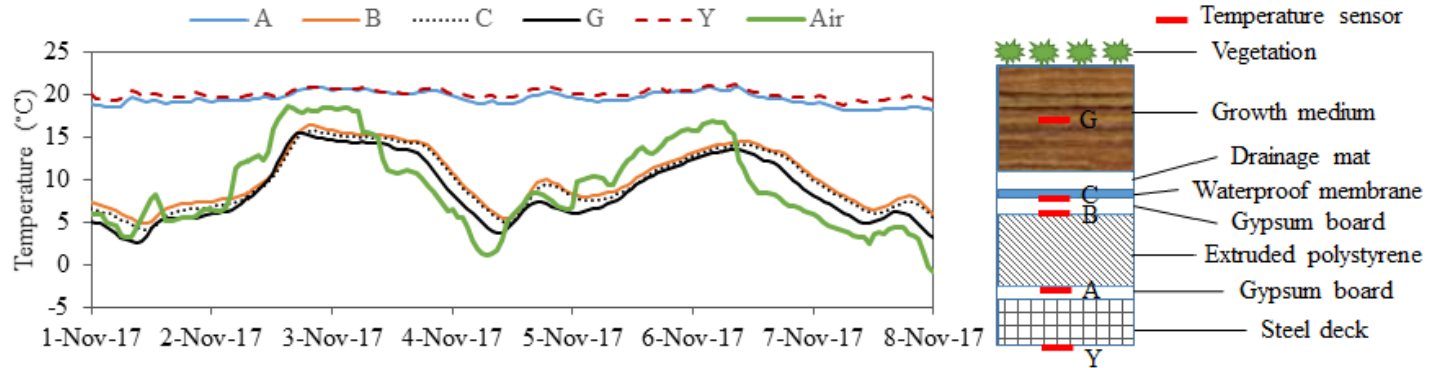


Figure 4.6. Temperature profile time series of the green roof during a winter week in November (no snow).

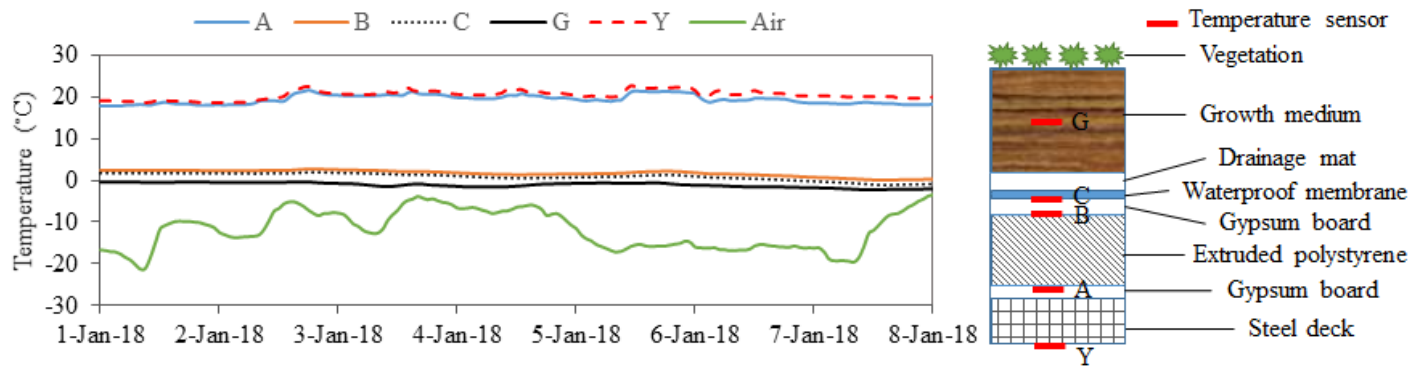


Figure 4.7. Temperature profile time series of the green roof during a winter week in January (snow cover).

### 4.3.3 Model Validation

The green roof model in CHAMPS was validated using the data of the first week of August and the first week of November. The simulated growth medium temperature was compared with the measured data (temperature sensor G, Fig. 4.8). Reasonable agreement between simulated and monitored temperature of soil was observed. For November, the CHAMPS model overpredicted the measured temperature by 17%. For August, the root mean square error (RMSE) between the simulated and monitored data was 1.7°C. Overall, around 80% of the simulated data were within +/- 10% of the measured values. These observed differences could be uncertainty in the certain input, such as the albedo, or approximation of the ET values. CHAMPS does not account for the energy of photosynthesis by the sedum, which might explain the overprediction of the temperature. The simulated green roof model appeared to be reliable in both summer and winter and can be used to simulate the traditional roof and the green roof.

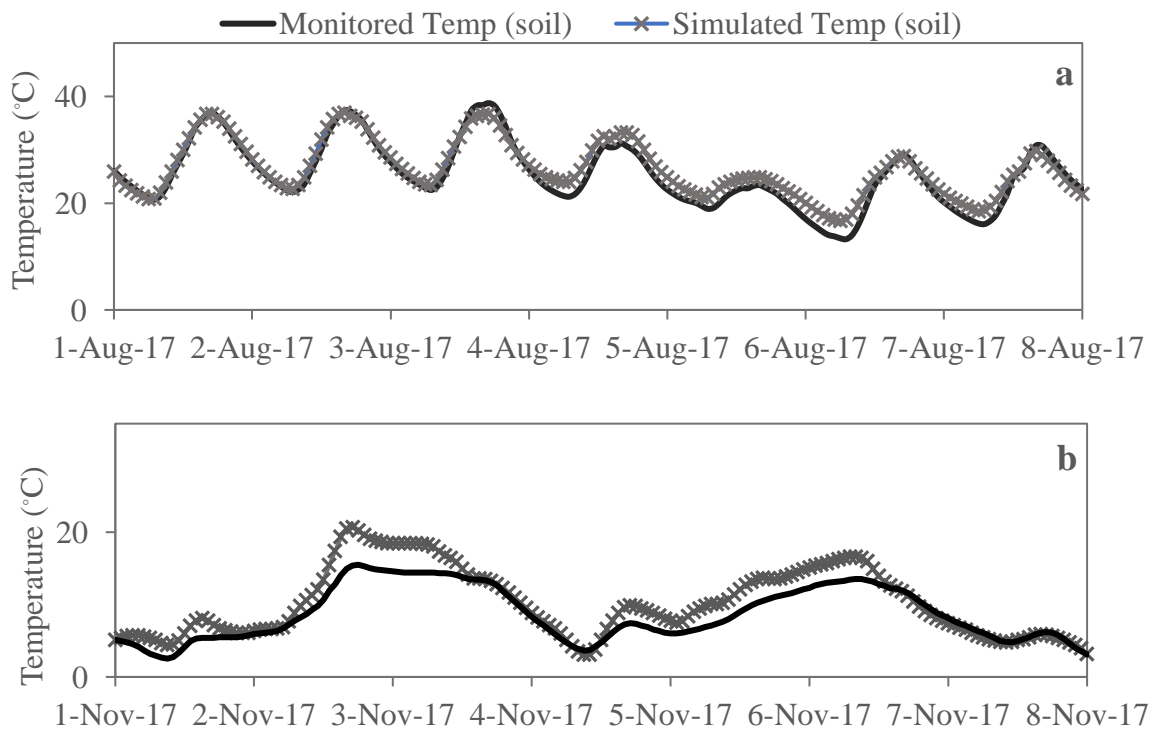


Figure 4.8. Comparison of simulated and measured temperatures of the growth medium on the green roof for the first week of August (a) and the first week of November (b).

#### **4.3.4 Thermal Impacts of Green Roofs in Summer**

An important benefit of green roofs is the reduction of the external surface temperature in summer, mitigating the urban heat island effect. Urban heat island mitigation represents the ability to reduce extreme air temperatures caused by the many heat sources in an urban area (Foustalieraki, et al., 2016). The comparison of surface temperature for the first week of August between the green roof and the traditional roof is shown in Fig. 4.9. Although the temperatures on these two roofs were not statistically different (ANOVA,  $p > 0.05$ ), a reduction in peak temperature was to be expected. The traditional roof had peak surface temperatures exceeding 40 and exhibited larger diurnal amplitudes than the green roof. An average of three hours delay in peak surface temperature of the green roof was evident in simulations.

The difference in surface temperature between the traditional and green roofs is due to a combination of albedo effect and latent heat loss. Since less incoming solar radiation is reflected on a traditional roof, more heat energy is transformed into the roofing system, leading to higher surface temperature. Cool roof is a strategy to decrease surface temperature of traditional roofs by adding a highly reflective paint, sheet covering, or highly reflective tiles or shingles to increase albedo (Coutts et al., 2013). Green roofs achieve surface temperature reduction not only through raising the albedo, but also through shading, storing heat in the plants, and losing latent heat through ET. The reduction of surface temperature also proves the green roof can serve as a thermal mass, damping thermal fluctuations through the system.

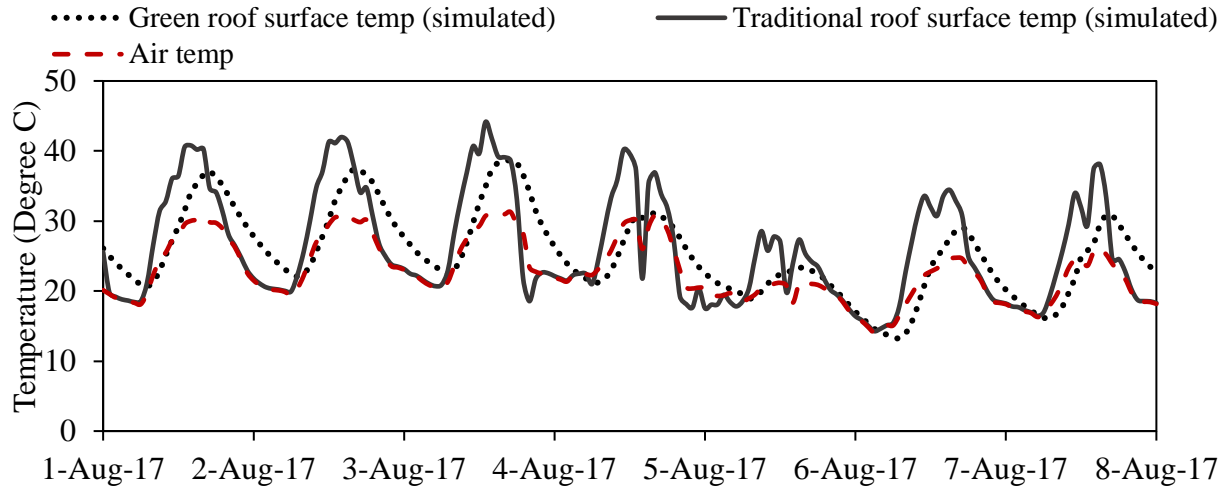


Figure 4.9. Comparison of the measured soil temperature of the green roof and simulated temperature of a traditional roof. The measured curve is identical to the curve in Figure 5.7 a.

Another benefit of a green roof is the reduction in the temperature fluctuation of the roof membrane, increasing its durability (She and Pang, 2010). Temperature fluctuation is the difference between daily maximum and minimum temperature. A significant statistical difference between the green roof and traditional roof of temperature fluctuation was indicated (ANOVA,  $p = 0.0008$ ). The membrane temperature fluctuation of a traditional roof was simulated to be 10°C higher than the green roof in August (Fig. 4.10). The green roof reduced the temperature fluctuation by 48% compared to the traditional roof. For the traditional roof, the membrane absorbs solar radiation during the day and emits heat at night.

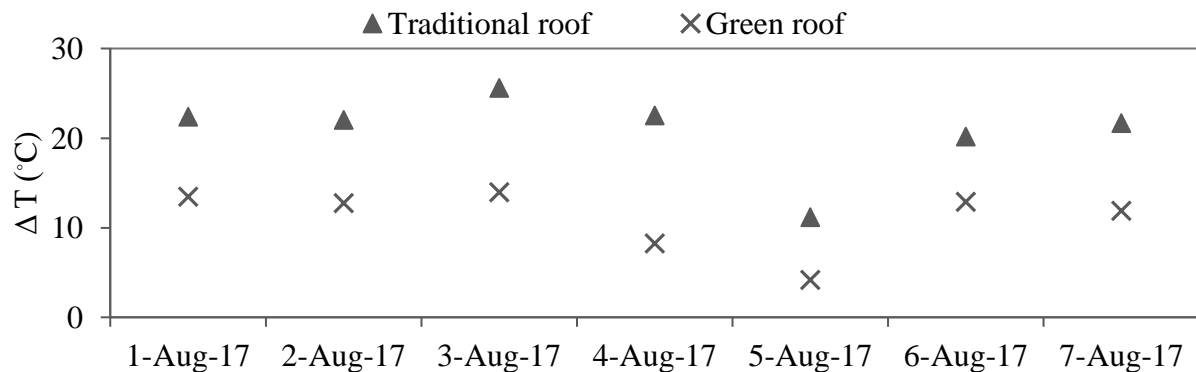


Figure 4.10. Temperature fluctuations at the membrane of the simulated traditional roof and measured on the green roof in summer.

Another benefit of a green roof is the reduction of heat flux through the roofing system, decreasing cooling load or heating load. Heat flux through the insulation has been used to estimate the flow of energy that enters or leaves the building. The green roof effectively decreased the heat flow through the roofing system compared to the traditional roof (Fig. 4.11). Further statistical analysis by ANOVA demonstrated that heat flux through the green roof and the traditional roof were statistically different ( $p < 0.05$ ). Even though the difference of overall R values between the green and traditional roof was very small ( $R_{\text{growth medium}}=0.2 \text{ m}^2\text{KW}^{-1}$ ), the heat flux was still significantly reduced mainly due to the reduction in surface temperature, which was caused by the albedo and ET effects. Gaffin et al. (2010) found a similar reduction of 37% in heat flux values through a green roof compared to a black roof in New York City. During dry periods in summer (8/1-8/3), CHAMPS simulations showed the traditional roof experienced negative (downward) heat flow in the afternoon and positive (upward) heat flow in the mornings and evenings. However, the green roof experienced negative heat flow most of the interval during the dry period, which means the accumulated heat from the day continues to enter the building at night. After rainfall events (8/6-8/7), positive heat flows occurred during the daytime on the green roof, likely due to the ET effect.

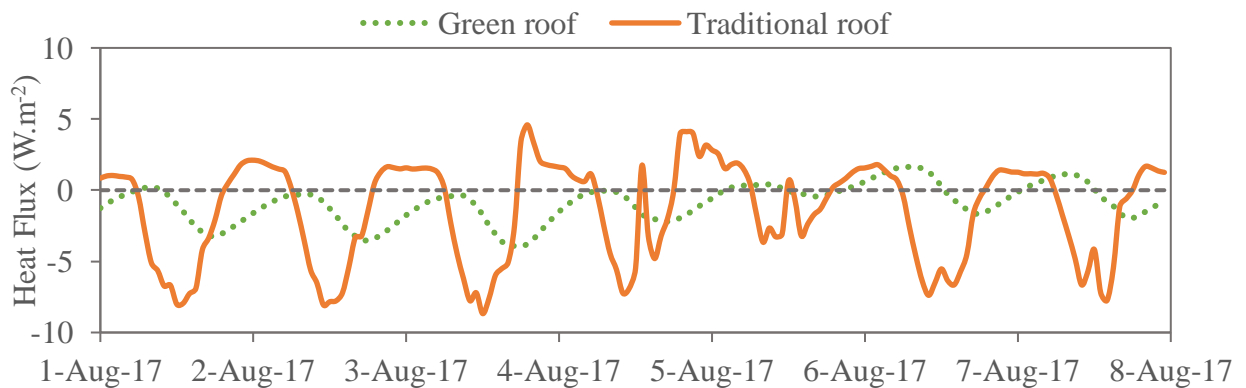


Figure 4.11. Comparison of heat flow through the insulation for the green roof and the traditional roof during a typical summer week (Aug 1-7, 2017).

The estimated energy demand for building cooling of the OnCenter during summer (June, July, and August) based on the average daily heat flux is summarized in Table 4.1 when considering only the heat flow through the roof. In this estimation, a seasonal energy efficiency ratio (SEER) of 13 BTU/W h was assumed for the central air conditioners in the OnCenter building (DOE, 2011). An electricity price of 16 cent/kWh was used, as it was the average price in New York State in the summer 2017 (NYSERDA, 2019). The green roof has reduced summer heat gain around 40% compared to the traditional roof. In addition, only accounting for the heat flow through the roofing system, the green roof is estimated to result in a total savings of \$295 in cooling costs compared to the traditional roof during summer. The difference in energy costs of the two roofs is not dramatic, which can be explained by two reasons: low cost of electricity and the fact that the effective extruded polystyrene insulation layer exists in both roofs. Even though the temperature fluctuation are significant, heat flows through both green and traditional roofs are relative small, due to the dominant thermal resistance of the insulation layer ( $R_{\text{insulation}}=2.5 \text{ m}^2\text{KW}^{-1}$ ) (Squier and Davidson, 2016).

Table 4.1. Estimated summer energy demand and cost for 5600 m<sup>2</sup> green roof and traditional roof.

	Average daily heat flux (W/m <sup>2</sup> )	Summer total cooling energy (kWh)	Summer electricity Cost (\$)
Green Roof	21	2808	449
Traditional Roof	35	4649	744

#### 4.3.5 Thermal Impacts of Green Roofs in Winter

Simulations showed the temperature fluctuations of the membrane on the traditional roof were far greater than those measured on the green roof in early winter (Fig. 4.12). The reduction of

temperature fluctuation in November was close to the magnitude of reduction simulated for August.

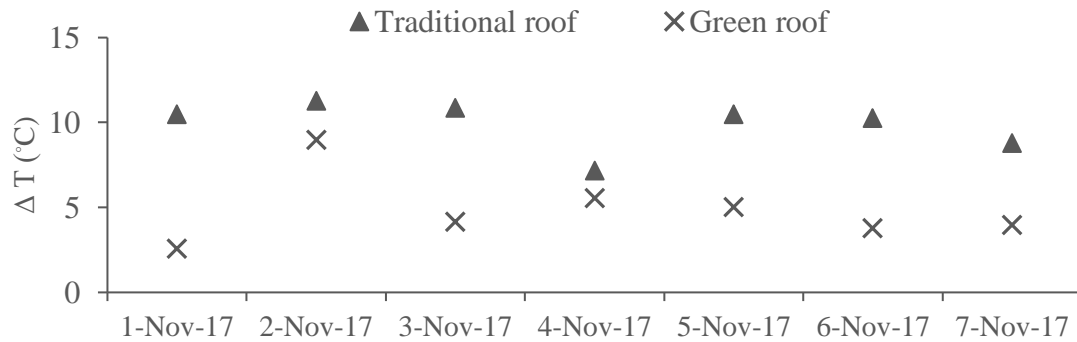


Figure 4.12. Temperature fluctuations at the membrane of the simulated traditional roof and measured on the green roof in winter.

To determine the effect of snow cover, the thermal profile of the green roof was simulated without snow cover using early January meteorological data in CHAMPS. The membrane temperatures with and without snowpack are shown in Fig. 4.13. The membrane temperatures of the green roof with and without snowpack were statistically different (ANOVA,  $p = 0.02$ ). Snow accumulation plays an important role in reducing temperature fluctuations. Without snow cover, under the same weather conditions, the membrane temperature could range from  $-18^{\circ}\text{C}$  to  $0^{\circ}\text{C}$ . Under snow cover, the protection provided by the growth medium becomes negligible compared with insulation associated with the snowpack. The thermal benefit of having a green roof decreases in cold weather. Similar results have been reported in other studies. Lundholm et al. (2014) found a positive relationship between average snow depth and average temperature of growth medium. They also suggested that greater snow coverage tended to decrease the differential benefits of green roofs against traditional roofs, but led to lower overall energy consumption. Zhao et al. (2015) reported that the green roof could reduce the building energy consumption for heating by 5% with a snow layer compared to a traditional roof. Without snowpack, the green roof was able to reduce the building energy consumption by 23%.

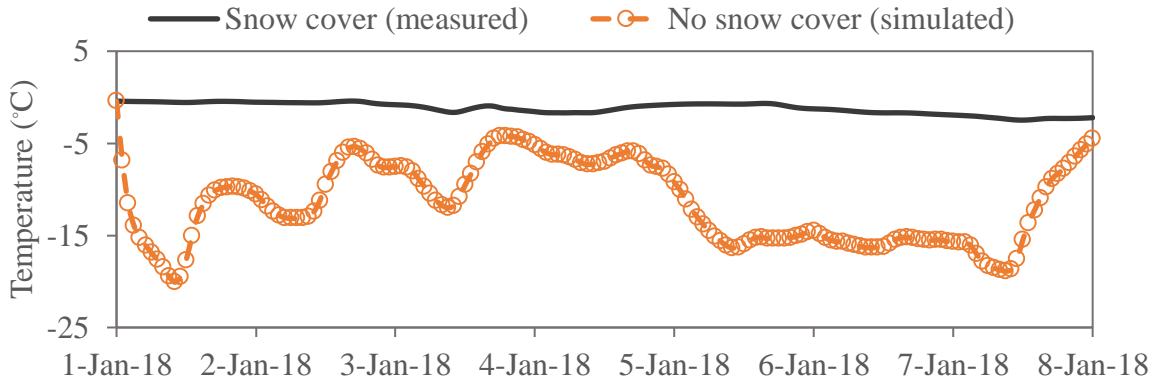


Figure 4.13. Temperature of the membrane for two conditions: simulated result with no snow cover and measurements with snow cover.

### 4.3.6 Parametric Studies

The green roof model was simulated with and without the water balance in CHAMPS. The soil temperature from measured and simulated results are shown in Figure 4.14. During dry weather conditions, the performance of the coupled heat and moisture transfer model and the heat only transfer model were similar. However, when rainfall occurs, the coupled heat and moisture transfer model had a smaller deviation from measured temperature values than the model that does not include moisture. Models with the water balance count for two effects: (1) the change of soil moisture content based on rainfall, runoff, and the ET cycle, and (2) the change of thermal conductivity of the growth medium as a function of moisture content.

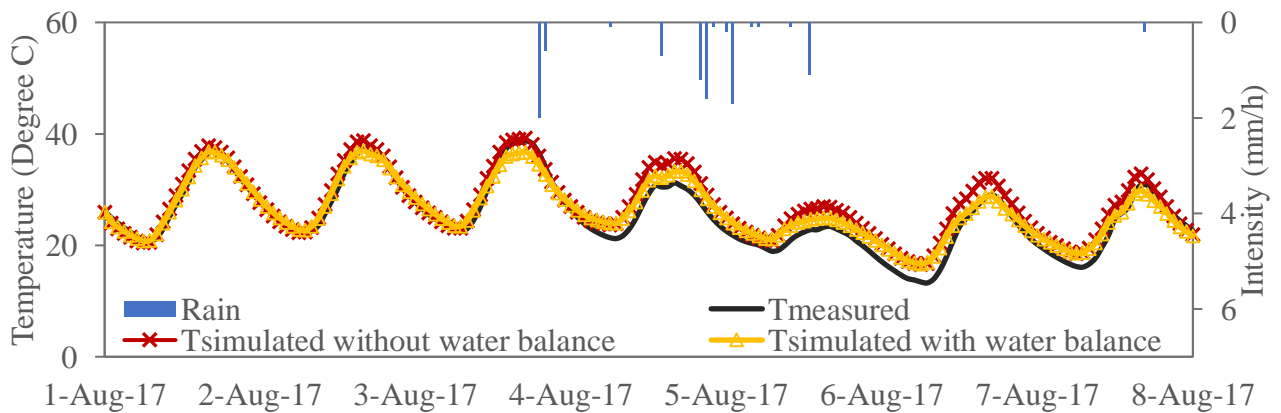


Figure 4.14. Comparison between measured and simulated (with and without water balance) soil temperature for the green roof.

During the roof model simulation, the albedo is a dominant parameter governing the soil temperature output. The variability in soil temperature is greatly reduced as the albedo increases (Fig. 4.15). Model simulations suggest that when a roof has an albedo as low as 0.1, the peak soil temperature can reach 55°C in August in Central New York. For a green roof, the albedo is related to ground cover, biomass, plant types, and moisture content of the growth medium. Blanus et al. (2013) showed that vegetation offers a cooling effect by direct shading and transpiration of water through stomata. In a parametric study, Theodosiou (2003) found the foliage density was the most important parameter governing the albedo compared to other parameters such as foliage height and soil layer thickness. Zhao et al. (2013) presented a simulation study of various plants and growth medium types, demonstrating how both plant types and growth medium types significantly affect the heat flux through the green roof.

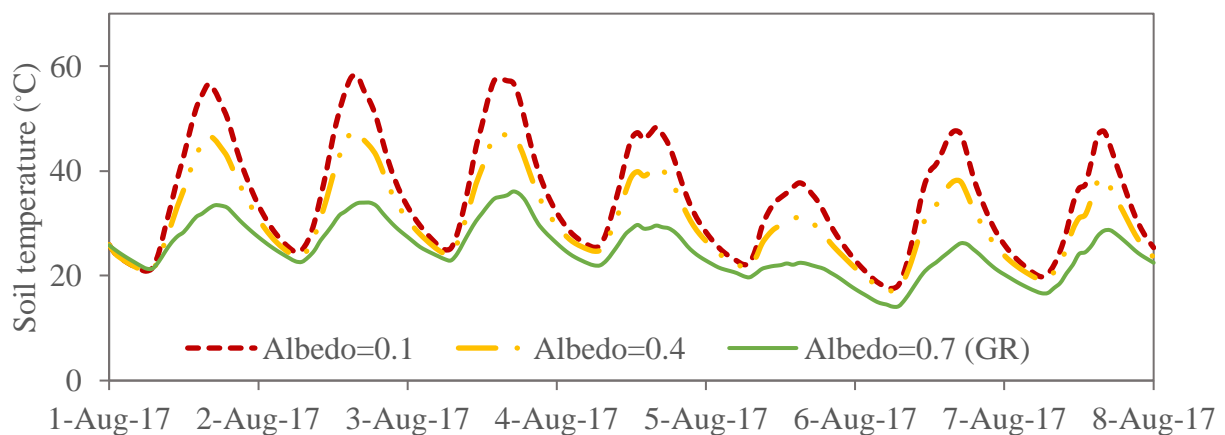


Figure 4.15. Soil temperature on the green roof for different albedo values.

#### 4.4 Conclusion

In this study, we performed field measurements to characterize the thermal performance of a green roof, and proposed a new approach to account for the evapotranspiration of vegetation in modeling the hygrothermal performance of the roof using CHAMPS-BES model. The CHAMPS

model takes into account both energy and water balances of a green roof in simulating the thermal dynamics of a roof system. By comparing the simulated results to measured data, this tool has demonstrated its ability to simulate heat and moisture transfer processes for a green roof. The analyses showed that the green roof with 7.6 cm growth medium could reduce the membrane temperature fluctuation by around 50% in both August and November. During early winter months, the plants and growth medium add thermal mass to decrease the membrane temperature fluctuations. In very cold weather, snow accumulation acts as effective natural insulation, isolating the roof from the ambient environment and this overrides any effect of the green roof on roof thermal protection. During warm periods, precipitation plays an important role in both temperature and heat flux through the roofing system. When the weather is dry, the soil temperature of the green roof and the surface temperature of the traditional roof are both higher than the air temperature. After rainfall events, the temperature of the green roof decreases close to the air temperature, while the traditional roof remains around 5°C higher than the air temperature. This phenomenon can be explained by the dissipated latent heat caused by ET. Also, the green roof significantly moderated the heat flow by 40% through the roofing system compared to the traditional roof. Only considering the heat flow through the roof, the 5600 m<sup>2</sup> green roof was estimated to save about \$295 on electricity for summer months compared with a traditional insulated roof. In addition, simulations demonstrated that adding a water balance to account for soil moisture and ET effects can improve the effectiveness of model simulations of roof temperature. A model sensitivity analysis showed that amplitude of the daily variation in temperature of the growth medium decreases with increasing albedo. The albedo of green roofs is related to plant type, biomass, and soil moisture content. In this study, details of energy and moisture flow through the plants were not considered. To improve the accuracy of the green roof

model, a plant layer could be developed in CHAMPS in the future. CHAMPS proved to be a useful tool for the quantitative evaluation of the energy benefits of green roofs under temperate climate. Further, it can add value to designers when considering retrofit additions of green roofs on buildings.

## Chapter 5

---

### CONCLUSIONS

#### 5.1 Key Findings

The overall goal of this PhD research is to advance knowledge of the hydrologic performance and thermal properties of a green roof, with emphases on the aging effect of soil media, the evapotranspiration (ET) process, and thermal modeling. Investigating the aging effect allows practitioners and policymakers to understand changes in hydrologic performance as the roof ages. Evaluating the ET process allows researchers and practitioners to quantify hydrologic and thermal benefits of green roofs. Establishing a thermal modeling tool allows designers and practitioners to estimate the energy cost saving and durability of a green roof before a traditional roof is replaced by a green roof retrofit. Overall, exploration of these areas can result in substantial theoretical and practical contributions to green roof design and maintenance as well as improved stormwater management and less costly thermal control in buildings.

This research focused on a green roof on the Nicholas J. Pirro Convention Center (OnCenter) in Syracuse, NY. The 5600 m<sup>2</sup> rectangular-shaped roof was retrofit on top of the existing structure in 2011. The roof is sloped at -1% from the centerline. Since 2015, the green roof has been instrumented with various sensors to record rainfall, runoff, soil moisture content, temperature in various roof layers, solar radiation, windspeed and direction, and relative humidity. The field data provided by this instrumentation are basis of this research.

In Chapter 2, the aging effect of the green roof is evaluated. Various key physical properties of virgin (2011) and aged samples (2018) were tested, and the impact of changes on hydrologic

retention and detention performance were assessed. The particles and pores tend to shift to smaller sizes as the roof ages. This pattern is similar to the findings in other studies (De-Ville et al., 2017; Hill et al., 2017). The reduction of pore sizes can be explained by root development, increases in soil organic matter, and growth medium consolidation. An increase of maximum water holding capacity in the aged sample suggests better hydrologic retention and detention performance. Meteorological conditions were similar in 2015 and 2017, so hydrologic performance of the roof during these two years was compared to investigate whether differences could be detected in the 6-year old roof compared with the 4-year old roof. Both retention and detention performances were slightly better in 2017. Furthermore, the HYDRUS-1D model was applied to simulate rainfall-runoff for five 24-hr design storms. The simulated results showed improvements in runoff retention, runoff delay and peak intensity delay in an aged green roof. This study offers a repeatable method to determine the effect of soil media aging. On the hydrologic function of a green roof, HYDRUS-1D shows potential to simulate green roof hydrologic performance.

Chapter 2 contributes to the existing literature on green roof aging by relating change in physical properties of the growth medium to the hydrologic performance. The methods used in this study can be repeated for other studies in aging effect research. The findings in this chapter offer insights to urban planners and practitioners on what to expect as a green roof ages. However, the two separate years of monitoring data analyzed to show the change of hydrologic performance due to aging were 2015 and 2017, only two years apart. Collecting data from years with greater separation is needed to better understand the effect of aging.

In Chapter 3, continuous daily ET measurements were conducted from May 2015 to November 2017 using the soil water balance method. Quantifying ET can enhance our knowledge of hydrologic processes, urban heat island mitigation, building energy saving, and reduction in heat loss through the roof. ET is restricted when the soil moisture is relatively low. The initial soil moisture content and the amount of solar radiation greatly influence the ET rates.

Since ET is difficult to measure, various models have been developed to predict values from available data. The models were mainly intended for agriculture but were applied to the OnCenter green roof. Since the green roof is not irrigated, a term to account for water availability has been added to the models. Fourteen models were evaluated with a crop coefficient, soil moisture extraction functions (SMEF), the Thornthwaite-Mather (T-M) equation, and the antecedent precipitation index (API). Comparison of measured and predicted ET rates revealed that the ASCE Penman-Monteith model performed the best. However, this model requires various onsite monitored data which are not commonly available for green roofs. Overall, it is proposed that when soil moisture data are available, the Blaney-Criddle and the Priestley-Taylor models together with SMEF and monthly crop coefficients are the best ET models due to their limited data input requirements. When soil moisture data are not available, the modified API model with monthly crop coefficients is recommended for application to Central New York.

Chapter 3 contributes to the existing literature by providing a low-cost methodology for estimating ET and evaluating of the suitability of various models to estimate ET, including those designed to account for water availability. Irrigation can enhance ET, reduce temperature, improve plant vitality, and improve overall hydrologic and thermal performance of a green roof.

With accurate measurements or predictions of ET, appropriate irrigation decisions can be made. ET is an important characteristic of hydrologic function, and better ET estimates can improve green roof hydrologic and thermal predictions, to maximize environmental benefits.

In Chapter 4, a combined energy and moisture model was developed using the Combined Heat, Air, Moisture, and Pollutant Simulation (CHAMPS) software to simulate heat flow and temperature profiles through the layers of the green roof. The simulated results were validated with the measured data in both August and November. In August, simulations showed the green roof reduced the temperature fluctuations of the membrane by 48%. The membrane absorbs solar radiation during the day and the roof temperature increases, and then the roof re-radiates the heat at night and the temperature decreases. In addition, by considering the water balance model, simulation of roof temperatures improved by accounting for soil moisture and ET. In November, without a snowpack, the simulated temperatures of the growth medium followed the diurnal cycle of ambient air temperatures with smaller amplitude than a traditional roof. In the coldest part of winter in January, when there is a snowpack on the roof surface, the growth medium remained slightly above freezing, since the snow acted as an insulator. In this study, details of energy and water flow through the plants were not considered, although the plants might be treated as a separate layer in future studies. Overall, CHAMPS showed its ability to quantify the energy benefits of green roofs under temperate climates.

Chapter 4 contributes to the existing literature by providing a thermal modeling tool to predict the thermal benefits of green roofs. For example, green roofs can serve as a passive cooling technique through insulation, thermal mass, and ET. CHAMPS can add a green roof layer to any

existing building to assess the thermal potential of adding a green roof as a retrofit. Simulating the energy flow through the layers of a proposed green roof before it is built can help urban planners and practitioners estimate and maximize the thermal benefits.

## **5.2 Proposed Areas of Future Work**

Several new opportunities for extending the research are presented below. Further, the methodologies presented in this dissertation can be applied to other green infrastructure.

Area 1: A standard physical test procedure is needed in the green infrastructure industry. Physical properties of green roofs provide important model parameters. Various studies applied different methods, testing saturated hydraulic conductivity, wilting point, field capacity, and other variables. Developing standard physical test procedures will allow researchers to compare their tested results, to further inform design.

Area 2: The focus of this work has been on the growth medium of the green roof. Plants are important factor affecting the hydrologic and thermal performance of the green roof. Specifically, vegetation is expected to change as the green roof ages. Future work is needed to identify the impact of aging vegetation.

Area 3: The rain simulator can help to assess the influence of growth medium depth, roof slope, plant type, plant coverage, and growth medium composition on hydrologic performance. Since a rain simulator can provide various rainfall intensities as required, a green roof plot with different features can be tested under this controlled setup. In addition, the results from the green roof plot

can be compared to monitored data from the full-scale green roof to evaluate how representative the lab experiments are.

Area 4: The soil water balance ET measurement method can be applied to a green infrastructure network, in which research is conducted on various types of green infrastructure at different locations. The soil water balance method is an affordable approach to measure ET that only requires soil moisture sensors. With portable sensors, this method can be widely used to estimate ET on various types of green infrastructure. The results can help quantify the benefits of green infrastructure, and assist with maintenance decisions.

## Appendix A

HYDRUS-1D mainly solves the Richards equation for saturated-unsaturated water flow (Eq.

A1). Van Genuchten –Mualem relationship is applied with Richards equation by determining the unsaturated hydraulic conductivity in terms of soil hydrologic parameters (Eq. A.2-A.4).

$$\frac{\partial \theta}{\partial t} = -\frac{\partial q}{\partial z} = \frac{\partial}{\partial z} \left[ K(\varphi_m) \left( \frac{\partial \varphi_m}{\partial z} + 1 \right) \right] \quad (\text{Eq. A1})$$

where  $\theta$  is the volumetric moisture content [ $L^3L^{-3}$ ];  $\varphi$  is the suction head [ $L$ ];  $K$  is the unsaturated hydraulic conductivity [ $LT^{-1}$ ];  $S$  is the volume of water removed from a unit volume of soil per unit time due to plant water uptake [ $L^3L^{-3}T^{-1}$ ].

$$\theta(P_c) = \theta_r + \frac{\theta_s - \theta_r}{[1 + |\alpha P_c|^n]^{1-1/n}} \quad (\text{Eq. A.2})$$

$$S_e = \left[ \frac{P_c}{P_e} \right]^{-\lambda} = (\theta - \theta_r) / (\theta_s - \theta_r) \quad (\text{Eq. A.3})$$

$$K(\theta) = K_s S_e^{0.5} \left[ 1 - \left( 1 - S_e^{\frac{1}{1-1/n}} \right)^{1-1/n} \right]^2 \quad (\text{Eq. A.4})$$

Where  $\theta_r$  and  $\theta_s$  are respectively the residual and saturated water content;  $P_c$  is soil pressure;  $P_e$  represents the entry pressure; the parameter  $\lambda$  is experimentally derived and it is related to the soil size distribution index;  $K(\theta)$  is hydraulic conductivity which related to the water content; parameter  $\alpha$  and  $n$  are independent parameters. Values of  $\alpha$  and  $n$  for twelve types of soils are shown in Table A.1.

Table A.1. Average values of  $\theta_s$ ,  $\theta_r$ ,  $\alpha$ ,  $n$ , Porosity and  $K_s$  of the Carsel and Parrish (1988) calibration data set.

Soil texture	Number of samples	$\theta_s$ ( $cm^3 cm^{-3}$ )	$\theta_r$ ( $cm^3 cm^{-3}$ )	$\alpha$ ( $cm^{-1}$ )	$n$	Porosity ( $cm^3 cm^{-3}$ )	$K_s$ (cm/hr)
Sand	246	0.43	0.045	0.145	2.68	0.384	29.7
Loamy sand	315	0.41	0.057	0.124	2.28	0.350	14.59
Sandy loam	1183	0.41	0.065	0.075	1.89	0.325	4.42
Loam	735	0.43	0.078	0.036	1.56	0.265	1.04
Silt	82	0.46	0.034	0.016	1.37	0.202	0.25
Silt loam	1093	0.45	0.067	0.020	1.41	0.210	0.45
Sandy clay loam	214	0.39	0.100	0.059	1.48	0.221	1.31
Clay loam	364	0.41	0.095	0.019	1.31	0.140	0.26
Silty clay loam	641	0.43	0.089	0.010	1.23	0.092	0.07
Sandy clay	46	0.38	0.100	0.027	1.23	0.113	0.12
Silty clay	374	0.36	0.070	0.005	1.09	0.023	0.02
Clay	400	0.38	0.068	0.008	1.09	0.033	0.2

## Appendix B

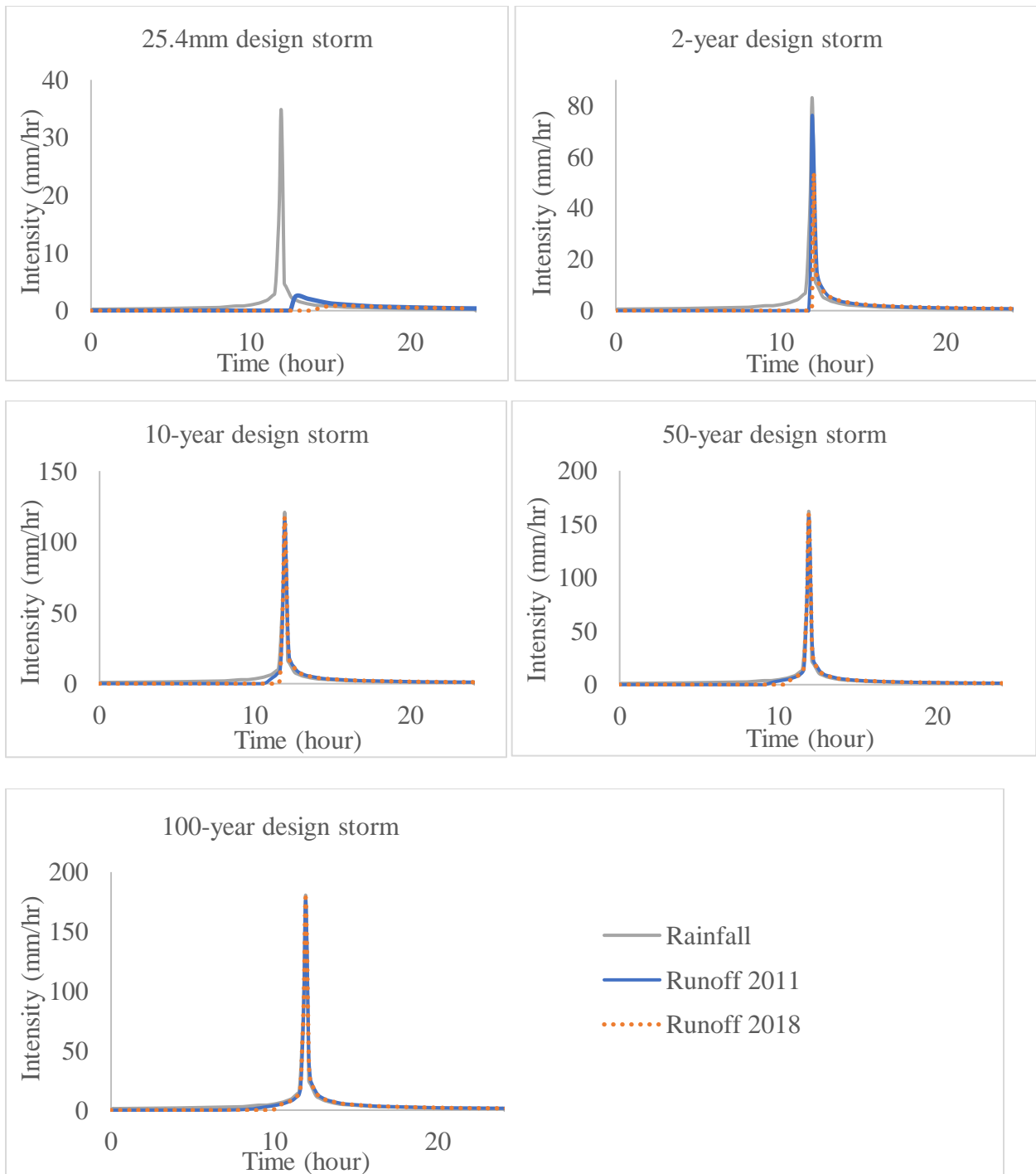


Figure B.1. Simulated hydrographs with rainfall (grey line), runoff for 2011 virgin soil (blue line), and runoff for 2018 aged soil (orange dot line).

## Appendix C

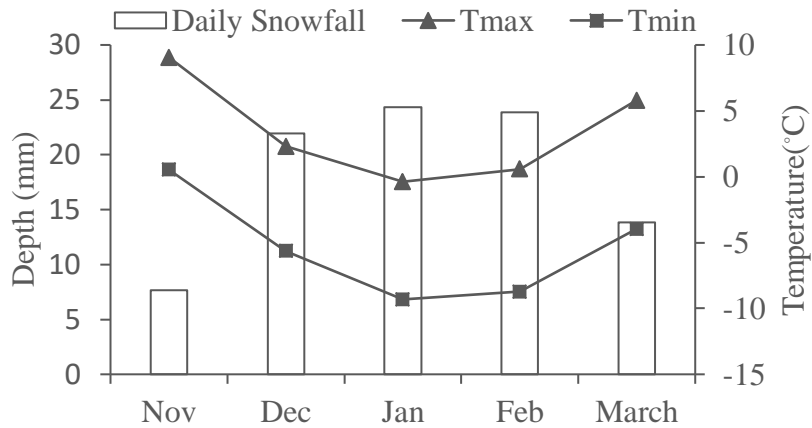


Figure C.1. Daily snowfall and daily minimum and maximum air temperature (1938-2016).

## Appendix D

Table D.1. Thermal properties of the Conventional Center green roof.

Layers	Thickness (cm)	Density (kg m <sup>-3</sup> )	Thermal conductivity (W m <sup>-1</sup> K <sup>-1</sup> )	Specific heat capacity (J kg <sup>-1</sup> K <sup>-1</sup> )
Growth Medium	7.62	790	0.36	1000
Drainage mat	0.63	1000	0.92	1000
Waterproof membrane	0.12	1400	0.43	1000
Gypsum board 2	1.59	700	0.16	870
Extruded polystyrene insulation	7.62	100	0.03	1300
Gypsum board 1	1.27	700	0.16	870
Steel	7.62	3600	20	700

\*Thickness, density, and thermal conductivity for all layers except growth medium are from the original construction files. Parameters for the growth medium were measured on the OnCenter roof.

## Appendix E

$$\frac{\partial}{\partial t} \rho_{REV}^{m_{w+v}} = -\frac{\partial}{\partial x} [j_{conv}^{m_w} + j_{conv}^{m_v} + j_{diff}^{m_v}] + \sigma_{REV}^{m_{w+v}} \quad (\text{Eq. E.1})$$

$$\frac{\partial}{\partial t} \rho_{REV}^{m_a} = -\frac{\partial}{\partial x} (j_{conv}^{m_a}) + \sigma_{REV}^{m_a} \quad (\text{Eq. E.2})$$

$$\frac{\partial}{\partial t} \rho_{REV}^U = -\frac{\partial}{\partial x} [j_{cond}^Q + h_v j_{diff}^{m_v} + \mu_w j_{conv}^{m_w} + \mu_v j_{conv}^{m_v} + \mu_a j_{conv}^{m_a}] + \sigma_{REV}^U \quad (\text{Eq. E.3})$$

$$j_{conv}^{m_w} = -K_l(\theta_l) \left( \frac{\partial p_l}{\partial x} + \rho_l g \right) \quad (\text{Eq. E.4})$$

$$j_{conv}^{m_v} = \frac{\rho_v}{\rho_a + \rho_v} j_{conv}^{m_g} \quad (\text{Eq. E.5})$$

$$j_{conv}^{m_a} = \frac{\rho_a}{\rho_a + \rho_v} j_{conv}^{m_g} \quad (\text{Eq. E.6})$$

$$j_{conv}^{m_g} = -K_g(\theta_l) \left( \frac{\partial p_g}{\partial x} + \rho_g g \right) \quad (\text{Eq. E.7})$$

$$j_{diff}^{m_v} = -\frac{D_v(\theta_l, T)}{R_v T} \frac{\partial p_v}{\partial x} \quad (\text{Eq. E.8})$$

$$j_{cond}^Q = -\lambda(\theta_l) \frac{\partial T}{\partial x} \quad (\text{Eq. E.9})$$

where  $\rho_{REV}^{m_{w+v}}$  is moisture (liquid water + vapor) density in reference volume in  $\text{kg/m}^3$ ,  $j_{conv}^{m_w}$  is convective liquid water flux in  $\text{kg/m}^2 \text{s}$ ,  $j_{conv}^{m_v}$  is convective water vapor flux in  $\text{kg/m}^2 \text{s}$ ,  $j_{diff}^{m_v}$  is diffusive water vapor flux in  $\text{kg/m}^2 \text{s}$ ,  $\sigma_{REV}^{m_{w+v}}$  is moisture sources/sinks in the reference volume in  $\text{kg/m}^3 \text{s}$ ,  $\rho_{REV}^{m_a}$  is air mass density in reference volume in  $\text{kg/m}^3$ ,  $j_{conv}^{m_a}$  is convective air mass flux in  $\text{kg/m}^2 \text{s}$ ,  $\sigma_{REV}^{m_a}$  is air sources/sinks in reference volume in  $\text{kg/m}^3 \text{s}$ ,  $\rho_{REV}^U$  is internal energy density in reference volume in  $\text{J/m}^3$ ,  $j_{cond}^Q$  is heat conduction flux in  $\text{W/m}^2$ ,  $h_v$  is specific enthalpy of water vapor in  $\text{J/kg}$ ,  $\mu_w, \mu_v, \mu_{air}$  are specific internal energy of water, vapor, and air in  $\text{J/kg}$ ,  $\sigma_{REV}^U$  is energy sources/sinks in reference volume in  $\text{J/m}^3$ .  $K_l$  is liquid water conductivity

in s,  $\theta_l$  is water content in  $\text{m}^3/\text{m}^3$ ,  $p_l$  is liquid water pressure in Pa,  $\rho_l$  is intrinsic density of liquid phase in  $\text{kg}/\text{m}^3$ ,  $g$  is gravity constant in  $\text{m}/\text{s}^2$ ,  $p_v$  is water vapor pressure in gas phase in Pa,  $p_a$  is air pressure in gas phase in Pa,  $j_{conv}^{m_g}$  is convective flux of the gas phase in  $\text{kg}/\text{m}^2 \text{ s}$ ,  $K_g$  is gas permeability of material in s,  $\rho_g$  is intrinsic density of gas phase in  $\text{kg}/\text{m}^3$ ,  $D_v$  is vapor diffusivity in  $\text{m}^2/\text{s}$ ,  $R_v$  is gas constant of water vapor in  $\text{J}/\text{kg K}$ ,  $T$  is temperature in K,  $\lambda$  is thermal conductivity of material in  $\text{W}/\text{m K}$ .

## References

- Abudi, I., Carmi, G., & Berliner, P. (2012). Rainfall simulator for field runoff studies. *Journal of Hydrology*, 454–455, 76–81. <https://dx.doi.org/10.1016/j.jhydrol.2012.05.056>.
- Akdogan, Z., & Guven, B. (2016). Assessing the sensitivity of SWMM to variations in hydrological parameters: a case study for the city of Istanbul. *Global NEST Journal*, 18(4), 831-841. <https://doi.org/10.30955/gnj.001717>.
- Alfredo, K., Montalto, F., & Goldstein, A. (2010). Observed and modeled performances of prototype green roof test plots subjected to simulated low- and high-intensity precipitations in a laboratory experiment. *Journal of Hydrologic Engineering*, 15(6), 444–457. [https://doi.org/10.1061/\(ASCE\)HE.1943-5584.0000135](https://doi.org/10.1061/(ASCE)HE.1943-5584.0000135).
- Ali, M. F., & Mawdsley, J. A. (1987). Comparison of two recent models for estimating actual evapotranspiration using only regularly recorded data. *Journal of Hydrology*, 93(3–4), 257–276. [https://doi.org/10.1016/0022-1694\(87\)90099-0](https://doi.org/10.1016/0022-1694(87)90099-0).
- Allen, P. D. R. (2012). Estimating reference evapotranspiration under inaccurate data conditions. *Irrigation and Drainage Systems*, 16, 33–45. <https://doi.org/10.1023/A:1015508322413>.
- Allen, R. G., Pereira, L. S., Raes, D., & Smith, M. (1998). Crop evapotranspiration - Guidelines for computing crop water requirements - FAO Irrigation and drainage paper 56 (Rome, IT). Retrieved from <http://www.fao.org/docrep/x0490e/x0490e00.htm#Contents>.
- Arshad, M.A., Lowery, B., & Grossman, B. (1996). Physical tests for monitoring soil quality. In: Doran, J.W. and Jones, A.J., Eds., Methods for assessing soil quality, *Soil Science Society of America Special Publication 49*, SSSA, Madison, WI, 123-142.
- Ayata, T., Tabares-Velasco, P. C., & Srebric, J. (2011). An investigation of sensible heat fluxes at a green roof in a laboratory setup. *Building and Environment*, 46 (9), 1851-1861.

<https://doi.org/10.1016/j.buildenv.2011.03.006>.

Barrio, E. P. Del. (1998). Analysis of the green roofs cooling potential in buildings. *Energy and Buildings*, 27(2), 179–193. [https://doi.org/10.1016/S0378-7788\(97\)00029-7](https://doi.org/10.1016/S0378-7788(97)00029-7).

Berghage, R., Jarrett, A., Beattie, D., Kelley, K., Husain, S., Rezai, F., Long, B., Negassi, A., Cameron, R. (2007). Quantifying evaporation and transpirational water losses from green roofs and green roof media capacity for neutralizing acid rain. *National Decentralized Water Resources Capacity Development Project (NDWRCP) Research Project*, 1–94.

Berndtsson, J. C., Bengtsson, L., & Jinno, K. (2009). Runoff water quality from intensive and extensive vegetated roofs. *Ecological Engineering*, 35(3), 369–380.

<https://doi.org/10.1016/j.ecoleng.2008.09.020>.

Berretta, C., Poë, S., & Stovin, V. (2014). Moisture content behaviour in extensive green roofs during dry periods: The influence of vegetation and substrate characteristics. *Journal of Hydrology*, 516, 37–49. <https://doi.org/10.1016/j.jhydrol.2014.04.001>.

Besir, A. B., & Cuce, E. (2018). Green roofs and facades: A comprehensive review. *Renewable and Sustainable Energy Reviews*, 82, 915–939. <https://doi.org/10.1016/j.rser.2017.09.106>.

Bianchini, F., & Hewage, K. (2012). How “green” are the green roofs? Lifecycle analysis of green roof materials. *Building and Environment*, 48(1), 57–65.

<https://doi.org/10.1016/j.buildenv.2011.08.019>.

Blaney H.F, Criddle W.D. (1950). Determining water requirements in irrigated areas from climatological irrigation data. *Soil Conservation Service Tech Paper No. 96, US Department*.

Blanusa, T., Vaz Monteiro, M. M., Fantozzi, F., Vysini, E., Li, Y., & Cameron, R. W. F. (2013). Alternatives to Sedum on green roofs: Can broad leaf perennial plants offer better “cooling

service”? *Building and Environment*, 59, 99–106.

<https://doi.org/10.1016/j.buildenv.2012.08.011>.

Boivin, M. A., Lamy, M. P., Gosselin, A., & Dansereau, B. (2001). Effect of artificial substrate depth on freezing injury of six herbaceous perennials grown in a green roof system.

*HortTechnology*, 11(3), 409–412. <https://doi.org/10.21273/HORTTECH.11.3.409>.

Bouzouidja, R., Rousseau, G., Galzin, V., Claverie, R., Lacroix, D., & Séré, G. (2018). Green roof ageing or Isolatic Technosol’s pedogenesis? *Journal of Soils and Sediments*, 18(2),

418–425. <https://doi.org/10.1007/s11368-016-1513-3>.

Bowyer-Bower, T. A. S., & Burt, T. P. (1989). Rainfall simulators for investigating soil response to rainfall. *Soil Technology*, 2(1), 1–16. [https://doi.org/10.1016/S0933-3630\(89\)80002-9](https://doi.org/10.1016/S0933-3630(89)80002-9).

Breña Naranjo, J. A., Weiler, M., & Stahl, K. (2011). Sensitivity of a data-driven soil water balance model to estimate summer evapotranspiration along a forest chronosequence.

*Hydrology and Earth System Sciences*, 15(11), 3461–3473. <https://doi.org/10.5194/hess-15-3461-2011>.

Bricker, S. B., Longstaff, B., Dennison, W., Jones, A., Boicourt, K., Wicks, C., & Woerner, J. (2008). Effects of nutrient enrichment in the nation’s estuaries: A decade of change.

*Harmful Algae*, 8(1), 21–32. <https://doi.org/10.1016/j.hal.2008.08.028>.

Burszta-adamiak, E., & Mrowiec. (2013). Modelling of Green roofs’ hydrologic performance using EPA’s SWMM. *Water Science and Technology*, 68(1), 36–42.

<https://doi.org/10.2166/wst.2013.219>.

Carpenter, C. M. G., Todorov, D., Driscoll, C. T., & Montesdeoca, M. (2016). Water quantity and quality response of a green roof to storm events: Experimental and monitoring observations. *Environmental Pollution*, 218, 664–672.

<https://doi.org/10.1016/j.envpol.2016.07.056>.

Carsel, R., & Parrish, R. (1988). Developing joint probability distributions of soil water retention characteristics. *Water Resources Research*, 24(5), 755–769.

<https://doi.org/10.1029/WR024i005p00755>.

Carson, T. B., Marasco, D. E., Culligan, P. J., & McGillis, W. R. (2013). Hydrological performance of extensive green roofs in New York City: observations and multi-year modeling of three full-scale systems. *Environmental Research Letters*, 8(2), 024036.

<https://doi.org/10.1088/1748-9326/8/2/024036>.

Carson, T., Keeley, M., Marasco, D. E., McGillis, W., & Culligan, P. (2017). Assessing methods for predicting green roof rainfall capture: A comparison between full-scale observations and four hydrologic models. *Urban Water Journal*, 14(6), 589–603.

<https://doi.org/10.1080/1573062X.2015.1056742>.

Centinari, M., Poni, S., Filippetti, I., Magnanini, E., & Intrieri, C. (2009). Evaluation of an open portable chamber system for measuring cover crop water use in a vineyard and comparison with a mini-lysimeter approach. *Agricultural and Forest Meteorology*, 149(11), 1975–1982.

<https://doi.org/10.1016/j.agrformet.2009.07.005>.

Chow, M. F., Fadhlullah, M., Bakar, A., & Sidek, L. M. (2018). A Review on the Controlling Factors that Affecting the Stormwater Retention Performance of Green Roof. *IOP Conference Series: Earth and Environmental Science*, 159, 012045.

<https://doi.org/10.1088/1755-1315/159/1/012045>.

Cirkel, D. G., Voortman, B. R., van Veen, T., & Bartholomeus, R. P. (2018). Evaporation from (Blue-) Green Roofs: Assessing the benefits of a storage and capillary irrigation system based on measurements and modeling. *Water (Switzerland)*, 10(9), 1–21.

<https://doi.org/10.3390/w10091253>.

Cohen, L. R., Raz-Yaseef, N., Curtis, J. B., Young, J. M., Rahn, T. A., Wilson, C. J., ...

Newman, B. D. (2015). Measuring diurnal cycles of evapotranspiration in the Arctic with an automated chamber system. *Ecohydrology*, 8(4), 652–659.

<https://doi.org/10.1002/eco.1532>.

Coles, A. E., & McDonnell, J. J. (2018). Fill and spill drives runoff connectivity over frozen ground. *Journal of Hydrology*, 558, 115–128. <https://doi.org/10.1016/j.jhydrol.2018.01.016>.

Coma, J., de Gracia, A., Chàfer, M., Pérez, G., & Cabeza, L. F. (2017). Thermal characterization of different substrates under dried conditions for extensive green roofs. *Energy and Buildings*, 144, 175–180. <https://doi.org/10.1016/j.enbuild.2017.03.031>.

Coutts, A. M., Daly, E., Beringer, J., & Tapper, N. J. (2013). Assessing practical measures to reduce urban heat: Green and cool roofs. *Building and Environment*, 70, 266–276. <https://doi.org/10.1016/j.buildenv.2013.08.021>.

Crago, R., & Brutsaert, W. (1992). A comparison of several evaporation equations. *Water Resources Research*, 28(3), 951–954. <https://doi.org/10.1029/91WR03149>.

Dalton, J. (1802). Experimental essays on the constitution of mixed gases; on the force of steam of vapour from waters and other liquids in different temperatures, both in a torricellian vacuum and in air on evaporation and on the expansion of gases by heat. *Memoirs and proceedings of the Manchester Literary & Philosophical Society*, 5, 535–602.

Davidson, E. A., Savage, K., Verchot, L. V., & Navarro, R. (2002). Minimizing artifacts and biases in chamber-based measurements of soil respiration. *Agricultural and Forest Meteorology*, 113(1–4), 21–37. [https://doi.org/10.1016/S0168-1923\(02\)00100-4](https://doi.org/10.1016/S0168-1923(02)00100-4).

De-Ville, S., Menon, M., Jia, X., Reed, G., & Stovin, V. (2017). The impact of green roof ageing

- on substrate characteristics and hydrological performance. *Journal of Hydrology*, 547, 332-344. <https://doi.org/http://dx.doi.org/10.1016/j.jhydrol.2017.02.006>.
- De-Ville, S., Menon, M., & Stovin, V. (2015). Using X-ray microtomography to identify physical changes in green roof substrates as a result of ageing. *Proceedings, The Annual Postgraduate Research Student Conference*, April 8-13, 2015, Sheffield, UK. Retrieved from <http://www.gruppofrattura.it/ocs/index.php/gigf/aprsc2015/paper/viewFile/12152/11540>.
- DelVecchia, A. G., Bruno, J. F., Benninger, L., Alperin, M., Banerje, O., & De Dios Morales, J. (2014). Organic carbon inventories in natural and restored Ecuadorian mangrove forests. *PeerJ*, 2014(1), 1–18. <https://doi.org/10.7717/peerj.388>.
- DeNardo, J.C., Jarrett, A.R., Manbeck, H.B., Beattie, D.J., & Berghage, R.D., 2005. Stormwater mitigation and surface temperature reduction by green roofs. *Transactions of the American Society of Agricultural Engineers*, 48 (4), 1491–1496. <http://dx.doi.org/10.13031/2013.19181>.
- Dexter, A.R., (1987). Compression of soil around roots. *Plant Soil*, 97, 401–406. <http://dx.doi.org/10.1007/bf02383230>.
- Digiovanni, K., Montalto, F., Gaffin, S., & Rosenzweig, C. (2013). Applicability of classical predictive equations for the estimation of evapotranspiration from urban green spaces : green roof results. *Journal of Hydrologic Engineering*, 18, 99–107. [https://doi.org/10.1061/\(ASCE\)HE.1943-5584.0000572](https://doi.org/10.1061/(ASCE)HE.1943-5584.0000572).
- DiGiovanni, K., Montalto, F., Gaffin, S., & Rosenzweig, C. (2013). Applicability of Classical Predictive Equations for the Estimation of Evapotranspiration from Urban Green Spaces: Green Roof Results. *Journal of Hydrologic Engineering*, 18(1), 99–107.

[https://doi.org/10.1061/\(asce\)he.1943-5584.0000572](https://doi.org/10.1061/(asce)he.1943-5584.0000572).

Djedjig, R., Ouldboukhitine, S.-E., Belarbi, R., & Bozonnet, E. (2012). Development and validation of a coupled heat and mass transfer model for green roofs. *International Communications in Heat and Mass Transfer*, 39(6), 752–761.

<https://doi.org/10.1016/j.icheatmasstransfer.2012.03.024>.

Dussailant, A., Cozzetto, K., Brander, K., & Potter, K. (2003). Green-Ampt model of a rain garden and comparison to Richards equation model. *Sustainable World*, 6, 891–900.

<https://doi.org/10.2495/SPD030841>.

Emilsson, T., & Rolf, K. (2004). Comparison of establishment methods for extensive green roofs in southern Sweden. *Urban Forestry and Urban Greening*, 3(2), 103–111.

<https://doi.org/10.1016/j.ufug.2004.07.001>.

DOE (Department of Energy). (2004). EnergyPlus Manual. *Quick Hits for New Faculty: Successful Strategies by Award-Winning Teachers*. Retrieved from

[https://doi.org/10.1007/978-3-540-44397-1\\_3](https://doi.org/10.1007/978-3-540-44397-1_3).

DOE (Department of Energy). (2011). Energy Conservation Program : Energy Conservation Standards for Residential Central Air Conditioners and Heat Pumps (Vol. 76). 1786-1858. Retrieved from

[https://www.energy.gov/sites/prod/files/2016/12/f34/CAC\\_HP\\_Direct\\_Final\\_Rule.pdf](https://www.energy.gov/sites/prod/files/2016/12/f34/CAC_HP_Direct_Final_Rule.pdf).

Eumorfopoulou, E., & Aravantinos, D. (1998). The contribution of a planted roof to the thermal protection of buildings in Greece. *Energy and Buildings*, 27(1), 29–36.

[https://doi.org/10.1016/s0378-7788\(97\)00023-6](https://doi.org/10.1016/s0378-7788(97)00023-6).

Fassman-Beck, E., Voyde, E., Simcock, R., & Hong, Y. S. (2013). 4 Living roofs in 3 locations: Does configuration affect runoff mitigation? *Journal of Hydrology*, 490, 11–20.

<https://doi.org/10.1016/j.jhydrol.2013.03.004>.

Feng, C., Meng, Q., & Zhang, Y. (2010). Theoretical and experimental analysis of the energy balance of extensive green roofs. *Energy and Buildings*, 42 (6), 959-965.

<https://doi.org/10.1016/j.enbuild.2009.12.014>.

Feng, Y., Burian, S. J., & Pardyjak, E. R. (2018). Observation and estimation of evapotranspiration from an irrigated green roof in a rain-scarce environment. *Water (Switzerland)*, 10(3), 13–21. <https://doi.org/10.3390/w10030262>.

Fioretti, R., Palla, A., Lanza, L. G., & Principi, P. (2010). Green roof energy and water related performance in the Mediterranean climate. *Building and Environment*, 45(8), 1890–1904. <https://doi.org/10.1016/j.buildenv.2010.03.001>.

FLL (Forschungsgesellschaft Landschaftsentwicklung Landschaftsbau) (1995). Guidelines for the planning, execution and upkeep of green-roof sites. In *Forschungsgesellschaft Landschaftsentwicklung Land- schaftsbau, Bonn*.

Foustalieraki, M., Assimakopoulos, M. N., Santamouris, M., & Pangalou, H. (2016). Energy performance of a medium scale green roof system installed on a commercial building using numerical and experimental data recorded during the cold period of the year. *Energy and Buildings*, 135, 33–38. <https://doi.org/10.1016/j.enbuild.2016.10.056>.

Gaffin, S. R., Rosenzweig, C., Eichenbaum-Pikser, J., Khanbilvardi, R., & Susca, T. (2010). A temperature and seasonal energy analysis of green, white, and black roofs. *Water Resources*, 19. Retrieved from <http://ccsr.columbia.edu/cig/greenroofs>.

Gao, F., Feng, G., Ouyang, Y., Wang, H., Fisher, D., Adeli, A., & Jenkins, J. (2017). Evaluation of reference evapotranspiration methods in arid, semiarid, and humid regions. *Journal of the American Water Resources Association*, 53(4). <https://doi.org/10.1111/1752-1688.12530>.

- Getter, K. L., Rowe, D. B., & Andresen, J. A. (2007). Quantifying the effect of slope on extensive green roof stormwater retention. *Ecological Engineering*, 31(4), 225–231. <https://doi.org/10.1016/j.ecoleng.2007.06.004>.
- Getter, K. L., Rowe, D. B., Andresen, J. A., & Wichman, I. S. (2011). Seasonal heat flux properties of an extensive green roof in a Midwestern U.S. climate. *Energy and Buildings*, 43(12), 3548–3557. <https://doi.org/10.1016/j.enbuild.2011.09.018>.
- Gregoire, B. G., & Clausen, J. C. (2011). Effect of a modular extensive green roof on stormwater runoff and water quality. *Ecological Engineering*, 37(6), 963–969. <https://doi.org/10.1016/j.ecoleng.2011.02.004>.
- Gunkel, A., & Lange, J. (2017). Water scarcity, data scarcity and the Budyko curve—An application in the Lower Jordan River Basin. *Journal of Hydrology: Regional Studies*, 12(5), 136–149. <https://doi.org/10.1016/j.ejrh.2017.04.004>.
- Hakimdavar, R., Culligan, P. J., Finazzi, M., Barontini, S., & Ranzi, R. (2014). Scale dynamics of extensive green roofs: Quantifying the effect of drainage area and rainfall characteristics on observed and modeled green roof hydrologic performance. *Ecological Engineering*, 73, 494–508. <https://doi.org/10.1016/j.ecoleng.2014.09.080>.
- Hansen, S. (1984). Estimation of potential and actual evapotranspiration. *Nordic Hydrological Conference*, 15, 205–212. <http://doi.org/10.2166/nh.1984.0017>.
- Hargreaves, G. H. (1975). Moisture availability and crop production. *Transactions of the American Society of Agricultural Engineers (ASAE)*, 18(5): 980–984.
- Hargreaves, G.H., Samani, Z.A. (1985). Reference crop evapotranspiration from temperature. *Transactions of the American Society of Agricultural Engineers (ASAE)*, 1(2):96–99.
- Henderson-Sellers, B. (1984). A new formula for latent heat of vaporization of water as a

- function of temperature. *Quarterly Journal of the Royal Meteorological Society*, 110(466), 1186–1190. <https://doi.org/10.1002/qj.49711046626>.
- Heusinger, J., & Weber, S. (2017). Surface energy balance of an extensive green roof as quantified by full year eddy-covariance measurements. *Science of the Total Environment*, 577, 220–230. <https://doi.org/10.1016/j.scitotenv.2016.10.168>.
- Hill, J., Drake, J., Sleep, B., & Margolis, L. (2017). Influences of four extensive green roof design variables on stormwater hydrology. *Journal of Hydrologic Engineering*, 22(8), 04017019. [https://doi.org/10.1061/\(ASCE\)HE.1943-5584.0001534](https://doi.org/10.1061/(ASCE)HE.1943-5584.0001534).
- Hiltner, R. N., Lawrence, T. M., & Tollner, E. W. (2008). Modeling stormwater runoff from green roofs with HYDRUS-1D. *Journal of Hydrology*, 358(3–4), 288–293. <https://doi.org/10.1016/j.jhydrol.2008.06.010>.
- Howell, T. A., Evett, S. R. (1965). The Penman-Monteith method. *USDA-Agricultural Research Service Conservation & Production Research Laboratory*, 5646(806). Retrieved from [www.cprl.ars.usda.gov](http://www.cprl.ars.usda.gov).
- Hudson, B. D. (1994). Soil organic matter and available water capacity. *Journal of Soil & Water Conservation*, 49(2), 189–194. <https://doi.org/10.1081/e-enrl-120049130>.
- Jaffal, I., Ouldboukhitine, S. E., & Belarbi, R. (2012). A comprehensive study of the impact of green roofs on building energy performance. *Renewable Energy*, 43, 157–164. <https://doi.org/10.1016/j.renene.2011.12.004>.
- Jensen, M.E., Burman, R.D., Allen, R.G. (1990). Evapotranspiration and irrigation water requirements. *ASCE Manuals and Reports on Engineering Practice No. 70*, ASCE, New York.
- Jim, C. Y., & Tsang, S. W. (2011). Ecological energetics of tropical intensive green roof. *Energy*

- and Buildings*, 43, 2696-2704. <https://doi.org/10.1016/j.enbuild.2011.06.018>.
- Johannessen, B., Muthanna, T., & Braskerud, B. (2018). Detention and retention behavior of four extensive green roofs in three nordic climate zones. *Water*, 10(6), 671. <https://doi.org/10.3390/w10060671>.
- Kirkham, M. (2004). *Principles of Soil and Plant Water Relations*. Burlington, MA: Academic Press.
- Kohler, M., & Linsley, R. (1951). Predicting the Runoff From Storm Rainfall. *Washington: U.S. Dept. of Commerce, Weather Bureau*. Retrieved from <https://www.nrc.gov/docs/ML0819/ML081900279.pdf>.
- Kumar, R., & Kaushik, S. C. (2005). Performance evaluation of green roof and shading for thermal protection of buildings. *Building and Environment*, 40(11), 1505–1511. <https://doi.org/10.1016/j.buildenv.2004.11.015>.
- Lazzarin, R. M., Castellotti, F., & Busato, F. (2005). Experimental measurements and numerical modelling of a green roof. *Energy and Buildings*, 37(12), 1260–1267. <https://doi.org/10.1016/j.enbuild.2005.02.001>.
- Legates, D. R., & McCabe Jr., G. J. (1999). Evaluating the use of “goodness-of-fit” measures in hydrologic and hydroclimatic model validation. *Water Resources Research*, 35(1), 233–241. <https://doi.org/10.1029/1998WR900018>.
- Li, Y., & Babcock, R. W. (2015). Modeling Hydrologic Performance of a Green Roof System with HYDRUS-2D. *Journal of Environmental Engineering*. 141(11), 1–9. [https://doi.org/10.1061/\(ASCE\)EE.1943-7870.0000976](https://doi.org/10.1061/(ASCE)EE.1943-7870.0000976).
- Li, Y. Y., Chung, P. R., Chen, C. Y., Chao, C. C., Chiu, F. Y., & Tzeng, P. C. (2017). The Study on the Evaluation of Thermal Insulation Efficiency with Typical Plant Species of Roof

- Greenery in Kaohsiung. *Procedia Engineering*, 180, 252–260.  
<https://doi.org/10.1016/j.proeng.2017.04.184>.
- Litvak, E., Bijoor, N. S., & Pataki, D. E. (2014). Adding trees to irrigated turfgrass lawns may be a water-saving measure in semi-arid environments. *Ecohydrology*, 7(5), 1314–1330.  
<https://doi.org/10.1002/eco.1458>.
- Liu, K., & Baskaran, B. (2003). Thermal performance of green roofs through field evaluation. *Proceedings, the First North American Green Roof Infrastructure Conference*. May 29-30, 2003, Chicago, IL. Retrieved from <http://archive.nrc-cnrc.gc.ca/obj/irc/doc/pubs/nrcc46412/nrcc46412.pdf>.
- Liu, K. K. Y., & Minor, J. (2005). Performance evaluation of an extensive green roof. *Proceedings, Greening Rooftops for Sustainable Communities*, . May 5-6, 2005, Washington, D.C. <https://doi.org/10.1109/ICEOE.2011.6013104>.
- Long, S. P., Farage, P. K., & Garcia, R. L. (1996). Measurement of leaf and canopy photosynthetic CO<sub>2</sub> exchange in the field. *Journal of Experimental Botany*, 47(11), 1629–1642. <https://doi.org/10.1093/jxb/47.11.1629>.
- Lu, J., Yuan, J. gang, Yang, J. zhi, & Yang, Z. yi. (2014). Responses of morphology and drought tolerance of *Sedum lineare* to watering regime in green roof system: A root perspective. *Urban Forestry and Urban Greening*, 13(4), 682–688.  
<https://doi.org/10.1016/j.ufug.2014.08.003>.
- Lundholm, J. T., Weddle, B. M., & Macivor, J. S. (2014). Snow depth and vegetation type affect green roof thermal performance in winter. *Energy and Buildings*, 84, 299–307.  
<https://doi.org/10.1016/j.enbuild.2014.07.093>.
- Ma, Y., Feng, S., Su, D., Gao, G., & Huo, Z. (2010). Modeling water infiltration in a large

- layered soil column with a modified Green – Ampt model and HYDRUS-1D. *Computers and Electronics in Agriculture*, 40–47. <https://doi.org/10.1016/j.compag.2009.07.006>.
- Mahringer, W. (1970). Verdunstungsstudien am Neusiedler See. *Arch. Met. Geoph. Biokl. B.* 18, 1–20. <https://doi.org/10.1007/BF02245865> .
- Makkink, G.F. (1957). Testing the Penman Formula by means of lysimeters. *Journal of the Institution of Water Engineers*, 11(3), 277–288.
- Marasco, D. E. (2014). Alternative Metrics of Green Roof Hydrologic Performance : Evapotranspiration and Peak Flow Reduction (Doctoral thesis, Columbia University). Retrieved from <https://academiccommons.columbia.edu/doi/10.7916/D89G5JZQ>.
- Marasco, D. E., Culligan, P. J., & McGillis, W. R. (2015). Evaluation of common evapotranspiration models based on measurements from two extensive green roofs in New York City. *Ecological Engineering*, 84, 451–462. <https://doi.org/10.1016/j.ecoleng.2015.09.001>.
- Marasco, D. E., Hunter, B. N., Culligan, P. J., Gaffin, S. R., & McGillis, W. R. (2014). Quantifying evapotranspiration from urban green roofs: A comparison of chamber measurements with commonly used predictive methods. *Environmental Science and Technology*, 48(17), 10273–10281. <https://doi.org/10.1021/es501699h>.
- Martens, R., Bass, B., & Alcazar, S.S. (2008). Roof–envelope ratio impact on green roof energy performance. *Journal of Urban Economics*, 11 (4), 399–408.
- Mawdsley, J. A., & Ali, M. F. (1985). Estimating Nonpotential Evapotranspiration by Means of the Equilibrium Evaporation Concept. *Water Resources Research*, 21(3), 383–391. <https://doi.org/10.1029/WR021i003p00383>.
- McLaren, R. G., & Cameron, K. C. (1996). *Soil science: Sustainable production and*

*environmental protection, 2nd Ed.*, Oxford University Press, Oxford, U.K.

Meng, Y., Wang, H., Chen, J., & Zhang, S. (2014). Modelling hydrology of a single bioretention system with HYDRUS-1D. *Scientific World Journal*, 2014.

<https://doi.org/10.1155/2014/521047>.

Mentens, J., Raes, D., & Hermy, M. (2006). Green roofs as a tool for solving the rainwater runoff problem in the urbanized 21st century? *Landscape and Urban Planning*, 77(3), 217–226. <https://doi.org/10.1016/j.landurbplan.2005.02.010>.

Metselaar, K. (2012). Water retention and evapotranspiration of green roofs and possible natural vegetation types. *Resources, Conservation and Recycling*, 64, 49–55.

<https://doi.org/10.1016/j.resconrec.2011.12.009>.

Nagase, A., & Dunnett, N. (2012). Landscape and Urban Planning Amount of water runoff from different vegetation types on extensive green roofs : Effects of plant species, diversity and plant structure. *Landscape and Urban Planning*, 104(3–4), 356–363.

<https://doi.org/10.1016/j.landurbplan.2011.11.001>.

Nash, J. E., & Sutcliffe, J. V. (1970). River flow forecasting through conceptual models part I - A discussion of principles. *Journal of Hydrology*, 10(3), 282–290.

[https://doi.org/10.1016/0022-1694\(70\)90255-6](https://doi.org/10.1016/0022-1694(70)90255-6).

Nawaz, R., McDonald, A., & Postoyko, S. (2015). Hydrological performance of a full-scale extensive green roof located in a temperate climate. *Ecological Engineering*, 82, 66–80.

<https://doi.org/10.1016/j.ecoleng.2014.11.061>.

Nektarios, P. A., Ntoulas, N., Nydrioti, E., Kokkinou, I., Bali, E. M., & Amountzias, I. (2014). Drought stress response of *Sedum sediforme* grown in extensive green roof systems with different substrate types and depths. *Scientia Horticulturae*, 181, 52–61.

<https://doi.org/10.1016/j.scienta.2014.10.047>.

Niachou, A., Papakonstantinou, K., Santamouris, M., Tsangrassoulis, A., & Mihalakakou, G.

(2001). Analysis of the green roof thermal properties and investigation of its energy performance. *Energy and Buildings*, 33(7), 719–729. [https://doi.org/10.1016/S0378-7788\(01\)00062-7](https://doi.org/10.1016/S0378-7788(01)00062-7).

NOAA (National Oceanic and Atmosphere administration). (2018). National Weather Service,

Daily record for Syracuse. Retrieved from

<https://www.weather.gov/bgm/climateSYRDailyRecords>.

NOAA (National Oceanic and Atmosphere administration). (2018). National Operational

Hydrologic Remote Sensing Center, Snowfall observations near Syracuse, NY.

Retrieved from

<https://www.nohrsc.noaa.gov/nearest/index.html?year=2020&month=4&day=13&city=Syracuse,%20NY&county=Onondaga>.

Novotny, V. (2002). *Water Quality: Diffuse Pollution and Watershed Management*, Wiley. pp.

422.

NYDEC (New York State Department of Environmental Conservation). (2010). New York State

Stormwater Management Design Manual. Retrieved from

[https://www.dec.ny.gov/docs/water\\_pdf/swdm2010entire.pdf](https://www.dec.ny.gov/docs/water_pdf/swdm2010entire.pdf).

NYSERDA (New York State Energy Research and Development Authority). (2019). Energy

price and weather data. Retrieved from <https://www.nyserda.ny.gov/Researchers-and-Policymakers/Energy-Prices>.

Ouldboukhitine, S. E., Belarbi, R., & Djedjig, R. (2012). Characterization of green roof

components: Measurements of thermal and hydrological properties. *Building and*

- Environment*, 56, 78–85. <https://doi.org/10.1016/j.buildenv.2012.02.024>.
- Palla, A., Gnecco, I., & Lanza, L. G. (2009). Unsaturated 2D modelling of subsurface water flow in the coarse-grained porous matrix of a green roof. *Journal of Hydrology*, 379(1–2), 193–204. <https://doi.org/10.1016/j.jhydrol.2009.10.008>.
- Palla, A., & Gnecco, I. (2015). Hydrologic modeling of Low Impact Development systems at the urban catchment scale. *Journal of Hydrology*, 528, 361–368. <https://doi.org/10.1016/j.jhydrol.2015.06.050>.
- Palla, A., Gnecco, I., & Barbera, P. La. (2018). Assessing the hydrologic performance of a green roof retrofitting scenario for a small urban catchment. *Water*, 10(8), 1052. <https://doi.org/10.3390/w10081052>.
- Penman, A. H. L. (2008). Natural Evaporation from Open Water, Bare Soil and Grass. *Proceedings of the Royal Society of London. Series A, Mathematical and Physical Sciences*, 193(1032), 120–145.
- Penn State University Agricultural Analytical Services Laboratory, Green roof media testing. Retrieved from <https://agsci.psu.edu/aasl/green-roof-media-testing>.
- Permpituck, S., & Namprakai, P. (2012). The energy consumption performance of roof lawn gardens in Thailand. *Renewable Energy*, 40(1), 98–103. <https://doi.org/10.1016/j.renene.2011.09.023>.
- Pickering, N. B., Jones, J. W., & Boote, K. J. (1993). Evaluation of the portable chamber technique for measuring canopy gas exchange by crops. *Agricultural and Forest Meteorology*, 63(3–4), 239–254. [https://doi.org/10.1016/0168-1923\(93\)90062-M](https://doi.org/10.1016/0168-1923(93)90062-M).
- Poë, S. (2016). The influence of a green roof configuration's moisture balance on hydrological performance (Doctoral thesis, University of Sheffield). Retrieved from

<http://etheses.whiterose.ac.uk/16102/>.

Poë, S., Stovin, V., & Berretta, C. (2015). Parameters influencing the regeneration of a green roof's retention capacity via evapotranspiration. *Journal of Hydrology*, *523*, 356–367.

<https://doi.org/10.1016/j.jhydrol.2015.02.002>.

Priestley, C. H., & Taylor, R. (1972). On the assessment of surface heat flux and evaporation using large-scale parameters. *Weather Review*, *100*(2), 81–92. [https://doi.org/10.1175/1520-0493\(1972\)100%3C0081:OTAOSH%3E2.3.CO;2](https://doi.org/10.1175/1520-0493(1972)100%3C0081:OTAOSH%3E2.3.CO;2).

Ran, J., & Tang, M. (2017). Effect of Green Roofs Combined with Ventilation on Indoor Cooling and Energy Consumption. *Energy Procedia*, *141*, 260–266.

<https://doi.org/10.1016/j.egypro.2017.11.103>.

Reicosky, D. C., & Peters, D. B. (1977). A Portable Chamber for Rapid Evapotranspiration Measurements on Field Plots. *Agronomy Journal*, *69*, 729–732.

Reicosky, D. C., Sharratt, B. S., Ljungkull, J. E., & Baker, D. G. (1983). Comparison of alfalfa evapotranspiration measured by a weighing lysimeter and a portable chamber. *Agricultural Meteorology*, *28*(3), 205–211. [https://doi.org/10.1016/0002-1571\(83\)90026-2](https://doi.org/10.1016/0002-1571(83)90026-2).

Rosenzweig, C., Gaffin, S., & Parshall, L. (2006). Green roofs in the New York metropolitan region, Research report. *Columbia University Center for Climate Systems Research and NASA Goddard Institute for Space Studies*. Retrieve from [https://pubs.giss.nasa.gov/docs/2006/2006\\_Rosenzweig\\_ro05800e.pdf](https://pubs.giss.nasa.gov/docs/2006/2006_Rosenzweig_ro05800e.pdf).

Rossman, L.A. (2004). Storm water management model User's manual version 5.0. Water Supply and Water Resources Division, National Risk Management Research Laboratory, Cincinnati (USA).

Sailor, D. J. (2008). A green roof model for building energy simulation programs. *Energy and*

- Buildings*, 40(8), 1466–1478. <https://doi.org/10.1016/j.enbuild.2008.02.001>.
- Saxton, K. E., & Rawls, W. J. (2006). Soil water characteristic estimates by texture and organic matter for hydrologic solutions. *Soil Science Society of America*, 1578, 1569–1578. <https://doi.org/10.2136/sssaj2005.0117>.
- Schendel, U. (1967). *Vegetations wasserverbrauch und wasserbedarf. Habilitation*, Kiel, pp. 137.
- Schneider, D. (2011). Quantifying evapotranspiration from a green roof analytically (Master thesis, Villanova University). Retrieved from <https://pdfs.semanticscholar.org/a077/b5245ce2afef9a8d9a1727e5b23184002643.pdf>.
- Schwager, J., & Schaal, L. (2015). Emission of trace elements and retention of Cu and Zn by mineral and organic materials used in green roofs. *Journal of Soils Sediments*, 15, 1789–1801. <https://doi.org/10.1007/s11368-014-0962-9>.
- Schwarz, C. (2015). Green roof energy balances for native grasses and sedum (thesis, University of Nebraska). Retrieved from <https://digitalcommons.unl.edu/cgi/viewcontent.cgi?article=1115&context=natresdiss>.
- Schwen, A., Bodner, G., Scholl, P., Buchan, G. D., & Loiskandl, W. (2011). Temporal dynamics of soil hydraulic properties and the water-conducting porosity under different tillage. *Soil and Tillage Research*, 113(2), 89–98. <https://doi.org/10.1016/j.still.2011.02.005>.
- Science, W., Burszta-adamiak, E., & Mrowiec, M. (2015). Modelling of Green roofs' hydrologic performance using EPA's SWMM. *Water Science & Technology*, 68(1), 36-42. <https://doi.org/10.2166/wst.2013.219>.
- Sharma, A., Conry, P., Fernando, H. J. S., Hamlet, A. F., Hellmann, J. J., & Chen, F. (2016). Green and cool roofs to mitigate urban heat island effects in the Chicago metropolitan area:

- evaluation with a regional climate model. *Environmental Research Letters*, 11(6), 064004.  
<https://doi.org/10.1088/1748-9326/11/6/064004>.
- She, N., & Pang, J. (2010). Physically based green roof model. *Journal of Hydrologic Engineering*, 15(6), 458–464. [https://doi.org/10.1061/\(ASCE\)HE.1943-5584.0000138](https://doi.org/10.1061/(ASCE)HE.1943-5584.0000138).
- Sherrard, J. A., & Jacobs, J. M. (2011). Vegetated roof water-balance model: experimental and model results. *Journal of Hydrologic Engineering*, 17(8), 858–868.  
[https://doi.org/10.1061/\(asce\)he.1943-5584.0000531](https://doi.org/10.1061/(asce)he.1943-5584.0000531).
- Šimunek, J., Vogel, T. & Van Genuchten, M.T. (1994). The SWMS\_2D code for simulating water flow and solute transport in two-dimensional variably saturated media, Version 1.21. Research Report No. 132, Riverside, California (USA).
- Shuttleworth, J. (2008). Evapotranspiration Measurement Methods. *SouthWest Hydrology*, 2, 22–23.
- Singh, V. P., & Xu, C.Y. (1997). Evaluation and generalization of 13 mass-transfer equations for determining free water evaporation. *Hydrological Processes*, 11(3), 311–323.  
[https://doi.org/10.1002/\(sici\)1099-1085\(19970315\)11:3<311::aid-hyp446>3.3.co;2-p](https://doi.org/10.1002/(sici)1099-1085(19970315)11:3<311::aid-hyp446>3.3.co;2-p).
- Squier, M., & Davidson, C. I. (2016). Heat flux and seasonal thermal performance of an extensive green roof. *Building and Environment*, 107, 235–244.  
<https://doi.org/10.1016/j.buildenv.2016.07.025>.
- Starry, O., Lea-Cox, J., Ristvey, A., & Cohan, S. (2016). Parameterizing a water-balance model for predicting stormwater runoff from green roofs. *Journal of Hydrologic Engineering*, 21(12), 04016046. [https://doi.org/10.1061/\(ASCE\)HE.1943-5584.0001443](https://doi.org/10.1061/(ASCE)HE.1943-5584.0001443).
- Steenhuis et al. (1986). The Thornthwaite-Mather procedure as a simple engineering method to predict recharge. 84, 221–229.

- Stefferdud, S. (2016). Soil Moisture Measurements and Evapotranspiration in Extensive Green Roofs (Master thesis, Norwegian University of Science and Technology). Retrieved from <http://hdl.handle.net/11250/2433627>.
- Stewart, B. A., & Howell, T. A., (2003). *Encyclopedia of Water Science*, Marcel Dekker Inc. pp. 87–90.
- Stovin, V., Poë, S., De-Ville, S., & Berretta, C. (2015). The influence of substrate and vegetation configuration on green roof hydrological performance. *Ecological Engineering*, 85, 159–172. <https://doi.org/10.1016/j.ecoleng.2015.09.076>.
- Stovin, V., Poë, S., & Berretta, C. (2013). A modelling study of long term green roof retention performance. *Journal of Environmental Management*, 131, 206–215. <https://doi.org/10.1016/j.jenvman.2013.09.026>.
- Stovin, V., Vesuviano, G., & Kasmin, H. (2012). The hydrological performance of a green roof test bed under UK climatic conditions. *Journal of Hydrology*, 414–415, 148–161. <https://doi.org/10.1016/j.jhydrol.2011.10.022>.
- Sun, T., Yang, W., & Ni, G. (2014). Study on the Runoff Generation Mechanism of Green Roofs under Stormwater Scenarios. *Journal of Water Resources Research*, 3(1), 20–28.
- Tabares-Velasco, P. C., Zhao, M., Peterson, N., Srebric, J., & Berghage, R. (2012). Validation of predictive heat and mass transfer green roof model with extensive green roof field data. *Ecological Engineering*, 47, 165–173. <https://doi.org/10.1016/j.ecoleng.2012.06.012>.
- Teemusk, A., & Mander, Ü. (2010). Temperature regime of planted roofs compared with conventional roofing systems. *Ecological Engineering*, 36(1), 91–95. <https://doi.org/10.1016/j.ecoleng.2009.09.009>.
- Theodoridou, I., Karteris, M., Mallinis, G., Tsiros, E., & Karteris, A. (2017). Assessing the

- Benefits from Retrofitting Green Roofs in Mediterranean, Using Environmental Modelling, GIS and Very High Spatial Resolution Remote Sensing Data: The Example of Thessaloniki, Greece. *Procedia Environmental Sciences*, 38, 530–537.  
<https://doi.org/10.1016/j.proenv.2017.03.117>.
- Theodosiou, T. G. (2003). Summer period analysis of the performance of a planted roof as a passive cooling technique. *Energy and Buildings*, 35(9), 909–917.  
[https://doi.org/10.1016/S0378-7788\(03\)00023-9](https://doi.org/10.1016/S0378-7788(03)00023-9).
- Thomas, M.D., & Hill, G.R. (1937). The continuous measurement of photosynthesis, respiration, and transpiration of alfalfa and wheat growing under field conditions (I). *Plant Physiology*, 12, 285–307. <http://doi.org/10.1104/pp.12.2.285>.
- Todorov, D., Driscoll, C., & Todorova, S. (2018). Long-term and seasonal hydrologic performance of an extensive green roof. *Hydrological Processes*, 32(16), 2471–2482.  
<https://doi.org/10.1002/hyp.13175>.
- Trabert, W. (1896). Neue Beobachtungen über Verdampfungsgeschwindigkeiten. *Meteorol. Z.* 13, 261–263.
- Turc, L. (1961). Evaluation des besoins en eau d'irrigation, evapotranspiration potentielle, formule climatique simplifée et mise à jour. *Annales Agronomique*, 12 (1), 13–49 (in French).
- Urban, J., Ingwers, M., McGuire, M. A., & Teskey, R. O. (2017). Stomatal conductance increases with rising temperature. *Plant Signaling and Behavior*, 12(8).  
<https://doi.org/10.1080/15592324.2017.1356534>.
- USDA (U.S. Department of agriculture). (2009). Soil water characteristics. Retrieved from:  
<https://hrsl.ba.ars.usda.gov/soilwater/Index.htm>.

- Valiantzas, J.D. (2013). Simple  $ET_o$  forms of Penman's equation without wind and/or humidity data. II: comparisons with reduced set-FAO and other methodologies. *Journal of Irrigation and Drainage Engineering*, 139(1), 9–19. [http://doi.org/10.1061/\(ASCE\)IR.1943-4774.0000502](http://doi.org/10.1061/(ASCE)IR.1943-4774.0000502).
- VanDam, J. C. (1990). Water and solute movement in a coarse-textured water-repellent field soil. *Journal of Hydrology*, 120 (1-4), 359–379. [https://doi.org/10.1016/0022-1694\(90\)90159-U](https://doi.org/10.1016/0022-1694(90)90159-U).
- Van Genuchten, M.Th. 1980. A closed-form equation for predicting the hydraulic conductivity of unsaturated soils. *Journal of Soil Science Society of America*, 44:892– 898. <https://doi.org/10.2136/sssaj1980.03615995004400050002x>.
- Van Genuchten, M. Th., F. J. Leij, and S. R. Yates. (1991). The RETC code for quantifying the hydraulic functions of unsaturated soils. Report No. EPA/600/2-91/065. Ada, Okla.: *U.S. Environmental Protection Agency, R.S. Kerr Environmental Research Laboratory*. Retrieved from <https://www.pc-progress.com/Documents/programs/retc.pdf>.
- VanWoert, N. D., Rowe, D. B., Andresen, J. A., Rugh, C. L., Fernandez, R. T., & Xiao, L. (2005). Green roof stormwater retention. *Journal of Environment Quality*, 34(3), 1036. <https://doi.org/10.2134/jeq2004.0364>.
- Vijayaraghavan, K., & Raja, F. D. (2014). Design and development of green roof substrate to improve runoff water quality: Plant growth experiments and adsorption. *Water Research*, 63, 94–101. <https://doi.org/10.1016/j.watres.2014.06.012>.
- Villarreal, E. L., & Bengtsson, L. (2005). Response of a Sedum green-roof to individual rain events. *Ecological Engineering*, 25(1), 1–7. <https://doi.org/10.1016/j.ecoleng.2004.11.008>.
- Viola, F., Hellies, M., & Deidda, R. (2017). Retention performance of green roofs in

- representative climates worldwide. *Journal of Hydrology*, 553, 763–772.  
<https://doi.org/10.1016/j.jhydrol.2017.08.033>.
- Voyde, E., Fassman, E., & Simcock, R. (2010). Hydrology of an extensive living roof under subtropical climate conditions in Auckland, New Zealand. *Journal of Hydrology*, 394(3–4), 384–395. <https://doi.org/10.1016/j.jhydrol.2010.09.013>.
- Voyde, E., Fassman, E., Simcock, R., & Wells, J. (2010). Quantifying evapotranspiration rates for New Zealand Green Roofs. *Journal of Hydrologic Engineering*, 15(6), 395–403.  
[https://doi.org/10.1061/\(ASCE\)HE.1943-5584.0000141](https://doi.org/10.1061/(ASCE)HE.1943-5584.0000141).
- Wadzuk, B. M., Asce, M., Schneider, D., Feller, M., & Traver, R. G. (2013). Evapotranspiration from a Green-Roof Storm-Water Control Measure. *Journal of Irrigation and Drainage Engineering*, 139(12), 995–1003. [https://doi.org/10.1061/\(ASCE\)IR.1943-4774.0000643](https://doi.org/10.1061/(ASCE)IR.1943-4774.0000643).
- Wadzuk, B. M., Schneider, D., Feller, M., & Traver, R. G. (2013). Evapotranspiration from a green roof stormwater control measure. *Journal of Irrigation and Drainage Engineering*, 139(12), 995–1003. [https://doi.org/10.1061/\(ASCE\)IR.1943-4774.0000643](https://doi.org/10.1061/(ASCE)IR.1943-4774.0000643).
- Weil, R., & Brady, N. (2017). The nature and properties of soils (Fifteenth, Vol. 10). Peason.
- Willmott, C.J. (1981). On the validation of models. *Physical Geography*, 2, 184–194.  
<https://doi.org/10.1080/02723646.1981.10642213>.
- Witmer, L., & Brownson, J. (2011). An energy balance model of green roof integrated photovoltaics: A detailed energy balance including microclimatic effects. *Proceedings, 40th ASES National Solar Conference*, May 17-21, 2011, Raleigh, NC.  
<https://doi.org/10.1016/j.buildenv.2011.06.012>.
- Wong, G. K. L., & Jim, C. Y. (2014). Quantitative hydrologic performance of extensive green roof under humid-tropical rainfall regime. *Ecological Engineering*, 70, 366–378.

<https://doi.org/10.1016/j.ecoleng.2014.06.025>.

Wong, N. H., Cheong, D. K. W., Yan, H., Soh, J., Ong, C. L., & Sia, A. (2003). The effects of rooftop garden on energy consumption of a commercial building in Singapore. *Energy and Buildings*, 35(4), 353–364. [https://doi.org/10.1016/S0378-7788\(02\)00108-1](https://doi.org/10.1016/S0378-7788(02)00108-1).

Yang, Y., & Davidson, C. I. (2018). Thermal performance of a green roof based on CHAMPS model and experimental data during cold climatic weather. *Proceedings, 7th International Building Physics Conference*, September 23-26, 2018, Syracuse, NY.

Yio, M. H. N., Stovin, V., Werdin, J., & Vesuviano, G. (2013). Experimental analysis of green roof substrate detention characteristics. *Water Science and Technology*, 68(7), 1477–1486. <https://doi.org/10.2166/wst.2013.381>.

Zhang, L., Jin, M., Liu, J., & Zhang, L. (2017). Simulated study on the potential of building energy saving using the green roof. *Procedia Engineering*, 205, 1469–1476. <https://doi.org/10.1016/j.proeng.2017.10.369>.

Zhao, L., Xia, J., Xu, C. yu, Wang, Z., Sobkowiak, L., & Long, C. (2013). Evapotranspiration estimation methods in hydrological models. *Journal of Geographical Sciences*, 23(2), 359–369. <https://doi.org/10.1007/s11442-013-1015-9>.

Zhao, M., Srebric, J., Berghage, R. D., & Dressler, K. A. (2015). Accumulated snow layer influence on the heat transfer process through green roof assemblies. *Building and Environment*, 87, 82–91. <https://doi.org/10.1016/j.buildenv.2014.12.018>.

Zhao, M., Tabares-Velasco, P. C., Srebric, J., & Komarneni, S. (2013). Comparison of green roof plants and substrates based on simulated green roof thermal performance with measured material properties. *Proceedings, 13th Conference of International Building Performance Simulation Association*, August 26-28, 2013, Chambéry, France.

Zhao, M., Tabares-Velasco, P. C., Srebric, J., Komarneni, S., & Berghage, R. (2014). Effects of plant and substrate selection on thermal performance of green roofs during the summer. *Building and Environment*, 78, 199–211. <https://doi.org/10.1016/j.buildenv.2014.02.011>.

**VITA**  
**YIGE YANG**

**EDUCATION**

**Syracuse University, *PhD Candidate***, *Environmental Engineering*, May 2019

Specialization: Hydrological and thermal modeling of green roofs; Stormwater management

**Syracuse University, *M.S.***, *Environmental Engineering*, May 2015

Specialization: Managing Sustainability; Green Infrastructure; Hazardous Waste Management

**Sun Yat-sen University**, School of Environmental Science & Engineering, Guangzhou, China

*B.S., Environmental Science*, Minor: Public Relations, May 2013

**SKILLS**

*Water/Wastewater Engineering*: EPA-SWMM, Stormwater infrastructure design and calculation,

WaterCAD, HEC-RAS, HEC-HMS, Erosion control, Wastewater quality assessments

*Technical Software*: Civil 3D, AutoCAD, R, MATLAB, Hydraulic modeling, ArcGIS

*Language*: Mandarin, Cantonese, English

*Communication*: Proposal writing, technical writing, poster presentation, oral presentation

## **PROFESSIONAL EXPERIENCE (4 + years)**

**Civil Engineer Intern**, Environmental Design & Research, Landscape Architecture, Engineering & Environmental Services (Summer 2018)

- Conducted a novel project of helping a wind farm to pass a new state safety regulation. Applied a complex model to simulate the snow fall tracks from wind turbines and estimated the safe range using MATLAB
- Engineered stormwater management solutions to provide site planning, SWPPP compiling, MS4 Permits preparing, and 3D Auto CAD layout development
- Performed hydrologic modeling with HydroCAD to integrate project BMPs into clients' site designs

**Teaching Assistant**, Syracuse University, NY (08/2015 – 05/2017)

- Assist with Professors with lectures (*Wastewater Treatment, Intro to Sustainability, Fluid Mechanics*)
- Lead recitations providing additional examples, strategies for class work and projects

## **PROJECTS AND RESEARCH EXPERIENCE (4 + years)**

**Green roof aging effect on physical properties and hydraulic performance** (9/2018 – 1/2019)

- Analyzed structure and hydraulic properties of virgin and aged soil
- Evaluated retention and detention performance of a green roof based on monitoring data
- Plan to submit paper to *Journal of Sustainable Water in the Built Environment*.

**Evaluate energy performance and conducted thermal modeling of a green roof** (2/2017 – 1/2019)

- Designed and installed weather and temperature monitoring sensors in five layers of the roof
- Applied the combined heat, air, moisture and pollutant simulations in building envelope systems (CHAMPS-BES) model on the green roof and validated the model using field data
- Published paper “Thermal performance of a green roof based on CHAMPS model and experimental data during cold climatic weather” *7<sup>th</sup> International Building Physics Conference*

**Green roof monitoring and maintenance campaign** (9/2015 – present)

- Designed the monitoring system on the green roof: system design, sensor wiring, data logging
- Maintained the monitoring system over 4 years: sensor diagnostics

**COE Green roof Project, Syracuse University Campus as a Laboratory for Sustainability Grant** (9/2017 – 5/2018, \$1,5000)

- Applied Computational Fluid Dynamics (CFD) simulations to model atmospheric turbulence over the green roof and generate profiles of ambient air temperatures
- Designed an educational website for Green roofs

**The urban resilience to extremes sustainability research network (URExSRN)** (1/2017 – present)

- Work with 9 UREx network cities to co-create a set of decision tools that confront resiliency challenges

- Develop climatological hydrological, ecological, infrastructural and socio-economic databases for 9 cities

#### **Characterization of the growth medium on an extensive green roof (9/2015 – 9/2016)**

- Designed and ran tests to determine hydraulic conductivity, particle size distribution, bulk density, porosity, etc
- Connected the physical characteristics to the hydrological performance, built process based model to improve future design

#### **Develop InDeaTe Design Tool and Template for sustainable improvement (6/2015 - 6/2016)**

- Core member of the design team of InDeaTe Tool and Template, improved sustainability considerations
- Published Chapter “Supporting Sustainable Service-System Design: A Case study on Green-Roof Design with InDeaTe Template and Tool at Syracuse, New York.” *Research into Design for Communities*, Volume 2, pp.19-23

#### **The practical application of green infrastructure in US (8/2014 – 5/2015)**

- Built basic line of impervious surface ratio in 32 main cities with GIS technology

#### **Certificate and Fellowships**

##### **Certificate of Advanced Study in Sustainable Enterprise (CASSE), Syracuse University, NY**

- Applied sustainable theories to develop strategies for global enterprises facing environmental crisis.

- Collaborated with business students to evaluate the “Colgate Annual Report” through SWOT model.

- Designed effective environmental sustainable system for Honeywell.

**Education Model Program on Water-Energy Research (EMPOWER), Syracuse University, NY**

- An interdisciplinary approach that is focus on research of interface of water and energy use.

- Prepare students with the technical knowledge and professional skills needed to compete for careers.

**Syracuse University Water Initiative Fellowship (2017-2018)**

- One of the most prestigious fellowship (\$ 25,290).

**Poster winner in NYS Green Building Conference (Non architecture section) (03/2017)**

- Presented the poster “Green Roof Performance Influenced by Growth Medium Characteristics”.

**Professional Service, Affiliations and Activities**

American Society of Civil Engineers (ASCE), 2016 – present

American Society for Engineering Education (ASEE), 2016 – present

American Academy of Environmental Engineers & Scientists (AAEES), 2016 – present

Society of Women Engineers, 2015 – present

Women in Science and Engineering Future Professionals Program (WiSE), 2015 – present

Department Chair of Civil and Environmental Engineering, 2017 - present